DESY 18-106

Emerging chromo-natural inflation

Valerie Domcke[1], Ben Mares, Francesco Muia[2], Mauro Pieroni[3]

[1] *Deutsches Electronen Synchrotron (DESY), 22607 Hamburg, Germany*

[2] *ICTP, Strada Costiera 11, Trieste 34014, Italy,*

[3] *Instituto de Física Teórica UAM/CSIC C/ Nicolás Cabrera 13-15*
Universidad Autónoma de Madrid Cantoblanco, Madrid 28049, Spain

Abstract

The shift-symmetric coupling of a pseudo-scalar particle driving inflation to gauge fields provides a unique way of probing cosmic inflation. We show for an $SU(2)$ gauge group how a classical isotropic background gauge field develops from the standard quantum mechanical vacuum in the far past. Over the course of inflation, the theory dynamically evolves from an approximately abelian regime into an inherently non-abelian regime, with distinct predictions for the scalar and tensor power spectra. The latter regime closely resembles a setup known as chromo-natural inflation, although our main focus here is on a new part of the parameter space which has received little attention so far. For single-field slow roll inflation models, large scales may exit the horizon in the abelian regime, ensuring agreement with the observations of the anisotropies in the cosmic microwave background, whereas smaller scales experience the non-abelian effects. This results in a strong enhancement of the stochastic gravitational wave background at small scales, e.g. at frequencies accessible with ground-based interferometers. For the scalar power spectrum, a similar enhancement arises due to non-linear contributions.

Contents

1 Introduction

The paradigm of cosmic inflation, proposed to explain the puzzling homogeneity and flatness of the Hot Big Bang Universe [1], has been strikingly successful in predicting the anisotropies of the Cosmic Microwave Background (CMB), measured to great precision by the PLANCK satellite [2]. This paradigm however leaves open questions. What guarantees the required flatness of the inflationary potential? How is the inflation sector coupled to the Standard Model (SM) of particle physics? The lack of observable predictions on far sub-horizon scales makes it very difficult to find satisfactory and testable answers to these questions. In this context, a special role is played by pseudo-scalar inflation models, in which the inflaton ϕ (the particle driving inflation) couples to the field strength tensor $F_{\mu\nu}$ of massless gauge fields through the derivative coupling $\phi F_{\mu\nu}\tilde{F}^{\mu\nu}$. This coupling is compatible with a shift-symmetry of the inflaton ϕ protecting the flatness if the inflationary potential, it provides an immediate way to couple the inflation sector to a gauge field sector (which could be the SM or a hidden sector) and it leads to distinctive signatures, including a strongly enhanced chiral gravitational wave background [3–5].

The phenomenology of these models, both for Abelian and non-Abelian gauge fields, has recently received a lot of interest. In both cases, the gauge field sector experiences a tachyonic instability during inflation, leading to an explosive particle production which impacts the predictions of inflation. For Abelian gauge fields this instability is controlled by the inflaton velocity, implying large effects towards the end of inflation in single-field slow-roll inflation models whereas the CMB scales can be large unaffected, see Ref. [6] for an overview. The phenomenology of this model includes a strongly enhanced and non-Gaussian contribution to the scalar and tensor power spectra [6–10], which may lead to a distortion of the CMB black body spectrum [11], primordial black black hole (PBH) production [12–14] and an enhanced chiral gravitational wave signal in the frequency band of LIGO and LISA [3, 7, 8, 15–17]. Furthermore, the effective friction induced by the gauge field allows for inflation on rather steep potentials [18]. The interplay of the gauge fields with the production of charged fermions has been studied in [19]. The coupling to non-Abelian $SU(2)$ gauge fields, dubbed chromo-natural inflation (CNI) in [20], allows for inflationary solutions on steep potentials in the presence of a non-vanishing isotropic background gauge field configuration. An analysis of the perturbations [4, 5, 21, 22] revealed an enhanced tensor power spectrum, to the point of excluding the model as an explanation for the anisotropies in the CMB. This conclusion remains valid in the regime where the scalar field can be integrated out [23], referred to as gauge-flation [24, 25] (see also [26, 27]). Modifications of the original model can overcome this by employing different inflation potentials [28, 29], enlarging the field content of the model [30, 31] or considering a spontaneously broken gauge symmetry [32].

In this paper we study the dynamical emergence of CNI. In CNI, the gauge field background is assumed to be homogeneous, isotropic and have a sufficiently large vacuum expectation value, so that the background evolution of the inflaton is dominated by the gauge friction term. We show how such an isotropic background develops from the regular Bunch Davies initial conditions in the far past, providing justification for what is commonly taken for granted in CNI. For small gauge field amplitudes, the non-Abelian $SU(2)$ dynamics reduce to three copies of an Abelian gauge group. As

the inflaton velocity increases over the course of inflation, the tachyonic enhancement of the gauge fields in the Abelian regime triggers a classical, inherently non-Abelian background evolution. In this background, only a single helicity component of the gauge field features a regime of tachyonic instability. Contrary to the Abelian case, each Fourier mode experiences this instability only for a finite time interval. We provide analytical results which make only minimal assumptions about the values of the parameters involved. For the explicit parameter example which we study numerically, we find the gauge friction term to be subdominant in the non-Abelian regime, contrary to the usual assumption in CNI. This opens up a new part of parameter space of this model, which is moreover not plagued by the catastrophic instability in the scalar sector arising in part of the parameter space as pointed out in [4]. We emphasize that the transition from an effectively Abelian to a non-Abelian regime is generic in single field axion inflation models, and naturally removes the tension of the original CNI model with the PLANCK data by delaying the enhancement of the tensor power spectrum to smaller scales.

Throughout most of the paper we restrict ourselves to the linearized system of perturbations (see also [4, 5, 21, 22]). We however point out the importance of higher order contributions to the scalar perturbation sector, taking into account that two enhanced helicity 2 gauge field perturbation can source helicity 0 (i.e. scalar) modes. We estimate the impact of this on the scalar power spectrum, finding an enhancement which is exponentially sensitive to the inflaton velocity, similar to what was found in the Abelian case [12].[1]

The remainder of this paper is organized as follows. We begin with an executive summary in Sec. 1.1, to help guide the reader through the different points discussed in this paper, followed by an overview on our notation in Sec. 1.2. In Sec. 2, we review some of the key results and equations of Abelian and non-Abelian axion inflation, setting the notation for the following sections. Sec. 3 is dedicated to the study of the emerging non-trivial homogeneous isotropic gauge field background. In Sec. 4 we study the linearized system of perturbations in a general homogeneous isotropic gauge field background. This is applied to a specific parameter example in Sec. 5, showing explicitly the transition from the Abelian to the non-Abelian regime. We compute the resulting scalar and tensor power spectrum, taking into account non-linear contributions. We conclude in Sec. 6. Six appendices deal with the derivation of the linearized perturbation equations, including the gravitational modes not included in the main text (App. A), the explicit gauge field basis used in our linearized analysis (App. B) details on the computation of the non-linear contributions to the scalar power spectrum (App. C), technical details supporting the analysis of the gauge field background (App. D), mathematical properties of homogeneous isotropic gauge fields (App. E) and analytical approximations of the Whittaker function describing the enhanced perturbation mode of the non-Abelian regime (App. F).

[1] While this paper was being finalized, Refs. [33, 34] appeared, which also study the effects of the nonlinear coupling between the helicity 2 and helicity 0 perturbations. We briefly comment on these completely independent results in Sec. 5, finding overall good agreement within the expected uncertainties.

1.1 Executive summary

To help guide the reader through the different aspects of our analysis, we give a preview of our key equations and results in this section, skipping all technical details. These results will be derived in the subsequent sections.

Our main focus will lie on the linearized regime of $SU(2)$ axion inflation. The pseudo-scalar (axion-like) inflaton ϕ is coupled to the field strength tensor of the $SU(2)$ gauge fields through the derivative coupling $\phi F_{\mu\nu}\tilde{F}^{\mu\nu}$. In the linearized regime, the $SU(2)$ gauge fields A^a_μ can be decomposed into a homogeneous isotropic background $f(\tau)$ and perturbations δA^a_μ,[2]

$$A^a_\mu(\tau,\vec{x}) = f(\tau)\delta^a_\mu + \delta A^a_\mu(\tau,\vec{x})\,. \tag{1.1}$$

The classical evolution of the background gauge field is governed by

$$\frac{d^2}{d\tau^2}(ef) + 2(ef)^3 - \frac{2\xi}{(-\tau)}(ef)^2 = 0\,, \tag{1.2}$$

where e denotes the $SU(2)$ gauge coupling and ξ, encoding the velocity of the inflaton and defined in Eq. (2.7), is typically taken to be $\mathcal{O}(1-10)$ during the last 60 e-folds of inflation.

For a slowly evolving inflaton, $\xi \simeq const.$, the classical background evolution is focused around two attractor solutions[3],

$$ef(\tau) = c_i\,\xi(-\tau)^{-1} \quad \text{with } c_0 = 0\,, \quad c_2 = \tfrac{1}{2}(1+\sqrt{1-4/\xi^2})\,, \tag{1.3}$$

where the latter is only possible for $\xi \geq 2$. Beyond this classical motion, the background is also sourced by the fluctuations δA. These dominate the background evolution around the c_0-solution, and eventually trigger the transitions from the c_0 to the c_2 solution. For details see Sec. 3.

Out of the six physical degrees of freedom of the gauge field, the most important is the helicity $+2$ mode w_{+2}, which couples directly to the metric tensor mode, sourcing chiral gravitational waves (see also [4, 5]). In the c_2 background solution, its equation of motion

$$\frac{d^2}{dx^2}w_{+2}(x) + \left(1 - \frac{2\xi}{x} + 2\left(\frac{\xi}{x}-1\right)\frac{c_2\xi}{x}\right)w_{+2}(x) = 0\,, \tag{1.4}$$

(where $x = -k\tau$ with k the momentum of the Fourier mode w_{+2}) has an exact solution in terms of the Whittaker function in the limit of constant ξ:

$$w^{(e)}_{+2}(x) = \frac{e^{(1+c_2)\pi\xi/2}}{\sqrt{2k}} W_{-i\kappa,\,-i\mu}\left(-2ix\right)\,, \tag{1.5}$$

with $\kappa = (1+c_2)\xi$ and $\mu = \xi\sqrt{2c_2 - (2\xi)^{-2}}$. Due to a tachyonic instability in Eq. (1.4) in between $x_{\rm max,min} = (1+c_2 \pm \sqrt{1+c_2^2})\xi$, this solution is strongly enhanced just before horizon crossing. At and after horizon crossing, Eq. (1.5) is well approximated by

$$\sqrt{2k}\,w_{+2}(x) \simeq 2e^{(\kappa-\mu)\pi}\sqrt{\frac{x}{\mu}}\cos\left[\mu\ln(2x) + \theta_0\right]\,. \tag{1.6}$$

[2] Throughout this paper, we denote $SU(2)$ indices by $a, b, c, .. = \{1..3\}$, Lorentz indices by $\mu, \nu, .. = \{0..3\}$ and spatial indices by $i, j, .. = \{1..3\}$.

[3] In Sec. 3.3 and 5.1 we comment on the difference between the background evolution studied in this paper and the 'magnetic drift regime' of [4, 5, 20, 22].

With this solution at hand, we can approximately analytically solve the coupled helicity +2 gauge field - gravitational wave system (see Eq. (4.28)), obtaining for the gravitational wave amplitude $w_{+2}^{(\gamma)}$ after freeze-out on super-horizon scales,

$$x\, w_{+2}^{(\gamma)}(x)\big|_{x\geq 1} \simeq -\frac{2H\xi^{5/2}}{e}\frac{2^{3/4}}{\sqrt{2k}}e^{(2-\sqrt{2})\pi\xi}\,, \tag{1.7}$$

and consequently for the amplitude of the chiral stochastic gravitational wave background (see Eq. (5.23) for details),

$$\Omega_{\rm GW} \simeq \frac{1}{24}\Omega_r \left(\frac{\xi^3 H}{\pi M_P}\right)^2_{\xi=\xi_{\rm cr}} \left(\frac{2^{7/4}H}{e}\xi^{-1/2}e^{(2-\sqrt{2})\pi\xi}\right)^2_{\xi=\xi_{\rm ref}}\,. \tag{1.8}$$

The scalar perturbations are not enhanced at the linear level in the parameter space in the focus of this work. However, non-linear contributions, sourced by two enhanced helicity +2 gauge field modes, yield an exponentially enhanced contribution to the scalar power spectrum. We report analytical estimates for the resulting contribution to the scalar power spectrum in Eq. (5.16).

Combining the results on the background evolution and the analysis of the perturbations, the following picture emerges: At early times, deep in de-Sitter space with small values of ξ, the non-Abelian axion inflation model reduces to the Abelian regime. Two factors are necessary to trigger the transition to the inherently non-Abelian regime: The c_2 solution of the classical background emerges at $\xi \geq 2$ and the gauge field fluctuations have to reach a sufficient amplitude to trigger initial conditions for the classical motion which actually lead to the c_2 solution. As a proof of concept, we study a parameter example in Sec. 5 in which the CMB scales exit the horizon in the Abelian regime at relatively small ξ (thus ensuring agreement with all CMB observations), whereas smaller scales exit the horizon after the transition to the inherently non-Abelian regime. The resulting scalar and tensor power spectra are strongly enhanced at small scales, see Fig. 5.5 and 5.6.

1.2 Notation and conventions

We summarize here the main conventions used throughout this paper. The metric signature is $(-,+,+,+)$ and we mostly employ conformal time τ instead of cosmic time t. Derivatives with respect to the conformal time are denoted by a prime, while derivatives with respect to the cosmic time are denoted by a dot. We often use the dimensionless variable

$$x = -k\tau\,. \tag{1.9}$$

The first (second) derivative of the functional $F(\phi)$ with respect to the field ϕ is denoted by $F_{,\phi}$ ($F_{,\phi\phi}$). The Fourier transform of the function $F(\mathbf{x},t)$ (or equivalently $F(\mathbf{x},\tau)$) is given by

$$F(\mathbf{x},t) = \int \frac{d^3k}{(2\pi)^{3/2}}\,\tilde{F}(\mathbf{k},t)e^{-i\mathbf{k}\cdot\mathbf{x}}\,. \tag{1.10}$$

(Anti-)Symmetrization is defined as

$$S_{(ij)} = \frac{S_{ij}+S_{ji}}{2}\,, \qquad A_{[ij]} = \frac{A_{ij}-A_{ji}}{2}\,. \tag{1.11}$$

Greek letters refer to space-time indices ($\mu = 0, 1, 2, 3$), roman letters from the beginning of the alphabet refer to gauge indices (e.g. $a = 1, 2, 3$ for a $SU(2)$ gauge group) and roman letters from the middle of the alphabet refer to spatial indices ($i = 1, 2, 3$). We use the usual conventions for $SU(N)$ gauge fields $\mathbf{A}_\mu = A^a_\mu \mathbf{T}_a$. The field strength tensor is defined as

$$F^a_{\mu\nu}\mathbf{T}_a \equiv \mathbf{F}_{\mu\nu} \equiv \frac{i}{e}[\mathbf{D}_\mu, \mathbf{D}_\mu] = \partial_\mu \mathbf{A}_\nu - \partial_\nu \mathbf{A}_\mu - ie[\mathbf{A}_\mu, \mathbf{A}_\nu] \,, \tag{1.12}$$

where e is the coupling constant, $\mathbf{T}_a$ is the a-th generator of the group, $\mathbf{A}_\mu \equiv A^a_\mu \mathbf{T}_a$ and where we have used the definition of covariant derivative:

$$\mathbf{D}_\mu \equiv \partial_\mu - ie\mathbf{A}_\mu \equiv \partial_\mu - ieA^a_\mu \mathbf{T}_a \,. \tag{1.13}$$

With the commutation relation

$$[\mathbf{T}_a, \mathbf{T}_b] = i\varepsilon_{abc}\mathbf{T}_c \,, \tag{1.14}$$

the field strength can be expressed as

$$F^a_{\mu\nu} = \partial_\mu A^a_\nu - \partial_\nu A^a_\mu + e\varepsilon^{abc}A^b_\mu A^c_\nu \,. \tag{1.15}$$

The dual tensor to the field strength is defined as

$$\tilde{F}^{\mu\nu}_a = \frac{\varepsilon^{\mu\nu\rho\sigma}}{2\sqrt{-g}}F^a_{\rho\sigma} \,, \tag{1.16}$$

where we use the convention $\varepsilon^{0123} = 1$ for the anti-symmetric tensor. Additional conventions related to the computation of the equations of motion in the ADM formalism are reported in App. A.

2 The role of gauge fields during inflation

2.1 The Abelian limit

In the limit of small gauge couplings and/or small gauge field amplitudes, any non-Abelian $SU(N)$ gauge group will (approximately) act as $N^2 - 1$ copies of an Abelian group. Let us thus, also for later reference, begin by briefly reviewing the case of a pseudoscalar inflaton ϕ coupled to an Abelian gauge field A_μ [35–37] (for recent analyses see e.g. [6, 7, 16, 38]),

$$\mathcal{S} = \int \mathrm{d}^4x\sqrt{|g|}\left[m_p^2\frac{R}{2} - \frac{1}{2}\,\partial_\mu\phi\,\partial^\mu\phi - V(\phi) - \frac{1}{4}F_{\mu\nu}F^{\mu\nu} - \frac{\alpha}{4\Lambda}\phi F_{\mu\nu}\tilde{F}^{\mu\nu}\right] . \tag{2.1}$$

Here $V(\phi)$ denotes the inflaton potential, $F_{\mu\nu}$ ($\tilde{F}^{\mu\nu}$) is the (dual) field-strength tensor of the Abelian gauge group and α/Λ encodes the coupling between the inflaton and the gauge field. Since $F_{\mu\nu}\tilde{F}^{\mu\nu}$ is CP-odd, it will prove useful to work with the Fourier-modes of the gauge field in the chiral basis,

$$\vec{A}(\tau, \vec{x}) = \int \frac{\mathrm{d}^3k}{(2\pi)^{3/2}}\left[\sum_{\lambda=\pm}\tilde{A}_\lambda(\tau, \vec{k})\vec{e}_\lambda(\vec{k})\hat{a}(\vec{k})e^{i\vec{k}\cdot\vec{x}} + \tilde{A}^*_\lambda(\tau, \vec{k})\vec{e}^*_{\lambda'}(\vec{k})\hat{a}^\dagger(\vec{k})e^{-i\vec{k}\cdot\vec{x}}\right] , \tag{2.2}$$

with the polarization vectors fulfilling $\vec{e}_\lambda(\vec{k})\cdot\vec{k} = 0$, $\vec{e}_\lambda(\vec{k})\cdot\vec{e}_{\lambda'}(\vec{k}) = \delta_{\lambda\lambda'}$ and $i\vec{k}\times\vec{e}_\lambda(\vec{k}) = \lambda k\vec{e}_\lambda(\vec{k})$ with $k = |\vec{k}|$. $\hat{a}^{(\dagger)}$ denotes the annihilation (creation) operator and $\tilde{A}_\lambda(\vec{k})$ the corresponding Fourier coefficients. Here $\vec{k}$ and $\vec{x}$ denote the co-moving wave vector and coordinates,

$$ds^2 = g_{\mu\nu}\mathrm{d}x^\mu\mathrm{d}x^\nu = a^2(\tau)(-\mathrm{d}\tau^2 + \mathrm{d}\vec{x}^2) = a^2(\tau)\eta_{\mu\nu}\mathrm{d}x^\mu\mathrm{d}x^\nu \,, \tag{2.3}$$

with $a(\tau)$ the metric scale factor and $\eta_{\mu\nu}$ the Minkowski metric. Adopting temporal gauge, we have moreover set $A_0 = 0$. The equations of motion for the homogeneous inflaton field and for the gauge field then read,

$$\ddot{\phi} + 3H\dot{\phi} + \frac{\partial V}{\partial \phi} = \frac{\alpha}{\Lambda}\langle \vec{E} \cdot \vec{B} \rangle \ , \tag{2.4}$$

$$\tilde{A}''_{\pm}(\tau, \vec{k}) + \left[k^2 \mp k \, \frac{2\xi}{-\tau} \right] \tilde{A}^a_{\pm}(\tau, \vec{k}) = \ 0 \ , \tag{2.5}$$

where we have introduced the physical 'electric' and 'magnetic' fields as

$$\vec{E} \equiv -\frac{1}{a^2}\frac{\mathrm{d}\vec{A}}{\mathrm{d}\tau} \ , \qquad\qquad \vec{B} \equiv \frac{1}{a^2}\vec{\nabla} \times \vec{A} \ . \tag{2.6}$$

Here and in the following, dots denote derivatives with respect to cosmic time t whereas primes denote derivatives with respect to conformal time τ, where $dt = a\, d\tau$. The expectation values $\langle \bullet \rangle$ in Eq. (2.4) indicate the spatial average. The parameter ξ, encoding the tachyonic instability in Eq. (2.5), is given by

$$\xi \equiv \frac{\alpha \, \dot{\phi}}{2 \, \Lambda \, H} \ , \tag{2.7}$$

with $H = \dot{a}/a$ denoting the Hubble rate during inflation. In the following we will consider $\dot{\phi} > 0$ and hence $\xi > 0$ without loss of generality.

In the slow-roll regime, $|\ddot{\phi}| \ll H|\dot{\phi}|, |V_{,\phi}|$, we can neglect the change of ξ on the time-scales relevant in Eq. (2.5). This enables us to approximately decouple the equations and solve the equation of motion for the gauge fields analytically, with a parametric dependence on the parameter ξ,

$$\tilde{A}_{\lambda}(\tau, k) = \frac{1}{\sqrt{2k}} e^{\lambda \pi \xi / 2} W_{-i\lambda\xi, 1/2}(2ik\tau) \, . \tag{2.8}$$

Here $W_{k,m}(z)$ is the Whittaker function. For $\lambda = +$ this describes an oscillatory function which starts to grow exponentially around horizon crossing ($k|\tau| \sim 1$), before becoming approximately constant on super-horizon scales, see Fig. 2.1. The $\lambda = -$ mode does not exhibit this tachyonic instability and remains oscillatory. The overall normalization is obtained by matching to the Bunch–Davies vacuum in the infinite past, namely

$$\tilde{A}_{\lambda}(\tau, k) \approx \frac{e^{-ik\tau}}{\sqrt{2k}} \quad \text{as } \tau \to -\infty. \tag{2.9}$$

The explicit solution (2.8) in turn enables us to explicitly evaluate the right-hand side of Eq. (2.4). For $\xi \gtrsim 3$ this is well approximated by

$$\langle \vec{E} \cdot \vec{B} \rangle \simeq -2.4 \cdot 10^{-4} \frac{H^4}{\xi^4} e^{2\pi\xi} \, . \tag{2.10}$$

Recalling the definition of ξ in Eq. (2.7), this enables us to (numerically) solve Eq. (2.4). The resulting evolution of the Abelian gauge - inflaton system has been studied e.g. in Refs. [3, 6, 7, 12, 15, 16, 18], obtaining the following key results:

- The tachyonic enhancement of the A_+ modes leads to a significant back-reaction in the equation of motion for ϕ, which is exponentially sensitive to ξ. This can be interpreted as an additional friction term for the inflaton.

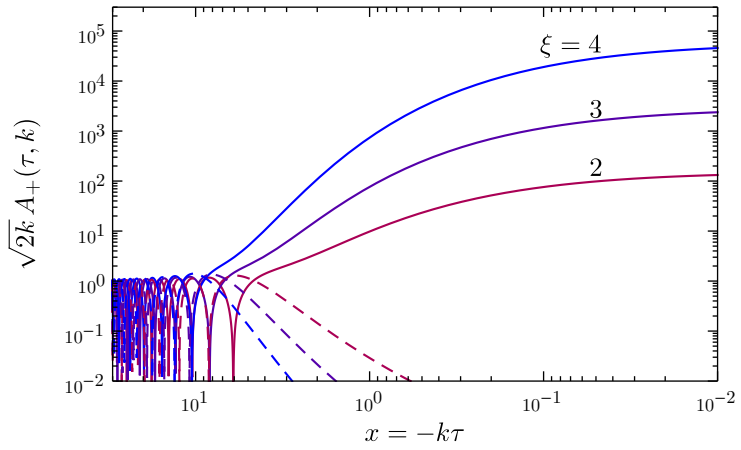

Figure 2.1: Enhanced helicity mode described by Eq. (2.8) for different values of ξ. The solid (dashed) curves show the absolute value of growing (decaying) component. For a suitable choice of the complex phase of the Whittaker function (see also App. F), the growing (decaying) component is the real (imaginary) part.

- In single field inflation models, $V_{,\phi}/V$ typically increases over the course of inflation, implying an increasing value of ξ. Constraints on non-gaussianities in the CMB impose $\xi_{\rm CMB} \lesssim 2.5$ whereas the back-reaction mentioned above dynamically limits the growth of ξ over the course of 50-60 e-folds of inflation, typically leading to $\xi \lesssim 10$.

- The presence of the gauge fields leads to an additional source term for the scalar and tensor power spectra. Eue to the increasing value of ξ this effect is typically largest at small scales (i.e. towards the end of inflation).

For later reference, let us discuss in detail three quantities which will be relevant for the analysis carried out in the next parts of this work: the gauge field variance, the homogeneity scale and decoherence time.

Variance. Isotropy ensures that averaged over the whole universe $\langle \vec{A} \rangle = 0$, but we may estimate the magnitude of the gauge fields in any Hubble patch by computing the variance,

$$\begin{aligned}
\langle 0|\vec{A}(\tau,\vec{x})\vec{A}(\tau,\vec{x})|0\rangle^{1/2} &= \left(\int \frac{\mathrm{d}^3 k}{(2\pi)^3} \left[\tilde{A}_+(\vec{k})\tilde{A}^*_+(\vec{k}) + \tilde{A}_-(\vec{k})\tilde{A}^*_-(\vec{k}) \right] \right)^{1/2} \\
&= e^{\pi\xi/2} \sqrt{\int \frac{\mathrm{d}k}{2\pi^2} \frac{k}{2} \left| W_{-i\xi,1/2}(2ik\tau) \right|^2} \\
&= \frac{aH}{2\pi} e^{\pi\xi/2} \sqrt{\int \mathrm{d}x\, x \left| W_{-i\xi,1/2}(-2ix) \right|^2} \\
&\simeq \frac{1}{(-\tau)}\, 0.008 \times e^{2.8\xi}\,, \qquad (2.11)
\end{aligned}$$

where we have introduced $x = -k\tau > 0$. Here we set the upper integration limit to $x_{UV} = 2\xi$, so as to not count the vacuum contribution. In agreement with Ref. [38], we find that all the integrals of this type performed in this paper are rather insensitive to the choice of x_{UV} for $\xi \gtrsim 3$.

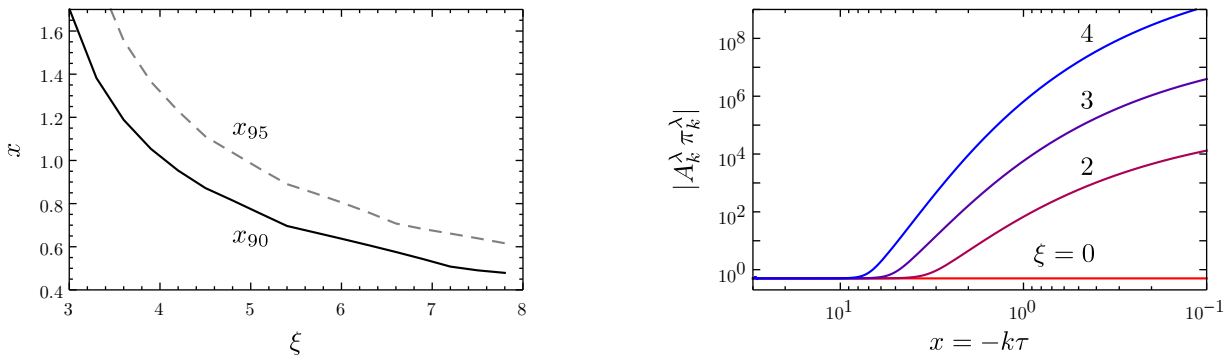

Figure 2.2: Properties of the gauge fields in the Abelian regime. *Left panel:* Scale of homogeneity for different values of ξ, defined such that 90% (95%) of the energy is contained in modes with $-k\tau = x > x_{90}$ ($x > x_{95}$). *Right panel*: $|A_k^\lambda \pi_k^\lambda|$ for $\xi = 0, 2, 3, 4$. Decoherence occurs once $|A_k^\lambda \pi_k^\lambda| \gg 1$.

Homogeneity. The energy density stored in the gauge fields can be computed as $(\vec{E}^2 + \vec{B}^2)/2$ with

$$\frac{1}{2}\langle \vec{E}^2 \rangle = \frac{1}{2a^4} \int \frac{d^3k}{(2\pi)^3} \left| \frac{\partial \tilde{A}_+^k(\tau)}{\partial \tau} \right|^2 = \frac{H^4}{8\pi^2} e^{\pi\xi} \int_0^{2\xi} dx\ x^3 \left| \frac{\partial W_{-i\xi,1/2}(-2ix)}{\partial x} \right|^2 , \tag{2.12}$$

$$\frac{1}{2}\langle \vec{B}^2 \rangle = \frac{1}{2a^4} \int \frac{d^3k}{(2\pi)^3} k^2 \left| \tilde{A}_+^k(\tau) \right|^2 = \frac{H^4}{8\pi^2} e^{\pi\xi} \int_0^{2\xi} dx\ x^3 \left| W_{-i\xi,1/2}(-2ix) \right|^2 . \tag{2.13}$$

We can now determine for each value of ξ, the value of x_{90} for which 90% of the energy is contained in modes with $x < x_{90}$, see left panel of Fig. 2.2. For any $x > x_{90}$, we can then safely model the gauge field as a homogeneous background field. We conclude that for (the phenomenologically interesting) large values of $\xi \gtrsim 3$, the homogeneity scale lies at $x_{90} \lesssim \mathcal{O}(1)$, so that on sub-horizon scales, this gauge field acts like a homogeneous background field. This approximation becomes better for larger values of ξ. For reference, the dashed line in Fig. 2.2 indicates the value of x for which 95% of the energy is contained within $x < x_{95}$.

Decoherence. For any given mode decoherence is reached if $|\tilde{A}_k^\lambda \pi_k^\lambda| \gg 1$ [39]. Using the free-field expression for the conjugate momentum, $\pi_k^\lambda = \partial_0 \tilde{A}_k^\lambda$, the right panel of Fig. 2.2 demonstrates that decoherence is reached at $x \sim \xi$. As a further check, in order to establish the transition to the classical behaviour, we computed the number of particles n_k in each mode (see [40]) and we checked at which point the regime $n_k \gg 1$ is reached. The results agree with those shown in Fig. 2.2: decoherence is reached at $x \sim \xi$.

In summary, we find that in the Abelian limit, any Hubble patch develops a classical, approximately homogeneous gauge field background, whose average magnitude grows exponentially with ξ as indicated in Eq. (2.11). In the next section, we will highlight the key changes to this picture in the non-Abelian regime.

2.2 Non-Abelian regime

Let us now consider the same action as in Eq. (2.1), but now in the case of an $SU(2)$ gauge group,

$$\begin{aligned}\mathcal{S} &= \int \mathrm{d}^4x\sqrt{|g|}\left[m_p^2\frac{R}{2} - \frac{1}{2}\,\partial_\mu\phi\,\partial^\mu\phi - V(\phi) - \frac{1}{4}F^a_{\mu\nu}F_a^{\mu\nu} - \frac{\alpha}{4\Lambda}\phi F^a_{\mu\nu}\tilde{F}_a^{\mu\nu}\right] \\ &\equiv \int d^4x\,\sqrt{-g}\,\left[\mathcal{L}_{\rm EH} + \mathcal{L}_\phi + \mathcal{L}_{\rm YM} + \mathcal{L}_{\rm CS}\right]\,. \end{aligned} \tag{2.14}$$

The resulting equations of motion for the homogeneous inflaton field $\phi(\tau)$ and the gauge fields $A^a_\mu(\tau,\vec{x})$ read:

$$\ddot{\phi} + 3H\dot{\phi} + V_{,\phi} + \frac{\alpha}{4\Lambda}\,\frac{\varepsilon^{\mu\nu\rho\sigma}}{a^3(t)}\,F^a_{\mu\nu}F^a_{\rho\sigma} = 0\,, \tag{2.15}$$

and

$$\begin{aligned}&\eta^{\nu\sigma}\left\{\Box A^a_\sigma - \partial_\sigma\left(\partial_\mu\eta^{\mu\rho}A^a_\rho\right) + e\varepsilon^{abc}\eta^{\mu\rho}\left[2A^b_\rho\partial_\mu A^c_\sigma + \left(\partial_\mu A^b_\rho\right)A^c_\sigma - A^b_\mu\partial_\sigma A^c_\rho\right] + \right. \\ &\left. + e^2\eta^{\mu\rho}\left[A^a_\rho\left(A^b_\mu A^b_\sigma\right) - A^a_\sigma\left(A^b_\mu A^b_\rho\right)\right]\right\} + \frac{\alpha}{2\Lambda}\phi'\varepsilon^{0\nu jk}\left[2\partial_j A^a_k + e\varepsilon^{abc}A^b_j A^c_k\right] = 0\,,\end{aligned} \tag{2.16}$$

where we have introduced the $\Box$-operator defined as usual as $\Box \equiv g^{\mu\nu}\partial_\mu\partial_\nu$ which here is expressed in co-moving coordinates.

The non-linear equation (2.16) is highly sensitive to the presence of a gauge field background as described in Sec. 2.1. An exact treatment of the system requires solving the non-linear coupled system of equations of motions in an exponentially expanding background, a very challenging task. Instead we will work in a linear approximation (as in Refs. [4, 5, 22]), expanding the gauge fields around a homogeneous background, denoted by $A^{(0)}(\tau)$, so that

$$A(\tau,\vec{x}) = A^{(0)}(\tau) + \delta A(\tau,\vec{x}). \tag{2.17}$$

We will discuss the (classical) evolution of the background in Sec. 3 and the (quantum) evolution of the fluctuations in Sec. 4. This treatment is valid as long as the evolution of the background is indeed governed by the classical equation of motion, i.e. as long as the growth of the fluctuations does not overcome the classical motion. To make the overall picture clear from the start, we highlight in the following some of the key results, the derivation of these will follow in Secs 3 and 4, correspondingly. We find that the background field dynamically evolves towards an isotropic configuration with two distinct asymptotic behaviours. On the one hand, for small initial conditions, the co-moving background evolves towards a constant value, and thus remains small compared to tachyonically enhanced fluctuations, see Eq. (2.11). In this regime, we are essentially back in the Abelian limit, i.e. the fluctuations are well described by Eq. (2.8) with 3 enhanced and 3 oscillating modes.[4] On the other hand,

[4] One may worry about the justification of the linearization (2.17) in this regime. From Eq. (2.16), we note that in the limit $A^{(0)}(\tau) \to 0$, a necessary condition for the linearization to be valid is $e\,(\delta A)^2 \ll \partial_\mu\delta A$, or in other words $e\,\delta A \ll k = x/(-\tau)$, indicating the regime where the non-Abelian terms become irrelevant. For modes crossing the horizon ($x = 1$), this condition holds if

$$0.008 \times \exp(2.8\,\xi) \ll 1/e\,, \tag{2.18}$$

where we have inserted Eq. (2.11). For far super-horizon modes, the non-Abelian terms become more important. However, at this point due to a red-shift in momentum and a decay in the amplitude, the contribution of these modes to e.g. the variance of the energy density is negligible. Note that the condition (2.18) is not sufficient to justify the linearization

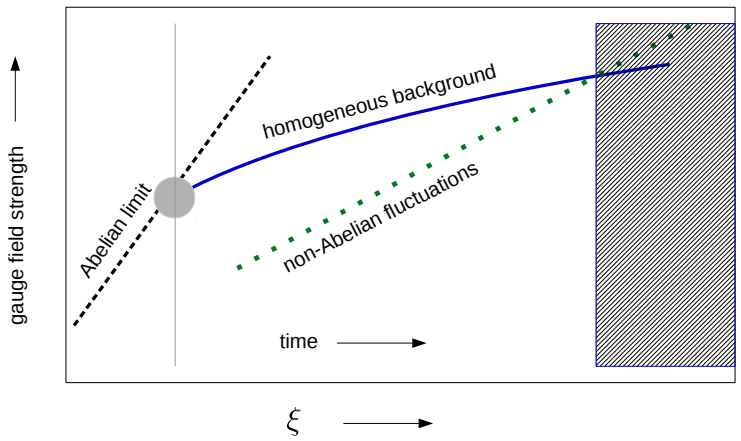

Figure 2.3: Sketch of the evolution of the average magnitude of the gauge fields from the Abelian to the non-Abelian regime. The vertical line marks the transition from the Abelian limit to the full non-Abelian theory, the gray circle indicates the requirement of matching the initial conditions accordingly. In the non-Abelian regime, the fluctuations grow slower, but may nevertheless at some point overcome the classically evolving background. This region of parameter space is beyond the scope of the present paper, as indicated by gray shaded region.

for sufficiently large initial conditions (and only if $\xi \geq 2$), there is an asymptotic solution for the background which grows as $1/|\tau|$. In this regime, the background significantly modifies the equation of motion for the fluctuations. Consequently, we find that only a single gauge field mode is enhanced, and the enhancement is moreover significantly suppressed compared to the Abelian case. Given the strong gauge field production in the Abelian regime and the increasing value of ξ over the course of inflation, eventually the growing background solution will be triggered. The point at which this happens depends on the gauge coupling e and the CP-violating coupling α/Λ. A sketch of this overall picture is given in Fig. 2.3.

3 The non-Abelian homogeneous gauge-field background

In this section we study the classical evolution of the non-Abelian gauge field background. In Sec. 3.1 we will discuss three distinct types of solutions. Among these, of particular interest is the type of solution which, in terms of comoving quantities, describes a background gauge field growing proportionally to the scale factor $a(\tau)$, or equivalently[5] proportionally to $(-\tau)^{-1}$. We will show that this solution is only possible for $\xi \geq 2$, is stable under perturbations, and we will specify the necessary

of the equation of motion for the inflaton (2.15). In the Abelian regime, the last term contains at least two powers of δA^a_μ, and its relative importance will depend on the coupling strength α/Λ. We will return to the importance of these non-linear effects in detail in Sec. 5.

[5]In the time scales we are considering, H is effectively constant.

conditions on the initial conditions to reach this type of solution. To this end we discuss the different types of solutions both at early and at late times. We close Sec. 3.1 by showing a phase space diagram of these solutions, illustrating the different the different types of solutions as well as the behaviour at early and late times. Based on this in-depth study of the non-equilibrium behavior of the classical equation of motion we will conclude that

- Once the magnitude of initial conditions reaches a particular threshold, the classical equation of motion for the gauge-field background evolves with high probability towards a growing homogeneous and isotropic background solution.

These initial conditions in turn are understood to be sourced by the enhanced gauge field perturbations generated before this growing solution developed. These perturbations will be the topic of Sec. 4. For now, we will only note that in the far past, these fluctuations are well described by the Abelian limit discussed in Sec. 2.1.
The analysis of Sec. 3.1 will assume an isotropic gauge field background. We will justify this in Sec. 3.2 by demonstrating that once a growing homogeneous background solution is triggered, the homogeneous background evolves towards isotropy. We will further see in Secs. 4 and 5, that this background suppresses the gauge field fluctuations. We therefore conclude that after the homogeneous background is triggered, the dynamics of the gauge-field background are accurately captured by the *classical* equation of motion for a homogeneous and isotropic gauge-field.
We conclude this discussion in Sec. 3.3 by including the dynamical evolution of the inflaton background. Technical details required to obtain the results of this section are relegated to Apps. D and E.

3.1 Equation of motion for an isotropic gauge-field background

In this section, we consider in detail the equation of motion for the non-Abelian gauge field background $A^{(0)}$. (For context, see the discussion around Eq. (2.17).) This is the zeroth order part of our approximation, so we ignore for now the inhomogeneous first-order perturbations δA which we will add later in Sec. 4. We make the following explicit assumptions on the background field:

- The background gauge field $A^{(0)}$ is homogeneous and isotropic. (We will show in Sec. 3.2 that isotropy is a valid assumption in our regime of interest. For a discussion on homogeneity in the Abelian limit, see Section 2.1.)

- The inflaton field ϕ is homogeneous and evolves in the slow-roll regime. In particular, we consider ξ to be constant. (See Eq. (2.7) and the subsequent comments.)

Any gauge field $A^{(0)}$ which is homogeneous and isotropic has (after applying a gauge transformation if needed) spatial components of the form

$$(A^{(0)})^a_i = \delta^a_i \, f(\tau). \tag{3.1}$$

We emphasize that although we make use of gauge freedom to express $A^{(0)}$ in this form, we have imposed no gauge-fixing condition.

The corresponding equation of motion for $f(\tau)$ is

$$\frac{d^2}{d\tau^2} ef(\tau) + 2\,(ef(\tau))^3 - \frac{2\,\xi}{-\tau}(ef(\tau))^2 = 0, \tag{3.2}$$

obtained by inserting Eq. (3.1) into Eq. (2.16). Our task is now to analyze the qualitative behavior of solutions to this ordinary differential equation, where e and ξ are constants.
It is helpful to observe the following symmetries of this equation.

- There is always a factor of e wherever $f(\tau)$ appears. Consequently, we focus our analysis on the quantity "$ef(\tau)$" instead of "$f(\tau)$." The coupling constant e is nothing but a scale factor.

- The substitution

$$ef(\tau) \mapsto -ef(\tau) \tag{3.3}$$

$$\xi \mapsto -\xi \tag{3.4}$$

  preserves solutions of Eq. (3.2). Thus solutions with $\xi < 0$, are identical (up to a sign) to solutions with $\xi > 0$. Thus, as in Section 2.1 we assume without loss of generality that $\xi \geq 0$.

- For any positive real number λ, the substitution

$$ef(\tau) \mapsto \lambda\, ef(\lambda\tau) \tag{3.5}$$

  preserves solutions of Eq. (3.2). This is easily understood as follows in terms of physical quantities (as opposed to comoving quantities). If we define

$$(-\tau H)\, ef(\tau) = Hg(N), \quad \text{where } \tau = \tau_0\, e^N \tag{3.6}$$

  so that N is the usual measure of e-folds during inflation, $N = -Hdt$, then Eq. (3.2) becomes

$$\frac{\mathrm{d}^2}{\mathrm{d}N^2} g(N) - 3\frac{\mathrm{d}}{\mathrm{d}N} g(N) + 2g(N)\left(g(N)^2 - \xi g(N) + 1\right) = 0\,. \tag{3.7}$$

  This is an autonomous [6] equation, so solutions are invariant under time translations of the form $g(N) \mapsto g(N + \ln\lambda)$. With comoving quantites, these time translations correspond precisely to the transformation (3.5). When this transformation is applied in the limit $\lambda \to 0^+$, it corresponds to the limiting behavior as $\tau \to 0^-$ (i.e. to the asymptotic future). Note that Refs. [4, 5, 20, 22] work directly with the physical gauge field background $g(N)$. When studying the asymptotic future it is more convenient to work with $g(N)$. However, we find that $ef(\tau)$ is more natural for studying the far past.

3.1.1 Three distinct types of solutions

Typical behavior of solutions

Before rigorously analyzing the behavior of solutions, we begin with an informal discussion of the two most common types of solution to Eq. (3.2). Typical examples of these are depicted as solid black lines in Fig. 3.1. Details and proofs will be provided below.

[6] *Autonomous* means that the time variable doesn't explicitly appear in the equation of motion. For example, the quartic oscillator equation $w''(x) + 2w(x)^3 = 0$ is autonomous, while the Airy equation $w''(x) - xw(x) = 0$ is not.

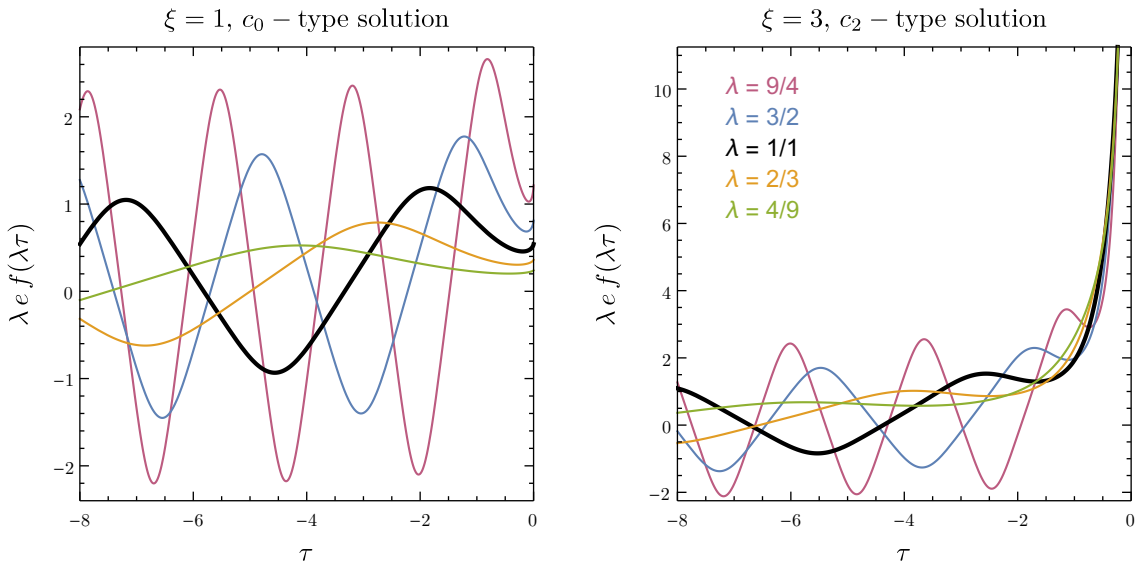

Figure 3.1: Typical solutions for the classical gauge field background. The thicker black curve ($\lambda = 1$) is obtained by numerically solving Eq. (3.2) for specific (but generic) initial conditions. The other curves, obtained by applying the transformation of symmetry in Eq. (3.5), allow to depict this solution at different points in time. The left panel shows a typical example of a bounded solution, the right panel a typical example of a growing background solution.

For large negative values of τ (the far past), solutions are typically oscillatory of a fixed amplitude. We caution the reader that in our model, this oscillatory behavior does not actually occur in the far past. This is because at early times, the gauge-field background is dominated by small but growing fluctuations from superhorizon modes, and so the classical equation of motion breaks down there.
On the other hand, we shall be primarily concerned with what happens as $\tau \to 0^-$ (the asymptotic future), and the influence of the initial conditions on this behavior. Based on the two parameters which determine the initial conditions, we can divide solutions into three categories based on their behavior as $\tau \to 0^-$.

c_0-type solutions The function $ef(\tau)$ remains bounded, and $ef(\tau)$ converges to a finite value as $\tau \to 0^-$. In this case, the physical gauge field background $f(\tau)/a(\tau)$ approaches zero and will remain small compared to the tachyonically enhanced gauge field fluctuations, see Eq. (2.11).

c_2-type solutions The function $ef(\tau)$ is unbounded as $\tau \to 0^-$. In this case, the growth of $ef(\tau)$ is always proportional to $(-\tau)^{-1}$. These are the growing background solutions which will be most relevant throughout this work, and which are responsible for the inherently non-Abelian regime of CNI. The physical gauge field background $f(\tau)/a(\tau)$ approaches a positive constant.

c_1-type solutions These solutions form the "saddle points" between c_0-type and c_2-type solutions. They arise only with finely-tuned initial conditions. Just like c_2-type solutions, their growth is proportional to $(-\tau)^{-1}$ as $\tau \to 0^-$, however with a smaller proportionality constant.

Asymptotic formulas for these three families of solutions are given in Appendix D.1.
Our central questions are as follows:

1. Given initial conditions for a solution to Eq. (3.2), will the solution be c_0-type or c_2-type?

2. For which initial conditions is the solution oscillatory? When so, at what time do the oscillations stop?

Ansatz

We can write down up to three explicit solutions to Eq. (3.2) with the ansatz

$$ef(\tau) = c\,\xi/(-\tau)\,, \tag{3.8}$$

where c is a constant. Solutions of this form arise by rescaling any general solution of Eq. (3.2) to its $\tau \to 0^-$ limit, namely by applying the transformation Eq. (3.5) in the limit as $\lambda \to 0$. (This fact is part of Theorem 2, and can be readily verified from the formulas of Appendix D.1.) Indeed, functions of the form of this ansatz are precisely the fixed points of Eq. (3.5).
We obtain a solution to Eq. (3.2) when c is one of

$$c_0 = 0\,, \quad c_1 = \tfrac{1}{2}(1 - \sqrt{1 - 4/\xi^2})\,, \quad c_2 = \tfrac{1}{2}(1 + \sqrt{1 - 4/\xi^2})\,, \tag{3.9}$$

motivating the nomenclature introduced above. Note that since $f(\tau)$ must be real, the c_1 and c_2 solutions exist only when $\xi \geq 2$. In this case,

$$0 + \xi^{-2} < c_1 \leq \tfrac{1}{2} \leq c_2 < 1 - \xi^{-2}\,, \tag{3.10}$$

and asymptotically as $\xi \to \infty$ we have

$$c_1 = 0 + \xi^{-2} + O(\xi^{-4}), \quad c_2 = 1 - \xi^{-2} + O(\xi^{-4})\,. \tag{3.11}$$

The reader will find it especially useful to keep in mind that $c_2 \approx 1$ for large ξ.
We shall see in Sec. 3.1.2 that the c_0 and c_2 solutions are stable under all small perturbations of the initial conditions. Thus they both have a two-parameter basin of attraction. The c_1-solution is stable under just one direction of perturbations, so it is just part of a one-parameter family. Appendix D.1 contains explicit asymptotic formulas for these families. The structure of these families is explained in Sec. 3.1.2.
The c_2 solution (which exists only when $\xi \geq 2$) plays a central role in our story because it is an explicit stable and growing solution:

$$ef(\tau) = c_2\,\xi/(-\tau) = \frac{\tfrac{1}{2}\left(1 + \sqrt{1 - 4/\xi^2}\right)\xi}{-\tau}\,. \tag{3.12}$$

Note We refer to the three particular solutions

$$ef(\tau) = c_i\,\xi/(-\tau), \quad i \in \{1, 2, 3\} \tag{3.13}$$

respectively as *the c_0 solution* (or simply *the zero solution*), *the c_1 solution* and *the c_2 solution*. In contrast there are three **families** of **c_i-type** *solutions*, of which the c_i solutions are respective members. A c_i-type solution approaches the corresponding c_i solution in the asymptotic future. More details on the families of c_i-type solutions are given in Appendix D.1.

Oscillatory behavior

We remind the reader that although the oscillatory regime for the classical background field equation Eq. (3.2) which we describe in this subsection extends to the infinite past, our model does not obey this classical equation at early times (see page 14). Nevertheless we will discover in Sec. 3.1.2 how the mathematical analysis of the oscillatory regime in the infinite past provides a nice criterion for determining which initial conditions lead to either c_0-type solutions or c_2-type solutions.
The oscillatory behavior of solutions is explained by the following conjecture.

Conjecture 1. *Any particular solution $ef(\tau)$ to Eq. (3.2) has two associated constants:*

- $\omega \geq 0$,
- $u_0 \in [0, 5.244)$.

These constants depend on the solution, so they are determined once initial conditions are fixed. The solution can be written in the form

$$ef(\tau) = \omega \cdot \mathrm{sn}(\omega\tau + u_0) + \epsilon(\tau)\,, \tag{3.14}$$

for some function $\epsilon(\tau)$ which satisfies

$$|\epsilon(\tau)| \leq \frac{4\xi}{-3\tau}\,. \tag{3.15}$$

Here $\mathrm{sn}(u)$ denotes the Jacobi $\mathrm{sn}(u|m)$ function with argument $m = -1$. We recall that the Jacobi sn function with argument m is periodic with quarter-period given by the complete elliptic integral $K(m)$. The precise range for the periodic parameter u_0 is thus $[0, 4K(-1))$. The constant ω is always uniquely determined by initial conditions. The constant u_0 is uniquely determined when $\omega \neq 0$.
The parameters (ω, u_0) transform under Eq. (3.5) as

$$(\omega, u_0) \mapsto (\lambda\omega, u_0)\,. \tag{3.16}$$

This conjecture tells us that when $\omega > 0$, $ef(\tau) \approx \omega \cdot \mathrm{sn}(\omega\tau + u_0)$ when $|\epsilon(\tau)| \ll \omega$. In particular combining this with Eq. (3.15), oscillation occurs at early times when

$$\tau \ll -\frac{\xi}{\omega}\,, \tag{3.17}$$

which is the definition of the oscillatory regime. In the case $\omega = 0$ we have simply that $|ef(\tau)| \leq \frac{4}{3}\xi/(-\tau)$ so that there are no oscillations.
This conjecture is expected to hold for the following reasons. Firstly, the conjecture respects (3.5): $ef(\tau)$ satisfies the conjecture if and only if $\lambda\, ef(\lambda\tau)$ does as well. Secondly, in the oscillatory regime, the last term in Eq. (3.2) is negligible, so that $ef(\tau)$ behaves like a quartic oscillator, whose solution is given by Eq. (3.14) with $\epsilon(\tau) = 0$. Outside the oscillatory regime, $f(\tau)$ grows at most like the c_2-solution, plus perturbations. The factor of $\frac{4}{3}$ seems to be sufficient to encompass all such perturbations, and we have verified this numerically.
We remark that this conjecture is consistent with the results obtained with the ansatz (3.8). Namely the c_i solutions correspond to $\omega = 0$ and $\epsilon(\tau) = ef(\tau) = c_i\xi/(-\tau)$. To explain why $\omega = 0$ is necessary

for the c_i solutions, recall that the c_i solutions are fixed points of the transformation Eq. (3.5). Thus by Eq. (3.16) we have $\omega = \lambda\omega$ for all positive λ , and hence $\omega = 0$. Regarding $\epsilon(\tau)$, it satisfies Eq. (3.15) because $|c_i| \leq \frac{4}{3}$.

Eq. (3.17) is unfortunately not very practical for determining the oscillatory regime for a given solution because ω is difficult to compute. As a remedy, the following theorem provides a very simple criterion in terms of just $ef(\tau)$ and $ef'(\tau)$. It introduces a function $\omega_1(\tau)$ which serves as an approximation to the constant ω.

Theorem 1. *(Criterion for oscillation) Let $ef(\tau)$ be a particular solution to Eq.* (3.2)*. Define the associated function*

$$\omega_1(\tau) \equiv \sqrt[4]{(ef'(\tau))^2 + (ef(\tau))^4}. \tag{3.18}$$

Then

$$\omega = \lim_{\tau \to -\infty} \omega_1(\tau), \tag{3.19}$$

where ω is the number defined in Conjecture 1. Furthermore, the solution is oscillatory (i.e. $\omega > 0$) if there exists any time τ such that either

- $\omega_1(\tau) > 0$ *when* $0 \leq \xi < 2$*, or*
- $\omega_1(\tau) > \frac{4}{3}\xi/(-\tau)$.

The proof is given in Appendix D.2.

The criterion of this theorem may be used to identify the transition between the oscillatory and non-oscillatory time as occuring when

$$\sqrt[4]{(ef'(\tau))^2 + (ef(\tau))^4} \approx \frac{4\xi}{-3\tau}\,. \tag{3.20}$$

This answers the second question of page 15. As will become clear from the discussion in Sec. 3.1.2, we can use this to estimate the necessary amplitude of the gauge field fluctuations which is required to trigger a growing c_2-type solution.

Here we pause to take account of the various notions of "oscillatory" that we have developed so far. Such a solution is, according to Conjecture 1, oscillatory in the far past if the constant ω associated to the solution is positive. In that case, the solution is oscillatory when $\tau \ll -\frac{\xi}{\omega}$. Thus $-\omega\tau \sim \xi$ sets the scale of the transition. Finally, a particular criterion which is well-suited for checking initial conditions for oscillatory behavior is $-\tau\omega_1(\tau) > \frac{4}{3}\xi$ with $\omega_1(\tau)$ defined in Eq. (3.18).

For solutions with $\omega \neq 0$, we may normalize the amplitude of oscillations to $\omega = 1$ by applying the transformation of Eq. (3.5) with $\lambda = \omega^{-1}$. (In terms of the physical quantities, this entails time-shifting the solutions so that they all exit the oscillatory regime at the same point in time.) This enables us to show how the solutions of Eq. (3.2) (normalized to $\omega = 1$) depend the remaining free phase parameter u_0, see Fig. 3.2. Again we note that the left panels with $\xi = 1$ do not admit unbounded solutions as $\tau \to 0^-$, whereas the right panels ($\xi = 3$) admit both bounded and un-bounded solutions. The value of u_0 is color coded, and we point out that for $\xi = 3$, the c_0-type solutions have colors which range

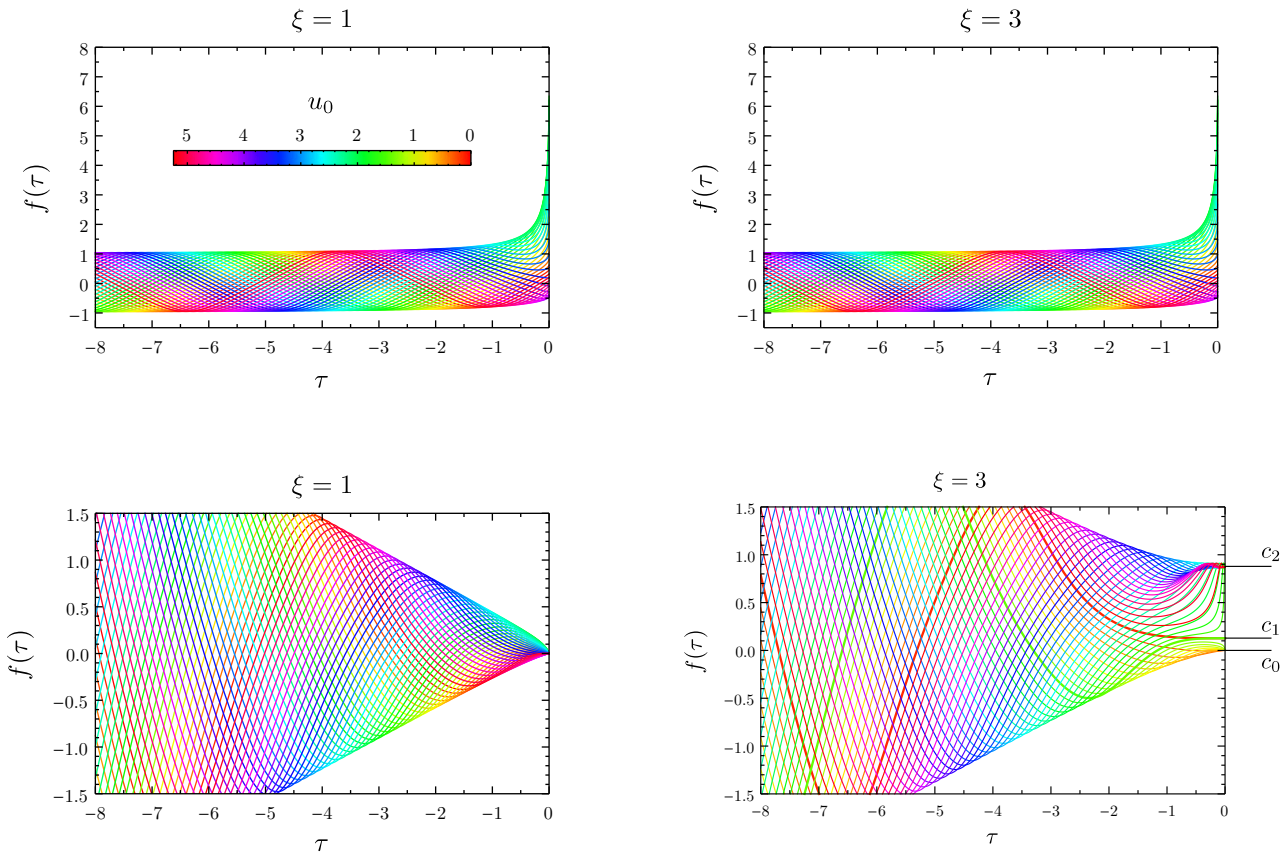

Figure 3.2: Systematic study of all possible solutions to the classical background equation (3.2) for two different values of ξ. All solutions have been normalized to unit amplitude ($\omega = 1$) and the phase u_0 is indicated by color. The lower panels are obtained from the upper panels by multiplication with $\xi^{-1}\tau$. This illustrates that the limiting values as $\tau \to 0^-$ are c_0, c_1 or c_2, and the value of the phase u_0 determines which of these c_i is reached. The two special c_1-type solutions are indicated by thicker lines.

only from orange-red to yellow-green. More precisely, this is the interval $u_0 \in (0.136, 1.409)$, which is approximately one fourth of the phase range. When $\xi = 3$ and the phase u_0 is random, the probability of a c_0-type solution is 24.3%, and the probability of a c_2-type solution is 75.7%.
The distinct categories of solutions are particularly evident in the lower panels of Fig. 3.2 depicting the physical gauge field amplitude. This is at the core of the following theorem:

Theorem 2. *When $\xi \neq 2$, all solutions of Eq. (3.2) satisfy*

$$\lim_{\tau \to 0^-} -\tau\, e f(\tau) = c_i \xi \tag{3.21}$$

for some $i \in \{0, 1, 2\}$, where c_i is defined in Eq. (3.9). Furthermore, the $\lambda \to 0$ limit of the transformation Eq. (3.5) applied to any solution of Eq. (3.2) is the corresponding c_i solution.

The proof is provided in Appendix D.3, and uses the machinery developed in Sec. 3.1.2.
This theorem gives us a way to classify solutions into three distinct categories. Solutions with generic initial conditions are always of type c_0 or c_2. Fine-tuning the phase u_0 to achieve a solution exactly

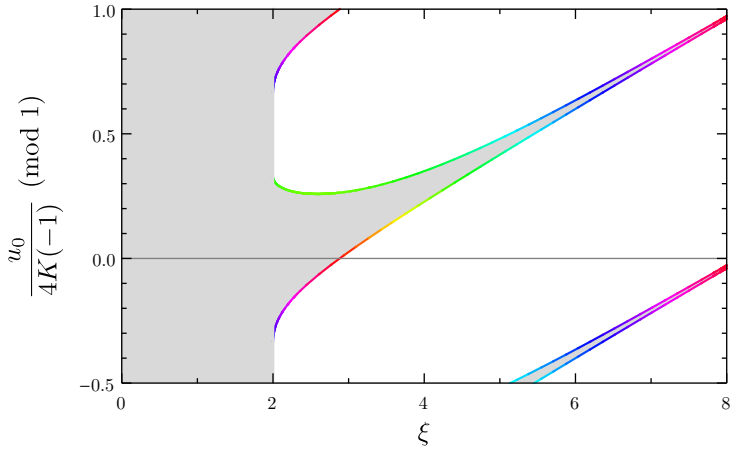

Figure 3.3: Parameter space leading a growing (c_2-type) solution for the classical background gauge field. The colored curves indicate the phase (normalized mod 1) of the two c_1-type solutions as a function of ξ. Note that the y-axis has period 1. The gray and white regions respectively indicate c_0- and c_2-type solutions.

between c_0 and c_2 leads to exactly two values of the phase which correspond to "c_1-type solutions." The corresponding red and green curves in the lower panels of Fig. 3.2 are indicated with thicker lines. Fig. 3.3 quantifies the phase intervals leading to the c_0 and c_1-type solutions, respectively, generalizing the above results to the entire ξ-range of interest. We note in particular that for $\xi \gtrsim 4$, the c_0-type solution becomes highly unlikely for random initial conditions. This will be a crucial ingredient in answering the first question on page 15.

3.1.2 Phase space diagram

Change of variables

As we saw in Eq. (3.6), there is a change of variables which puts Eq. (3.2) into the form of an autonomous system. Thus the dynamics are captured by a 2-dimensional phase space diagram. This will enable us to re-phrase the results obtained in Sec. 3.1.1 in a more intuitive way.
Rather than choose $(g(N), g'(N))$ as phase space coordinates, we find a different choice more convenient. In particular, we choose

$$q(\tau) \equiv (\tau/\tau_0)\, ef(\tau)\,, \quad p(\tau) \equiv (\tau/\tau_0)^2 ef'(\tau)\,, \quad \tau_0 \equiv -1\,, \tag{3.22}$$

where τ_0 is an arbitrary constant which for simplicitly we have set to -1. The equations of motion under these new coordinates then become

$$\frac{dq}{d\tau} = \frac{p(\tau) - q(\tau)}{-\tau}, \quad \frac{dp}{d\tau} = \frac{-2\left(q(\tau)^3 - \xi\, q(\tau)^2 + p(\tau)\right)}{-\tau}\,. \tag{3.23}$$

The denominator of $-\tau$ can be eliminated via the substitution $\tau = -e^{-v}$, rendering the system autonomous:

$$\frac{dq}{dv} = p - q\,, \quad \frac{dp}{dv} = -2(q^3 - \xi\, q^2 + p)\,. \tag{3.24}$$

The transformation Eq. (3.5) now corresponds to the time-translation

$$v \mapsto v - \ln \lambda \,. \tag{3.25}$$

This differential equation is solved by the flow lines of the vector field

$$\Big(p - q, -2\left(q^3 - \xi\, q^2 + p\right)\Big) \,, \tag{3.26}$$

in the q-p plane.

We now begin a complete classification of solutions to Eq. (3.2) based on an analysis of this vector field (3.26). For simplicity we exclude the degenerate case when $\xi = 2$ exactly.

The zeroes of this vector field are readily verified to be

$$(q, p) = (c_i \xi, c_i \xi) \,, \tag{3.27}$$

for c_i defined by Eq. (3.9), and the corresponding constant trajectories are, up to the change of variables, the c_i solutions of Eq. (3.9). Therefore for $\xi < 2$ there is a unique zero of (3.26) at $(q, p) = (0, 0)$. At $\xi = 2$, a pair of zeroes are created at $(1, 1)$ corresponding to the c_1 and c_2 solutions. Thus for $\xi > 2$ there are three zeroes. The zeroes at $(c_0\xi, c_0\xi)$ and $(c_2\xi, c_2\xi)$ are stable, while $(c_1\xi, c_1\xi)$ is a saddle point. Thus the stable trajectories of c_0 and c_2 form two-parameter families, while the stable trajectories of c_1 form a only one-parameter family. These families correspond to the "c_i-type solutions" described on page 14.

Visualizing solutions with a phase-like diagram

Using the change of variables from Eq. (3.22), we can visualize the structure of solutions to Eq. (3.2) in a very effective manner. Solutions to Eq. (3.2) can be plotted, via the change of variables, as trajectories in the q-p plane. Two solutions parameterize the same trajectory if and only if they are related by Eq. (3.5). In this case, they are related by a shift in the time variable v according to Eq. (3.25). In the first row of Fig. 3.4 we plot various such trajectories. Since the phase u_0 defined by Conjecture 1 is invariant under Eq. (3.5), each trajectory has a well-defined phase which is indicated by color in the first row of Fig. 3.4, with the same color coding as in Fig. 3.2. Oscillation is represented by the spirals in the top right panel of Fig. 3.4. Solutions spiral inwards along a trajectory of fixed color, and each crossing of the p-axis corresponds to a zero of the solution.

Already at this point, since no two trajectories are allowed to cross, we observe that the boundary between the basins of attraction for the c_0-type solutions and the c_2-type solutions is given precisely by the two trajectories of c_1-type solutions (plus of course their limit point, which corresponds to the c_1-solution.) These are depicted as red and green lines in the second row of Fig. 3.4.

We can construct a natural coordinate system on the q-p plane by taking a coordinate complementary to the phase u_0. The complementary invariant ω of solutions is not a suitable candidate, because it transforms nontrivially under Eq. (3.5) according to Eq. (3.16). The quantity $-\omega\tau$ is however invariant under Eq. (3.5), and level curves are shown in the last row of Fig. 3.4 (with a spacing of $N/10$, see Eq. (3.6)). For a given trajectory, these level curves correspond to contours of fixed time, and hence

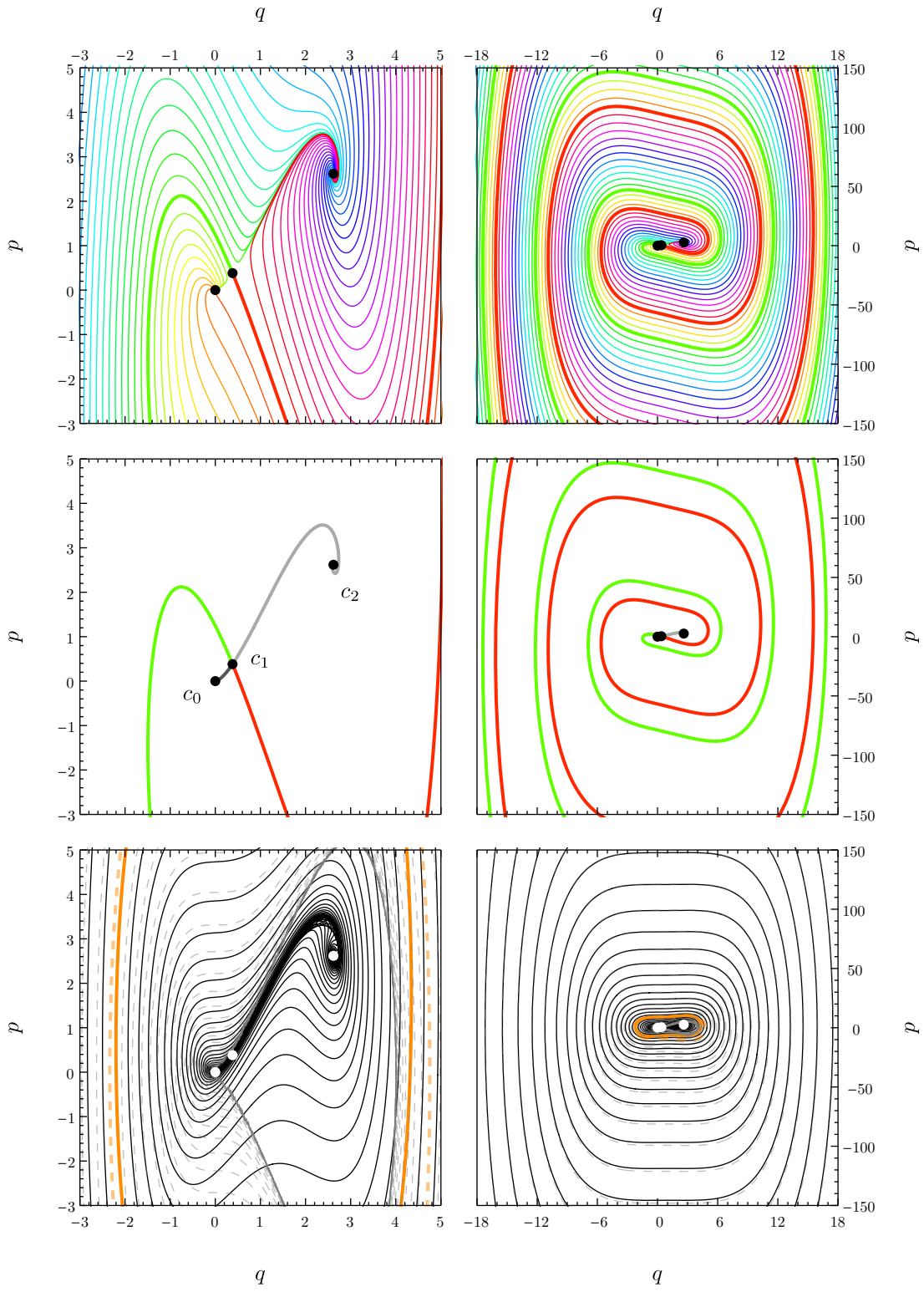

Figure 3.4: Evolution of the background gauge field in phase space, depicted by trajectories of the vector field Eq. (3.26) for $\xi = 3$. The dots are zeroes of the vector field, corresponding to the c_i solutions of Sec. 3.1.1. The left column shows the non-oscillatory regime around the zeroes, whereas the right column is a zoomed-out view showing the oscillatory regime. The second row shows some special trajectories, the third row depicts contours of constant $-\omega\tau$. For details see text.

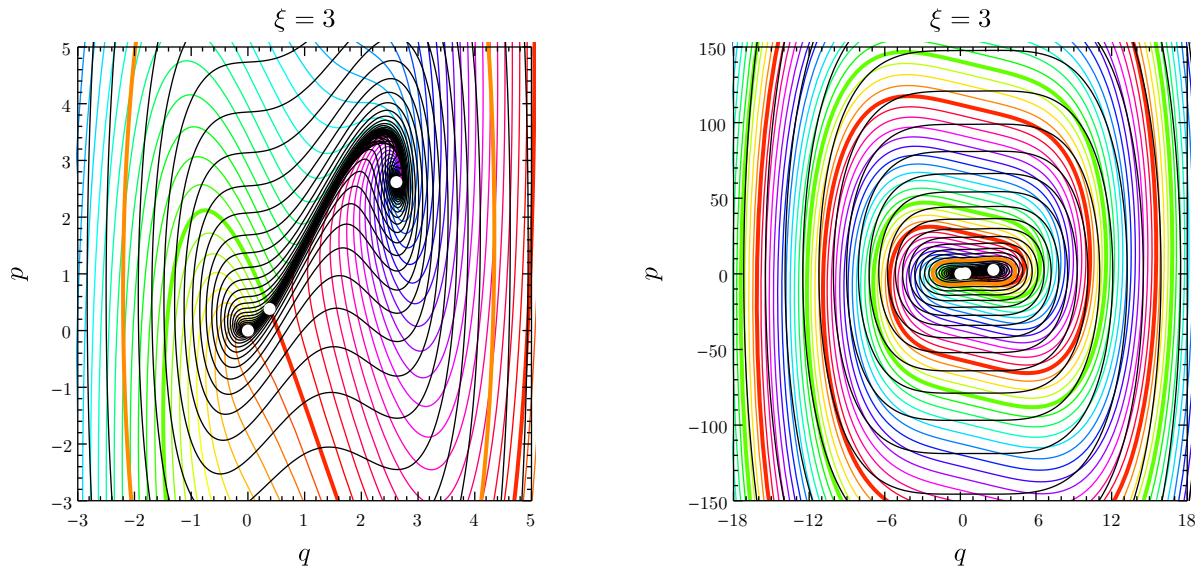

Figure 3.5: Summary of the evolution of the background gauge field. The colored lines are trajectories of the classical background field evolution in phase space, with the color coding corresponding to different phases u_0 as in Fig. 3.2. The black curves are contours of constant $-\omega\tau$.

the speed of approach to the respective c_i solution in encoded in the spacing of these level curves. The contour $\omega\tau = -\xi$ is highlighted in orange, indicating the transition between the oscillatory and the non-oscillatory regime (see Eq. (3.16)). Moreover, we indicate the level curves of $(-\tau\omega_2)$ (see Eq. (D.8)) as dashed lines, showing the excellent agreement between ω and the auxiliary function ω_2 in the oscillatory regime.

The resulting coordinate system is degenerate at $\omega = 0$. In the left panel of the middle row of Fig. 3.4, we show the $\omega = 0$ solutions corresponding to the two vacuum-to-vacuum transitions which tunnel from the c_1 solution in the infinite past to either the c_0 solution or c_2 solution in the asymptotic future as gray curves.

The asymptotic formula for the two such trajectories is Eq. (D.7) with $\rho > 0$ and $\rho < 0$ respectively. These instanton-type solutions, together with all the c_i solutions (which are the limit points), are all of the only non-oscillatory solutions to Eq. (3.2).

In this way, we understand the structure of all the solutions to Eq. (3.2) and how they fit together. The results are summarized in Fig. 3.5, which simply combines the first and last row of Fig. 3.4.

We see how if initial conditions are chosen to be oscillatory, they will spiral inwards towards either the c_0 or the c_2 solution. Finally, recall from Fig. 3.3 that c_2 is favored, overwhelmingly so as ξ increases. This explains why Eq. (3.20) can be used a a criterion for the required magnitude of the initial conditions necessary to trigger a growing c_2-type solution.

We note here that $c_1 \approx 0$ for large ξ, and hence the basin of attraction for c_2 comes very close to the c_1 solution. Thus it is quite likely that gauge-field fluctuations will trigger a c_2-type solution even before the oscillatory regime is entered. But given that the fluctuations grow exponentially with ξ we only need an order-of-magnitude estimate for the transition time.

3.2 Anisotropic background fields

Until now, throughout our analysis of the homogenous background we have assumed isotropy, so that

$$(A^{(0)})^a_i = \delta^a_i \, f(\tau). \tag{3.28}$$

Here we first consider anisotropic perturbations of the homogeneous background to linear order. As a verification, we numerically solve the full nonlinear equations of motion for a homogeneous anisotropic background. In both cases we observe the decay of anisotropies whenever a c_2-type solution develops. This justifies assuming isotropy when discussing c_2-type solutions.

Anisotropic perturbations to linear order

We begin with the scalar vector tensor (SVT) decomposition ansatz,[7]

$$(A^{(0)})^a_i = f(\tau)\delta^a_i + \left(v^j(\tau)\varepsilon_{ija} + T^a_i(\tau)\right)\epsilon + O(\epsilon^2)\,. \tag{3.29}$$

It's implicit here that the three $(A^{(0)})^a_0$ components are determined by the equation of motion (as constraint equations). Expanding out the remaining nine equations of motion, we obtain Eq. (3.2), together with ϵ multiplied by the rank-five equation

$$T'' + \frac{2\xi}{-\tau} e f(\tau)\, T = 0\,. \tag{3.30}$$

We find no equations of motion involving $v^j(\tau)$, indicating that they are the gauge degrees of freedom. The remaining three equations are equivalent to $0 = 0$.

As the isotropic component $f(\tau)$ grows in the positive direction, WKB theory dictates that T decays in proportion to $\left(-\tau^{-1} f(\tau)\right)^{-1/4}$ (see Eq. (F.33)). Thus when $ef(\tau)$ is any c_2-type solution, T decays in proportion to $\sqrt{-\tau}$. In the case of the c_2 solution, the exact solution is for $T(\tau)$ is

$$T(\tau) = T_0\sqrt{-\tau}\exp\left(\pm i\,\mu_2 \log(-\tau)\right) + \text{h.c}\,, \tag{3.31}$$

$$\mu_2 \equiv \xi\sqrt{2c_2 - (2\xi)^{-2}}\,, \tag{3.32}$$

where T_0 is a complex symmetric traceless tensor determined by the initial conditions.

No anisotropic steady states

We make the anisotropic analogue of our ansatz Eq. (3.8), namely

$$e\,(A^{(0)})^a_i(\tau) = C^a_i/(-\tau)\,. \tag{3.33}$$

The equations of motion yield the following equations:

$$\sigma_1(2 + \sigma_2^2 + \sigma_3^2) - 2\xi\sigma_2\sigma_3 = 0 \text{ and cyclic permutations}, \tag{3.34}$$

[7] We point out that this is different to the helicity decomposition we will work with in Sec. 4. SVT is based on the transformation properties of the diagonal subgroup of two $SO(3)$ symmetries (here one is from spatial rotations and the other is the adjoint group of the gauge symmetry). The helicity decomposition applies for a specific Fourier mode and measures the charges under $SO(2)$ rotations around the axis specified by the Fourier mode, see Sec. 4.2 for details.

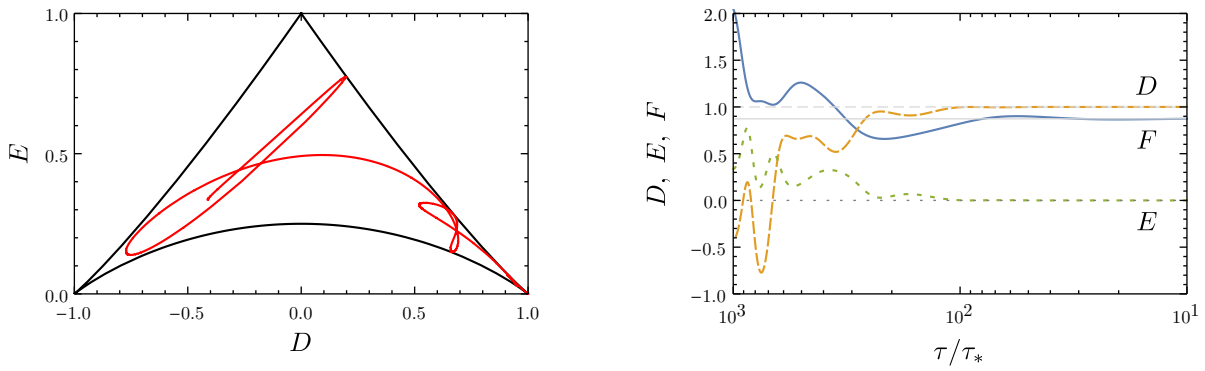

Figure 3.6: A c_2-type solution with random anisotropic initial conditions evolving towards isotropy for $\xi = 3$. Left panel: the positively orientated isotropic configuration corresponds to the bottom right corner. Right panel: For the same parameter point, time evolution (relative to an arbitrary time τ_*) of the quantities D, E and F as defined in the text. The horizontal lines denote the asymptotic values 1, c_2 and 0 (from top to bottom) characterizing an isotropic c_2 solution.

where σ_1, σ_2 and σ_3 are the singular values of C_i^a. As can be verified using a computer algebra system, the only solutions of this system of equations are equivalent to the three isotropic solutions we already found in Eq. (3.8).

Numerical solutions of full nonlinear anisotropic background

We showed above that any growing homogeneous background solution which has anisotropies at sub-leading order must evolve towards isotropy. While this supports the hypothesis that any system with a growing homogeneous background solution leads to isotropy, it doesn't apply to highly anisotropic backgrounds. For this we resort to numerical simulation. Specifically, we numerically solve the fully nonlinear system Eq. (2.16) for the twelve functions[8] $(A^{(0)})^a_\mu$ which determine the background field $A^{(0)}$.

With numerical solutions in hand, we must understand their properties in the non-isotropic case. As a substitute for $ef(\tau)$, we define for any nonzero 3×3 matrix A:

$$F(A) \equiv \frac{-\tau|A|}{\sqrt{3}\xi} \quad \text{where } |A| \equiv \sqrt{A_i^a A_i^a}. \tag{3.35}$$

When A is isotropic, $F(A) = -\tau|ef(\tau)|/\xi$. Thus if $A^{(0)}$ corresponds to an isotropic c_i-type solution, then $\lim_{\tau\to 0^-} F(A^{(0)}(\tau)) = c_i$. Next we must quantify the anisotropy of A. We define in Appendix E.2 two parameters $D(A)$ and $E(A)$ for this purpose, which are invariant under rotation, gauge symmetry, and multiplication by a positive scalar. Up to a normalization factor, $D(A) \in [-1, 1]$ is $(\det A)/\,|A|^3$, while the definition of $E(A)$ is more involved. The pair of values $(D(A), E(A))$ determines a point in a triangular-shaped region. The matrix A is isotropic when $D(A) = \pm 1$, or equivalently when $E(A) = 0$.

[8] We have twelve functions $(A^{(0)})^a_\mu$ subject to three constraint equations and six independent dynamical equations. To get a well-formed system, one must add three gauge-fixing constraints. We found it convenient to impose temporal gauge.

When $D(A) = +1$ (resp. -1) the gauge field is positively (resp. negatively) oriented [9].
In Fig. 3.6 we show a typical example of a c_2-type solution with random anisotropic initial conditions evolving towards isotropy. In our numerical simulations, we observe that after some evolution, all solutions converge converge towards an isotropic solution of the form Eq. (3.33), namely either a c_0-type solution or a c_2-type solution. The proportion of c_2-type solutions was even higher than predicted in Fig. 3.3. We conclude that

- the c_2-type solutions are stable against small anisotropic perturbations
- sufficiently large anisotropic initial conditions with $\xi > 2$ usually lead to c_2-type solutions
- the continuous sourcing of the background field through the enhanced Abelian super-horizon modes will therefore inevitably lead to an isotropic c_2-type background solution.

3.3 Coupled gauge field - inflaton background

In the previous section we took ξ to be a constant, external parameter in the equation of motion for the homogeneous gauge field background. We now turn to the complete dynamical background evolution, including also the evolution of the homogeneous inflaton field $\phi(\tau)$ and hence the (slow) evolution of ξ. This leads to the coupled system of equations

$$f''(\tau) + 2e^2 f^3(\tau) - e\frac{\alpha}{\Lambda}\phi' f^2(\tau) \;\; = 0\,, \tag{3.36}$$

$$\phi''(\tau) + 2aH\phi'(\tau) + a^2 V_{,\phi}(\phi) + \frac{6\alpha e}{\Lambda a^2} f^2(\tau) f'(\tau) = 0\,. \tag{3.37}$$

In single-field slow roll inflation, ξ typically increases over the course of inflation. This slowly evolving value of ξ slightly modifies some of the results of the previous subsections (e.g. the precises values for the range of phases which lead to the c_2-solution in Fig. 3.3 may be shifted), but the overall picture remains valid. After inserting the c_2-solution, Eq. (3.37) can be expressed as

$$\frac{\dot\phi}{H} + \frac{V_{,\phi}}{V} + 2e\frac{\alpha}{\Lambda}H^2(c_2\,\xi)^3 = 0\,, \tag{3.38}$$

where we have neglected the slow-roll suppressed term $\ddot\phi$. Assuming that the last term is sub-dominant, $\dot\phi/H$, $V_{,\phi}/V$ and ξ are all proportional to $\sqrt{\varepsilon}$, with $\varepsilon = \dot\phi^2/(2H^2) \simeq (V'/V)^2/2$ denoting the first slow-roll parameter. Moreover, for a quadratic or cosine potential as is usually considered in axion inflation models, H^2 is proportional to $1/\varepsilon$. In summary, the time-dependence of all terms in Eq. (3.37) is governed by the square root of the first slow-roll parameter. In particular, if the last term is sub-dominant at any point in time (after the c_2-solution has been reached), it will always remain sub-dominant. For the parameter example of Sec. 5, we find precisely this situation.

[9] We say that an isotropic gauge field $A_i^a = f(\tau)\delta_i^a$ is *positive* when $f(\tau)$ is positive. This has the following physical significance. An isotropic gauge field identifies an orthonormal basis of the Lie algebra with $|f(\tau)|$ times an orthonormal basis of 3-space (via contraction). The Lie algebra carries a natural orientation where the structure constants are $+2i\epsilon^{abc}$. For 3-space, the chiral term in our lagrangian picks out a preferred orientation (which corresponds to the standard orientation when $\xi > 0$). The relative orientation thus is the sign of $\xi f(\tau)$. Since we assume $\xi > 0$, the relevant sign is that of $f(\tau)$.

We note that this is a different regime than the 'magnetic drift' regime studied in Refs. [4, 5, 20, 22]. There, the friction term was taken to be large compared to the Hubble friction, $\xi\alpha H/(e\Lambda) \gg 1$. Also in this regime, there is a local attractor for the gauge field background which scales as $f(\tau) \sim 1/\tau$, with however a different constant of proportionality. Within the non-Abelian regime, the difference in our results with respect to these earlier works on CNI, in particular concerning the stability of the scalar sector, can be traced back to the fact that we do not restrict our analysis to this magnetic drift regime.

4 Linearized equations of motion

We now turn to the inhomogeneous equations of motion, adding perturbations to the homogeneous quantities discussed in the previous section. This includes the perturbations of the gauge field, the inflaton and the metric. We start by deriving the linearized equations of motions for all relevant degrees of freedom in Sec. 4.1, reproducing the results first obtained in Refs. [4, 5]. The helicity basis, introduced in Sec. 4.2, proves to be convenient to identify the physical degrees of freedom and simplify the system of equations. This becomes is particularly evident in Sec. 4.3 which discusses the resulting equations of motion for the pure Yang Mills sector. We can immediately identify the single enhanced mode and even give an exact analytical expression for the mode function in limit of constant ξ. Finally, Sec. 4.4 includes also the inflaton and metric tensor fluctuations. Limitations of the linearized treatment of the perturbations are pointed out in Sec. 4.4. They primarily affect the helicity 0 sector and we will return to this point in more detail in Sec. 5.2. Throughout Sec. 4.3 and 4.4, the parameter ξ is taken to be constant. Its evolution will be considered in Sec. 5.

4.1 Setup for the linearized analysis

In this section we will derive the system of first order differential equations for all gauge degrees of freedom and the inflaton fluctuations, assuming a homogeneous and isotropic gauge field background, for further details see App. A.

. The starting point is the action reported in Eq. (2.14). We work in the ADM formalism [41], i.e. we write the metric as

$$ds^2 = -N^2 d\tau^2 + h_{ij}\left(dx^i + N^i d\tau\right)\left(dx^j + N^j d\tau\right) , \tag{4.1}$$

and we decompose

$$h_{ij} = a^2\left[(1+A)\,\delta_{ij} + \partial_i\partial_j B + \partial_{(i}C_{j)} + \gamma_{ij}\right] . \tag{4.2}$$

Imposing the *spatially flat gauge* means that we can set

$$A = B = 0\,, \tag{4.3}$$

and we can use the remaining spatial reparametrization invariance to set $C_i = 0$, which implies

$$h_{ij} = a^2\left(\delta_{ij} + \gamma_{ij}\right) , \tag{4.4}$$

where γ_{ij} is the transverse traceless component of h_{ij}: $\gamma_{ii} = \partial_i \gamma_{ij} = 0$. As we numerically checked that the lapse and shift contributions to the subsequent discussion do not affect the results, we discard them in this section[10] for pedagogical reasons, and we refer to Appendix A for the complete expressions.

We expand the gauge fields and the inflaton field as (see also Eqs. (2.17) and (3.1))

$$A_i^a(\tau, \vec{x}) = f(\tau)\, \delta_i^a + \delta A_i^a(\tau, \vec{x})\,, \tag{4.5}$$

$$\phi(\tau, x) = \langle \phi(\tau) \rangle + \delta\phi(\tau, x)\,, \tag{4.6}$$

where δ_i^a is the Kronecker delta function, $f(\tau)\,\delta_i^a$ and $\langle\phi(\tau)\rangle$ comprise the homogeneous background, while $\delta A_i^a(\tau, \vec{x})$ and $\delta\phi(\tau, x)$ denote the quantum fluctuations around the homogeneous background. In order to infer equations of motion which are linear in the fluctuations, we need to expand the lagrangian up to quadratic order in all the field fluctuations. To make the computation easy to follow, we split it and the results into various terms arising from $\mathcal{S}_i = \int d^4x\, \sqrt{-g}\, \mathcal{L}_i$, following Eq. (2.14). The quadratic order of these terms take the following form

$$\delta^2 \mathcal{S}_\phi = \int d^4x \left[\frac{a^2}{2} \left((\delta\phi')^2 - (\partial_i \delta\phi)^2 - a^2 V_{,\phi\phi}\, (\delta\phi)^2 \right) \right], \tag{4.7}$$

$$\begin{aligned}
\delta^2 \mathcal{S}_{\rm YM} = \int d^4x \Bigg[& -\frac{1}{2} \delta A_0^a \partial_i \partial_i \delta A_0^a + \delta A_0^a \partial_0 \left(\partial_i \delta A_i^a - e f \varepsilon^{abi} \delta A_i^b \right) + \\
& + \delta A_0^a \left(2 e f' \varepsilon^{abi} \delta A_i^b + e f \varepsilon^{abi} \left(\partial_i \delta A_0^b \right) + e^2 f^2 \delta A_0^a \right) - \\
& - \frac{1}{2} \delta A_i^a \left(\delta A_i^a \right)'' + \frac{1}{2} \delta A_j^a \left(\partial_i \partial_i \delta A_j^a \right) + \frac{1}{2} (\partial_i \delta A_i^a)^2 - \\
& - e^2 f^2 \left((\delta A_a^a)^2 + \frac{1}{2} \left(\delta A_i^b \right)^2 - \frac{1}{2} \delta A_i^b \delta A_b^i \right) - e f \varepsilon^{abc} \left(\delta_i^b \partial_i \delta A_k^a \delta A_k^c + \delta_k^c \partial_i \delta A_k^a \delta A_i^b \right) + \\
& + \frac{(f')^2 - e^2 f^4}{4} \gamma^{jk} \gamma^{kj} - f' \gamma^{aj} \partial_0 \delta A_{j)}^{(a} - e f^2 \varepsilon^{abc} \gamma^{ij} \left(\delta_{(i}^b \partial_{j)} \delta A_c^a - \delta_{(i}^b \partial_{c} \delta A_{j)}^a \right) \Bigg],
\end{aligned} \tag{4.8}$$

$$\begin{aligned}
\delta^2 \mathcal{S}_{\rm CS} = \int d^4x \Bigg[& -\frac{\alpha}{\Lambda} \langle\phi\rangle \left(\varepsilon^{ijk} \left(\delta A_i^a \right)' \partial_j \delta A_k^a + 2 e f \left(\delta A_{[a}^a \right)' \delta A_{k]}^k + e f' \delta A_{[b}^b \delta A_{c]}^c \right) - \\
& - \frac{\alpha}{\Lambda} \delta\phi \left[f' \varepsilon^{ajk} \partial_j \delta A_k^a + 2 e f f' \delta A_a^a + e f^2 \left(\delta A_a^a \right)' - e f^2 \partial_i \delta A_0^i \right] \Bigg],
\end{aligned} \tag{4.9}$$

$$\delta^2 \mathcal{S}_{EH} = \int \mathrm{d}^4x\, \frac{a^2}{2} \left[\frac{\gamma_{ij} \partial_l \partial_l \gamma_{ij}}{4} + \frac{\gamma'_{ij} \gamma'_{ij}}{4} \right]. \tag{4.10}$$

As we will see in Sec. 4.2.1, the term proportional to δA_0^a in the first line of Eq. (4.8) vanishes after imposing the generalized Coulomb condition that reads (see Sec. 4.2.1 for further details):

$$\partial_i \delta A_i^a - e f \varepsilon^{abi} \delta A_i^b = 0\,. \tag{4.11}$$

The equation of motion for δA_0^a gives Gauss's law, which reads

$$\begin{aligned}
0 = & \left(\partial_i \partial_i - 2 e^2 f^2 \right) \delta A_0^a - \left(\partial_i \delta A_i^a - e f \varepsilon^{abi} \delta A_i^b \right) - \\
& - 2 e f' \varepsilon^{abi} \delta A_i^b - 2 e f \varepsilon^{abi} \left(\partial_i \delta A_0^b \right) + \frac{\alpha e}{\Lambda} f^2 \delta^{ai} \partial_i \delta\phi\,.
\end{aligned} \tag{4.12}$$

[10] Hence, we take $N = a$ and $N^i = 0$.

We write the linear equation of motion for the inflaton fluctuations in terms of the variable $(a\delta\phi)$ for later convenience

$$\begin{aligned} 0 = &- (a\delta\phi)'' + \partial_i\partial_i (a\delta\phi) + \frac{a''}{a}(a\delta\phi) - 2\mathcal{H}(a\delta\phi) + 2\mathcal{H}^2(a\delta\phi) - a^2 V_{,\phi\phi}(a\delta\phi) - \\ &- \frac{\alpha}{\Lambda a}\left[f'\varepsilon^{ijk}\partial_j\delta A^i_k + 2ef f'\delta A^a_a + ef^2(\delta A^a_a)' - ef^2\partial_i\delta A^i_0\right], \end{aligned} \tag{4.13}$$

where $\mathcal{H} = \frac{a'}{a}$. The linear equations of motion for the dynamical gauge field degrees of freedom are

$$\begin{aligned} 0 = &\delta A^{a\prime\prime}_i - \partial_j\partial_j\delta A^a_i + \partial_i\left(-\delta A^{a\prime}_0 - \partial_j\delta A^a_j\right) + \\ &- e\varepsilon^{abc}\left[-2\delta A^b_0\delta^c_i f' + 2f\delta^b_j\partial_j\delta A^c_i + f\delta^c_i(-\delta A^{b\prime}_0 + \partial_j\delta A^b_j) - f\delta^b_j\partial_i\delta A^c_j\right] - \\ &- e^2f^2\left[\delta^a_j\delta^b_j\delta A^b_i + \delta^a_j\delta^b_i\delta A^b_j + \delta^b_j\delta^b_i\delta A^a_j - 3\delta A^a_i - 2\delta^a_i\delta^b_j\delta A^j_b\right] - \\ &- \frac{\alpha}{2\Lambda}\left[\phi'\varepsilon_{ijk}\left[2\partial_j A^a_k + 2ef\varepsilon^{abc}\delta A^b_j\delta^c_k\right] + 2f'\varepsilon^{aji}\partial_j\delta\phi + 2ef^2\delta^a_i\delta\phi'\right] - \\ &- f''\gamma^a_i + f'(\gamma^a_i)' + ef^2\varepsilon^{ajk}\partial_k\gamma_{ij} + e^2f^3\gamma^a_i \equiv \mathbf{L}(\delta A, \phi, \gamma), \end{aligned} \tag{4.14}$$

where for later convenience we have defined the linear operator $\mathbf{L}$. Finally, we give the equation of motion for the metric fluctuations in terms of the variable $(a\gamma_{ij})$

$$\begin{aligned} \frac{a}{4}\left[(a\gamma_{ij})'' + \left(-\partial_l\partial_l - \frac{a''}{a}\right)(a\gamma_{ij})\right] = &\frac{f'^{\,2} - e^2f^4}{2a}(a\gamma_{ij}) - f'\partial_0\delta A^{(i}_{j)} + f'\partial_{(i}\delta A^{j)}_0 + \\ &+ ef^2\gamma^{ij}\left[\varepsilon^{aic}\partial_{[j}\delta A^a_{c]} + \varepsilon^{ajc}\partial_{[i}\delta A^a_{c]}\right] + e^2f^3\delta A^{(i}_{j)}. \end{aligned} \tag{4.15}$$

We point out that the right-hand side of this equation is given by the transverse traceless component of the anisotropic energy momentum tensor, and hence this equation is equivalent to the linearized Einstein equations used in gravitational wave physics [42].

4.2 Choice of gauge and basis

In the following we explain our choice of basis for dealing with the gauge field fluctuations, which will greatly simplify the analysis. After introducing the generalization of Coulomb gauge to a non-vanishing gauge field background, we decompose the 12 degrees of freedom of the gauge fields into helicity eigenstates. We further identify the degrees of freedom associated with gauge transformations and constraint equations, leaving us with six physical degrees of freedom. The explicit form of these basis vectors is given in App. B.

4.2.1 Generalized Coulomb gauge

In Eq. (3.1), we chose a particular representative $(A^0)^a_i = f(\tau)\delta^a_i$ for our homogeneous and isotropic background field. This is just one representative from the corresponding gauge-equivalence class. When considering physical fluctuations around this background configuration, we restrict ourselves to fluctuations which are orthogonal to the space spanned by gauge-equivalent configurations

$$U f(\tau)\delta^a_i U^\dagger + \frac{i}{e}U\partial_i U^\dagger, \quad \forall\, U = \exp(i\xi^a\mathbf{T}_a) \tag{4.16}$$

where ξ^a denotes a infinitesimal gauge transformation parameter. This condition should apply on each time slice. This orthogonality condition reads

$$0 = \langle D_i^{(A^0)} \xi^a \mathbf{T}_a | \delta A_i^c \mathbf{T}_c \rangle = \mathrm{Tr} \int (D_i^{(A^0)} \xi^a \mathbf{T}_a) \cdot (\delta A_i^c \mathbf{T}_c)\, d^3x \quad \forall\, \xi^a \,, \tag{4.17}$$

where

$$D_\mu^{(A)} \xi^a \mathbf{T}_a = \partial_\mu \xi^a \mathbf{T}_a - ie[A_\mu^b \mathbf{T}_b, \xi^a \mathbf{T}_a] \tag{4.18}$$

denotes the gauge-covariant derivative. After some algebra, Eq. (4.17) becomes

$$-\frac{1}{2} \int \xi^a (\partial_i \delta A_i^a + e\varepsilon_{abc} (A^0)_i^b \delta A_i^c)\, d^3x = 0 \quad \forall\, \xi^a \quad \Rightarrow \quad D_i^{(A^0)} \delta A_i^a = 0 \,. \tag{4.19}$$

Inserting Eq. (3.1) for A^0, we obtain the gauge fixing condition

$$\mathbf{C}(\delta A_i^a) \equiv \partial_i (\delta A_i^a) + ef(\tau) \varepsilon^{aic} \delta A_i^c = 0 \,. \tag{4.20}$$

In the following, we will in fact not fix the gauge, but we will choose a basis in which the 6 physical degrees of freedom (obeying Eq. (4.20)) and the 3 gauge degrees of freedom (contained in the subspace (4.16)) are explicit and orthogonal. This preserves gauge invariance as a consistency check at any point of the calculation, while clearly separating physical and gauge degrees of freedom. Together with the constraint equation (4.12), this splits the 12 degrees of freedom contained in the 3×4 matrix δA_μ^a into 6 physical, 3 gauge and 3 non-dynamical degrees of freedom, as expected for a massless $SU(2)$ gauge theory.

4.2.2 The helicity basis

In the absence of a background gauge field ($f(\tau) = 0$), Eq. (2.14) is invariant under two independent global $SO(3)$ rotations which act on the spatial and $SU(2)$ indices of the gauge fields $A_i^a(\tau, \vec{x})$. In the presence of the background Eq. (3.1), this symmetry is reduced to a single $SO(3)$ symmetry, which is the diagonal subgroup of $SO(3)_{\text{spatial}} \times SO(3)_{\text{gauge}}$. The Fourier decomposition introduces a preferred direction $\vec{k}$, which without loss of generality we will choose to be along the x-axis, $\vec{k} = k\hat{e}_1$. This breaks the diagonal $SO(3)$ symmetry down to an $SO(2)$ symmetry of rotations around $\vec{k}$. The generator of this symmetry is a helicity operator of massless particles. This generator is given explicitly by

$$\begin{aligned} \mathbf{H}(\delta A) &\equiv i\hat{e}_1 \times \delta\vec{A} + [\mathbf{T}_1, \delta\vec{A}], \\ \mathbf{H}(\delta A)_i^a &= i\varepsilon^{i1j} \delta A_j^a + i\varepsilon^{1ca} \delta A_i^c \,. \end{aligned} \tag{4.21}$$

Expressing the linearized system of equations of motion in terms of the linear operator $\mathbf{L}$, see Eq. (4.14), $\mathbf{L}(\delta A, \delta\phi, \gamma) = 0$, the symmetry properties above imply that this linear operator must commute with the helicity operator, $[\mathbf{L}, \mathbf{H}] = 0$. It will thus be useful to decompose δA into helicity eigenstates, which will lead to a block-diagonal structure for $\mathbf{L}$.

Let us look at the eigenvalues and multiplicities of these states. With respect to the diagonal $SO(3)$ group, the 3×3 matrix δA decomposes as $3 \otimes 3 = 1 \oplus 3 \oplus 5$: one scalar (S), one vector (V), one tensor (T) degree of freedom. The corresponding helicities are

$$(S) : 0 \,, \qquad (V) : -1, 0, +1 \,, \qquad (T) : -2, -1, 0, +1, +2 \,, \tag{4.22}$$

implying multiplicities 3, 2 and 1 for the helicities 0, ±1 and ±2 respectively. These nine degrees of freedom correspond to the six physical and three gauge degrees of freedom mentioned in the previous section. Since the gauge transformation acts only on the gauge indices and not the spatial indices (see e.g. Eq. (4.18)), the three gauge degrees of freedom form a vector (helicities $-1, 0, 1$). The helicities of the remaining six physical degrees of freedom must thus be $-2, -1, 0(\times2), +1, +2$. Hence in this basis, the linear operator $\mathbf{L}$ (and hence our equations of motions for δA_i^a) decomposes into four decoupled equations (for ±1 and ±2) and two (generically) coupled equations for the two helicity 0 modes. In the following we describe the basis we use for the gauge, constraint and physical degrees of freedom, the corresponding explicit basis vectors can be found in App. B. In Sec. 4.4 we will include also the inflaton (helicity 0) and tensor metric (helicity ±2) fluctuations, which will couple to the helicity 0 and ±2 gauge field modes, respectively.

Lets start by explicitly computing the basis vectors for the three gauge degrees of freedom[11],

$$(\delta\tilde{A}^a_\mu)_{\text{gauge}} = \sum_b (\hat{g}_b)^a_\mu w^{(g)}_b(x) = \sum_\lambda (\hat{g}_\lambda)^a_\mu \, w^{(g)}_\lambda(x)\,, \tag{4.23}$$

where $\hat{g}_b$ ($b = \{1,2,3\}$) denotes the basis vectors of the gauge degrees of freedom in $SU(2)$ space, $\hat{g}_\lambda$ with $\lambda = \{-,0,+\}$ denotes the basis vectors in terms of helicity states and we denote the corresponding coefficients with $w_{b,\lambda}$, respectively. The corresponding coefficients $w^{(g)}$ are subject to the equations of motion. As in the Abelian case we have introduced $x = -k\tau$ as a convenient parametrization of time. Expressing the infinitesimal gauge transformation (4.18) in matrix form defines the gauge basis vectors $\hat{g}$ (in the $SU(2)$ basis),

$$D^{(A_0)}_\mu w^{(g)}_a \mathbf{T}_a = (\hat{g}_b)^a_\mu w^{(g)}_b \mathbf{T}_a = (\hat{g}_\lambda)^a_\mu w^{(g)}_\lambda \mathbf{T}_a\,. \tag{4.24}$$

To decompose these into helicity states, we need to extend the helicity operator $\mathbf{H}$ to act on the $\mu = 0$ component. Since the time component does not transform under the any of the symmetries mentioned in this subsection, this can be trivially achieved by

$$\mathbf{H}(\delta A)^a_0 = 0 \quad \forall a\,. \tag{4.25}$$

The explicit form of the three basis vectors $\hat{g}_\lambda$ which simultaneously satisfy Eqs. (4.24) and (4.25) are given in App. B. We note that in any background which is a fixed point of Eq. (3.5) (e.g. if the background follows the c_2-solution), the k and τ dependence of the basis vectors is fully encoded in $x = -k\tau$ only.

So far, we have considered only the spatial components of δA. The time components δA_0 are subject to the constraint equations (4.12). We can solve these explicitly and substitute the solution back into the equation of motion for the spatial components. However in practice we will find it more convenient to introduce basis vectors also for these constraint degrees of freedom, extending the differential operator $\mathbf{L}$ to a differential-algebraic operator. The explicit form of the corresponding 'constraint' basis vectors in the helicity basis is given in App. B.

[11] Despite the functions $w(x)$ are the coefficients of the gauge fields in Fourier space $\delta\tilde{A}^a_\mu$, to ease the notation we do not use the tildas.

The remaining eigenspace of the helicity operator (4.25) is spanned by the basis vectors of the physical degrees of freedom $\hat{e}_\lambda$, see App. B for the explicit form. As anticipated, we find two states with helicity 0, and one state each with helicity $-2, -1, +1, +2$. One can immediately verify explicitly that the basis vectors presented here have the desired qualities, i.e. they are orthonormal, eigenfunctions of $\mathbf{H}$ with eigenvalues giving the helicity, $\mathbf{L}(\hat{g}_\lambda) = 0$ (gauge invariance) and $\mathbf{C}(\hat{e}_\lambda) = 0$ (compatibility with generalized Coulomb gauge, see (4.20)). The choice of basis derived here closely resembles the basis used in Refs. [4, 5, 22, 23]. The main difference is that we explicitly separate the $\pm\lambda$ states and normalize our basis vectors. As we will see in the next section, this simplifies the resulting equations of motion (in particular when considering only the degrees of freedom of the gauge sector).

4.3 Equations of motion for the gauge field fluctuations

In this section we will compute the equations of motion for the gauge field fluctuations in the canonically normalized helicity basis introduced above (see also App. (B)) and discuss their key properties. In Sec. 4.4 we will extend this to the inflaton and metric tensor fluctuations.
Expressing the δA in terms of the helicity basis,

$$\delta\tilde{A}^a_\mu(\tau, k) = \sum_\lambda (\hat{e}_\lambda)^a_\mu \, w^{(e)}_\lambda(x) + \sum_\lambda (\hat{f}_\lambda)^a_\mu \, w^{(f)}_\lambda(x) + \sum_\lambda (\hat{g}_\lambda)^a_\mu \, w^{(g)}_\lambda(x) \,, \tag{4.26}$$

we immediately obtain the equations of motions for the coefficients $w^{(x)}_\lambda$ with $x = \{e, f, g\}$ denoting the physical, constraint and gauge degrees of freedom, respectively. The three equations for the gauge degrees of freedom simply read $0 = 0$, reflecting gauge invariance. For the helicity ± 2 modes we obtain

$$\frac{\mathrm{d}^2}{\mathrm{d}x^2} w^{(e)}_{-2}(x) + \left(1 + \frac{2\xi}{x} + 2\left(\frac{\xi}{x} + 1\right) y_k(x)\right) w^{(e)}_{-2}(x) = 0 \,, \tag{4.27}$$

$$\frac{\mathrm{d}^2}{\mathrm{d}x^2} w^{(e)}_{+2}(x) + \left(1 - \frac{2\xi}{x} + 2\left(\frac{\xi}{x} - 1\right) y_k(x)\right) w^{(e)}_{+2}(x) = 0 \,, \tag{4.28}$$

with

$$y_k(x) \equiv \frac{e f(\tau)}{k} \,. \tag{4.29}$$

We can now appreciate some of the advantages of the canonically normalized helicity basis. The equations of motion for the ± 2 modes are fully decoupled, and moreover contain no terms involving the first derivatives $w'_\lambda(x)$. This makes them amenable to WKB analysis. We immediately see that for $\xi \geq 0$ and $y(x) \geq 0$ the -2 mode always has a positive effective squared mass, whereas the $+2$ mode can be tachyonic. Consider momentarily the limit where ξ is constant and $f(\tau)$ is one of the three fixed points of the symmetry (3.5), $y_k(x) = y(x) = c_i\xi/x$ for some $i \in \{0, 1, 2\}$, where c_i is defined in (3.9). In this case, the solutions of Eq. (4.28) are Whittaker functions:

$$w^{(e)}_{+2}(\tau) = \frac{e^{(1+c_i)\pi\xi/2}}{\sqrt{2k}} W_{-i(1+c_i)\xi,\, -i\sqrt{2\xi^2 c_i - 1/4}}(2ik\tau) \,, \tag{4.30}$$

with the normalization set by the Bunch–Davies vacuum (2.9) in the infinite past. For $c_i = c_0 = 0$, this solution coincides with the Abelian solution, Eq. (2.8). The region of tachyonic instability for the helicity $+2$ mode as well as some useful approximative expressions for Eq. (4.30) will be discussed below.

Next we turn to the ± 1 modes. Here we need to consider the two equations for the dynamical degrees of freedom and two constraint equations. For shorter notation, we introduce two reparameterizations of $y_k(x)$,

$$y_k(x) = \tfrac{1}{2}\left(\tan\theta_-(x) - 1\right) = \tfrac{1}{2}\left(\tan\theta_+(x) + 1\right). \tag{4.31}$$

with $\theta_\pm \in (-\pi/2, \pi/2)$. With this, the equations for the dynamical and constraint degrees of freedom read

$$\begin{aligned} 0 &= \frac{\mathrm{d}w^{(e)}_{\pm 1}(x)}{\mathrm{d}x^2} \pm \sqrt{2}i \sec\theta_\pm \left(\tfrac{\mathrm{d}}{\mathrm{d}x}\theta_\pm\right) w^{(f)}_{\pm 1}(x) + \\ &\quad + \left(-\left(\tfrac{\mathrm{d}}{\mathrm{d}x}\theta_\pm\right)^2 + \tfrac{1}{2}\left(1 \pm \sin(2\theta_\pm)\right) + \left(\frac{1}{2} \mp \frac{\xi}{x}\right)\left(2\cos^2\theta_\pm \mp \tan\theta_\pm\right)\right) w^{(e)}_{\pm 1}(x)\,, \\ 0 &= \sec\theta_\pm w^{(f)}_{\pm 1}(x) \pm 2\sqrt{2}i w^{(e)}_{\pm 1}(x) \tfrac{\mathrm{d}}{\mathrm{d}x}\theta_\pm\,. \end{aligned} \tag{4.32}$$

After inserting the constraint equations, this simplifies to

$$\begin{aligned} &\frac{\mathrm{d}w^{(e)}_{-1}(x)}{\mathrm{d}x^2} + \left(3\left(\tfrac{\mathrm{d}}{\mathrm{d}x}\theta_-\right)^2 + \tfrac{1}{2}\left(1 - \sin(2\theta_-)\right) + \left(\frac{1}{2} + \frac{\xi}{x}\right)\left(2\cos^2\theta_- + \tan\theta_-\right)\right) w^{(e)}_{-1}(x) = 0 \\ &\frac{\mathrm{d}w^{(e)}_{+1}(x)}{\mathrm{d}x^2} + \left(3\left(\tfrac{\mathrm{d}}{\mathrm{d}x}\theta_+\right)^2 + \tfrac{1}{2}\left(1 + \sin(2\theta_+)\right) + \left(\frac{1}{2} - \frac{\xi}{x}\right)\left(2\cos^2\theta_+ - \tan\theta_+\right)\right) w^{(e)}_{+1}(x) = 0. \end{aligned} \tag{4.33}$$

For the c_2 background attractor solution given in Eq. (3.12), the resulting effective masses are always positive. We will turn to a more detailed stability analysis in the next subsection.

Finally lets consider the two helicity zero modes. Since these expressions are somewhat more lenghty, we only give the final expression after substituting the constraint equation

$$-\sec^2\theta_0 w^{(f)}_0(x) - \sqrt{2}\sec\theta_0 \tfrac{\mathrm{d}}{\mathrm{d}x}\theta_0 w^{(e)}_{02}(x) = 0\,, \tag{4.34}$$

where we have introduced $\theta_0 \in [-\pi/2, \pi/2]$ as

$$y_k(x) = \tfrac{1}{\sqrt{2}}\tan\theta_0(x)\,. \tag{4.35}$$

With this,

$$\frac{\mathrm{d}}{\mathrm{d}x^2}\begin{pmatrix} w^{(e)}_{01}(x) \\ w^{(e)}_{02}(x)\end{pmatrix} + M_0(x)\begin{pmatrix} w^{(e)}_{01}(x) \\ w^{(e)}_{02}(x)\end{pmatrix} = 0 \tag{4.36}$$

with the 2×2 Hermitian mass matrix M_0 for the two e_{0i} modes given by

$$M_0 = \begin{pmatrix} 1 - \sqrt{2}\frac{\xi}{x}\tan\theta_0 + 2\tan^2\theta_0 & -\frac{2i}{\cos\theta_0}\left(\frac{\xi}{x} - \frac{1}{\sqrt{2}}\tan\theta_0\right) \\ \frac{2i}{\cos\theta_0}\left(\frac{\xi}{x} - \frac{1}{\sqrt{2}}\tan\theta_0\right) & \sin^2\theta_0 + \cos^{-2}\theta_0 - \frac{\xi}{\sqrt{2}x}\sin 2\theta_0 + 3\left(\tfrac{\mathrm{d}}{\mathrm{d}x}\theta_0\right)^2 \end{pmatrix}. \tag{4.37}$$

For the background solution of Eq. (3.12) and for $\xi \gg 1$, the off-diagonal elements vanish. Furthermore, on far sub-horizon scales ($x \gg 1$) and far super-horizon scales $x \ll 1$, the diagonals elements approach unity and $2\xi^2/x^2$, respectively. One may be tempted to diagonalize the general expression of M_0, but the diagonalization would be time-dependent and hence re-introduces first-derivatives of $w^{(e)}_{0i}$. We note that the helicity 0 sector is particularly sensitive to non-linear contributions neglected in our analysis so far, arising from two enhanced helicity 2 modes coupling to the helicity 0 modes, see also Eq. (4.53). We will discuss this effect in more detail in Sec. 5.2.

In summary and as anticipated, the modes with helicity ± 1 and ± 2 form four decoupled harmonic oscillators with the time-dependent mass terms specified in Eqs. (4.27), (4.28) and (4.33). The two helicity zero modes form a system of coupled, mass-dependent harmonic oscillators given by Eq. (4.36).

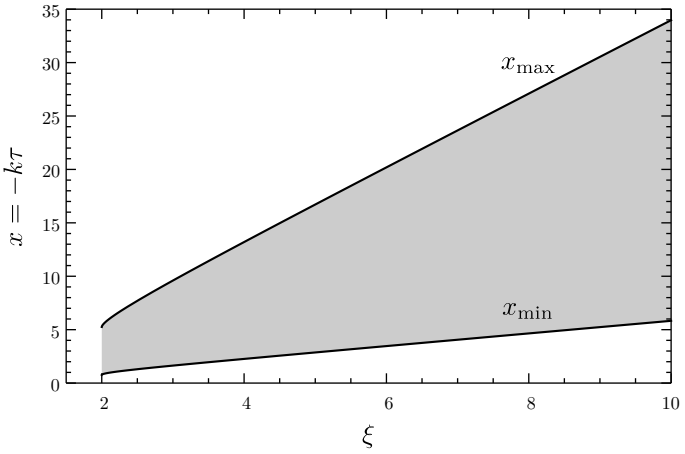

Figure 4.1: Tachyonic region of the +2 mode in a non-Abelian, c_2-background (shaded in gray). Contrary to the Abelian regime, the instability region is bounded from both sides and only affects a single mode.

Stability analysis

Let's look at these fluctuations in two different background limits (taking ξ to be constant): $f(\tau) \to 0$ and $ef(\tau) = c_2\,\xi/(-\tau)$ (see Eq. (3.9)). In the former case, defining $e_{\pm 0}(x) := (e_{01}(x) \mp i e_{02}(x))/\sqrt{2}$, the effective squared mass[12] of $e_{\pm 0}$, $e_{\pm 1}$, and $e_{\pm 2}$ is $1 \mp 2\xi/x$, so that as in the Abelian case, the '$-$' modes are unenhanced, while the '$+$' modes are enhanced for $x < 2\xi$. In this case, the spatial components of the helicity basis simplify to

$$e_{\pm 0} = \frac{1}{2}\begin{pmatrix} 0 & 0 & 0 \\ 0 & 1 & \pm i \\ 0 & \mp i & 1 \end{pmatrix}, \quad e_{\pm 1} = \frac{1}{\sqrt{2}}\begin{pmatrix} 0 & 1 & \pm i \\ 0 & 0 & 0 \\ 0 & 0 & 0 \end{pmatrix}, \quad e_{\pm 2} = \frac{1}{2}\begin{pmatrix} 0 & 0 & 0 \\ 0 & 1 & \pm i \\ 0 & \pm i & -1 \end{pmatrix}. \tag{4.38}$$

On the other hand, for $ef(\tau) = c_2\,\xi/(-\tau)$, the squared mass terms appearing in Eqs. (4.27) and Eq. (4.33) for $w^{(e)}_{-2}(x)$ and $w^{(e)}_{\pm 1}(x)$, respectively, are positive for all $x, \xi > 0$. Similarly the matrix M_0 in Eq. (4.36) is positive definite, as can be immediately checked by verifying that the trace and determinant are always positive. The only mode which can experience a tachyonic instability in a c_2-background is the e_{+2} mode. The mass term for this mode is then given by

$$m^2_{+2} = 1 - \frac{2\xi}{x} + \frac{\xi(\xi - x)}{x^2}\left(1 + \sqrt{1 - 4/\xi^2}\right) \to 1 - \frac{4\xi}{x} + \frac{2\xi^2}{x^2}\,, \tag{4.39}$$

where in the last step we have assumed $\xi \gg 2$. The region in which this mass term becomes tachyonic is shown as gray shaded region in Fig. 4.1 and is given by

$$x_{\min} \equiv \left[1 + c_2 - \sqrt{1 + c_2^2}\right]\xi < x < \left[1 + c_2 + \sqrt{1 + c_2^2}\right]\xi \equiv x_{\max}\,, \tag{4.40}$$

which for $\xi \gg 2$ yields

$$\xi(2 - \sqrt{2}) < x < \xi(2 + \sqrt{2})\,. \tag{4.41}$$

[12]Since we are considering ODEs as a function of x, $\frac{\mathrm{d}^2}{\mathrm{d}x^2}w(x) + m^2 w(x) = 0$, the 'squared mass' is dimensionless quantity.

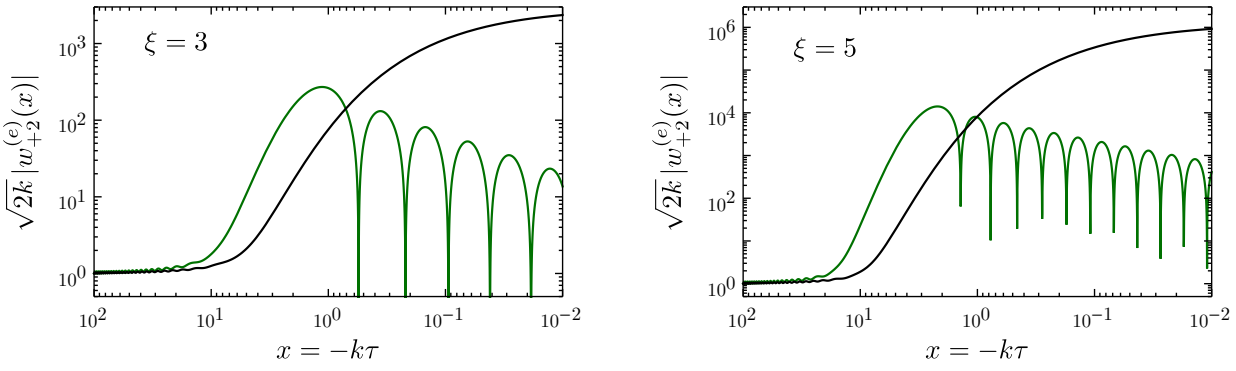

Figure 4.2: Evolution of the helicity +2 mode for $\xi = 3$ (left panel) and $\xi = 5$ (right panel). The black curves correspond to the Abelian regime ($f(\tau) \simeq 0$), the green curves to the non-Abelian regime ($e\,f(\tau) = c_2\xi/(-\tau)$.

In Fig. 4.2 we show the evolution of the helicity +2 mode in both regimes. The initial conditions are set by imposing the Bunch–Davies vacuum on far sub-horizon scales,

$$w^{(e)}_{+2}(x) = \frac{1}{\sqrt{2k}} e^{ix} \qquad \text{for } x \gg 1\,. \tag{4.42}$$

Note that (apart from the normalization factor $1/\sqrt{2k}$) these solutions are only functions of $x = -k\tau$ and ξ. They are in particular independent of the value of the gauge coupling e and the absolute time τ (although of course the slowly varying value of ξ will introduce an implicit dependence on τ).
A key observation here is that in the presence of a vanishing or c_0-type background solution, the helicity +2 mode of the linearized non-Abelian theory behaves very much like the enhanced helicity mode of the Abelian theory, see Fig. 2.1. With this in mind, we will refer to the time before the c_2-solution develops as the 'Abelian regime', in contrast to the 'non-Abelian regime' characterized by the inherently non-Abelian effects induced by the growing c_2-background solution.
In summary, in the Abelian regime ($f(\tau) = 0$), 3 modes become enhanced as soon as $x < 2\xi$. In the non-Abelian regime ($ef(\tau) = c_2\,\xi/(-\tau)$), only a single mode is enhanced. The enhancement occurs earlier (as soon as $x \lesssim \xi(2+\sqrt{2})$) compared to the Abelian regime but contrary to the Abelian regime only lasts for some finite period of time (for $\Delta x \simeq 2\sqrt{2}\xi$). As we will see below, these differences lead to a signifincant changes between the properties of gauge field fluctuations arising in the Abelian and non-Abelian regime. In particular, due to the helicity decomposition, the single enhanced mode of the non-Abelian regime can only source (at the linear level) tensor perturbations (i.e. gravitational waves) but not scalar perturbations (i.e. no curvature perturbations).

Approximate solutions for the enhanced helicity +2 mode

The tachyonically enhanced modes in the Abelian regime have been discussed in much detail in the literature (see Sec. 2.1). Here we focus on the enhanced mode in the inherently non-Abelian regime, i.e. the helicity +2 mode in a c_2 gauge-field background. In the limit of constant ξ, the exact solution

to Eq. (4.28) is given by Eq. (4.30),[13]

$$w_{+2}^{(e)}(\tau) = \frac{e^{\kappa\pi/2}}{\sqrt{2k}} W_{-i\kappa,\,-i\mu}\left(2ik\tau\right) , \tag{4.43}$$

with $\kappa = (1+c_2)\xi \simeq 2\xi$ and $\mu = \xi\sqrt{2c_2 - (2\xi)^{-2}} \simeq \sqrt{2}\xi$. For the c_2 background solution, we derive useful asymptotic expressions in App. F, approximating the enhanced component of Eq. (4.30) on super-horizon scales and around the epoch of maximal enhancement, respectively:

$$\sqrt{2k}\, w_{+2} \simeq 2e^{(\kappa-\mu)\pi}\sqrt{\frac{x}{\mu}}\cos\left[\mu\ln(2x) + \theta_0\right] \qquad \text{for } x \ll x_{\rm min}\,, \tag{4.44}$$

$$\sqrt{2k} w_{+2}(x) \simeq \sqrt{4\pi}\; e^{(\kappa-\mu)\pi}\left(\frac{\zeta(x)}{V(x)}\right)^{1/4} \mathrm{Ai}\left(\zeta(x)\right) \qquad \text{for } x \simeq x_{\rm min}\,, \tag{4.45}$$

with $\mathrm{Ai}(x)$ denoting the Airy Ai function and

$$V(x) = -\left(1 - \frac{2\kappa}{x} + \frac{\mu^2}{x^2}\right) , \qquad \zeta(x) \approx \left(2\mu^2 - 2\kappa x_{\rm min}\right)^{1/3} \ln\left(\frac{x}{x_{\rm min}}\right) . \tag{4.46}$$

These expressions will prove useful to obtain analytical estimates. For details see App. F.

4.4 Including the inflaton and gravitational wave fluctuations

With this understanding of the growth of the gauge field fluctuations, let us now include the scalar and metric tensor fluctuations. The former will couple to the helicity 0 gauge field modes, the latter to the helicity ± 2 modes.

Let us start with the helicity 0 modes. After inserting the constraint equation which now reads

$$-w_0^{(f)}(x) - \sqrt{2}\cos\theta_0 \tfrac{\mathrm{d}}{\mathrm{d}x}\theta_0 w_{02}^{(e)}(x) = -\frac{ik\alpha}{\sqrt{2}e\Lambda}\sin\theta_0^2\delta\phi\,, \tag{4.47}$$

the equations for the dynamical degrees of freedom read

$$\frac{\mathrm{d}}{\mathrm{d}x^2}\begin{pmatrix} w_{01}^{(e)}(x) \\ w_{02}^{(e)}(x) \\ a\delta\phi(x)\end{pmatrix} + N_0^k(x)\frac{\mathrm{d}}{\mathrm{d}x}\begin{pmatrix} w_{01}^{(e)}(x) \\ w_{02}^{(e)}(x) \\ a\delta\phi(x)\end{pmatrix} + \tilde{M}_0^k(x)\begin{pmatrix} w_{01}^{(e)}(x) \\ w_{02}^{(e)}(x) \\ a\delta\phi(x)\end{pmatrix} = 0\,, \tag{4.48}$$

with

$$N_0^k = \frac{\gamma x}{\sqrt{2}}\begin{pmatrix} 0 & 0 & \tan^2\theta_0 \\ 0 & 0 & -\frac{i}{\sqrt{2}}\sin\theta_0\tan^2\theta_0 \\ -\tan^2\theta_0 & -\frac{i}{\sqrt{2}}\sin\theta_0\tan^2\theta_0 & 0\end{pmatrix}, \tag{4.49}$$

$$\tilde{M}_0^k = \begin{pmatrix} (M_0)_{11} & (M_0)_{12} & \frac{\gamma}{\sqrt{2}}\tan^2\theta_0 \\ (M_0)_{21} & (M_0)_{22} & -\frac{i\gamma}{2}\left(\sin\theta_0\tan^2\theta_0 - 2x\cos\theta_0\theta_0'\right) \\ -\sqrt{2}\gamma x\frac{\tan\theta_0}{\cos^2\theta_0}\theta_0' & -\frac{i\gamma x}{16}\frac{(15+\cos(4\theta_0))}{\cos^3\theta_0}\theta_0' & m_{\phi\phi}^2\end{pmatrix}, \tag{4.50}$$

[13] To leading order in $1/\xi$, this expression agrees with the one given in [22]. The discrepancy at higher orders is due to the different background solution chosen (see also discussion in Sec. 3.3).

where $M_0(x)$ is given in Eq. (4.37), $\theta_0' = d\theta_0/dx$, $\gamma = \alpha H/(e\Lambda)$ and

$$m_{\phi\phi}^2 = 1 - \frac{2}{x^2} + \frac{\alpha^2 H^2 x^2}{e^2\Lambda^2}\frac{\sin^6\theta_0}{\sin^2(2\theta_0)} + \frac{V_{,\phi\phi}}{H^2 x^2}\,. \tag{4.51}$$

As long as the gauge coupling is not very small, $e \gg \xi H\alpha/\Lambda$, the coupling between the gauge field modes and the inflaton mode is supressed around horizon crossing, and the two helicity 0 gauge field modes are to good approximation described by the unperturbed system (4.36). Recalling that $\tan\theta_0 = y(x) = ef(\tau)/k$, we note that all off-diagonal terms, including the entire matrix N_0^k, vanish in the absence of a background gauge field, $f(\tau) = 0$. In the case of a gauge field background following the c_2-solution, $\tan\theta_0 = c_2\,\xi/x$, we note that all off-diagonal terms, including the matrix N_0^k, vanish for $x \to \infty$, i.e. in the infinite past, and the matrix $\tilde{M}_0^k$ reduces to the unit matrix, allowing us to impose Bunch Davies initial conditions in the infinite past.

In the opposite regime, on far super-horizon scales, the second term in Eq. (4.51) is responsible for the freezing out of the $\delta\phi$ fluctuations. In the limit $\alpha \to 0$, $x \ll 1$ and $V_{,\phi\phi} \to 0$, the equations of motion for $w_0^{(\phi)} = a\,\delta\phi$ simply reads

$$\left(w_0^{(\phi)}\right)''(x) - \frac{2}{x^2}\,w_0^{(\phi)}(x) = 0\,, \tag{4.52}$$

with the solution $x\,w_0^{(\phi)}(x) = Ax^3 + B$ with the integration constants A and B. For $x \to 0$ this leads to a decaying solution ($A = 1, B = 0$) and a constant solution ($A = 0, B = 1$). This is the usual freeze-out mechanism for scalar (and tensor) fluctuations. Note that the sign in Eq. (4.52) is crucial to obtain a constant solution. The last two terms in Eq. (4.51) could in principle interfere with this freeze-out mechanism, however the last term in ensured to be sub-dominant in slow-roll inflation and the second-last term only becomes large together with all the off-diagonal terms, in which case the full coupled system must be analyzed. We point out that the freeze-out of the inflaton perturbation, $(a\delta\phi) \propto 1/x$ also entails its decoupling from the helicity 0 gauge field modes on super horizon scales.

In the left panel of Fig. 4.3 we show the evolution of these helicity 0 modes for a parameter example of the benchmark scenario of the next section. Here $w_0^{(\phi)}$ denotes the coefficient of the co-moving scalar mode ($a\,\delta\phi$). We clearly see the freeze-out of the inflation fluctuations after horizon crossing. The oscillations visible on sub-horizon are induced by the time-dependence of the eigenstates of the system. We have verified that the sum of the absolute value squared of all three states is x-independent as expected in this regime.[14]

Contrary to Refs. [4, 22], we do not find any enhanced or instable scalar mode here for any value of ξ. Neglecting the first derivative terms in Eq. (4.36), this can be checked explicitly by investigating the positive definiteness of the matrix $\tilde{M}_0$ in Eq. (4.50). On sub-horizon scales, this matrix is safely positive definite, on super-horizon scales the loss of positive definiteness indicates the freeze-out of the inflaton perturbations. This picture however changes for much smaller gauge couplings, as required for the magnetic drift regime of Refs. [4, 22] (see Sec. 3.3). In this case and for $\xi \lesssim 2.12$, the trace of $\tilde{M}_0$ becomes negative already at $x \gg 1$, triggering an extremely enhanced scalar mode. This

[14] The time-dependence of these (interacting) eigenstates induces some ambiguity when imposing the Bunch Davies initial conditions at any finite value of x. We have verified that our final results are not affected by this.

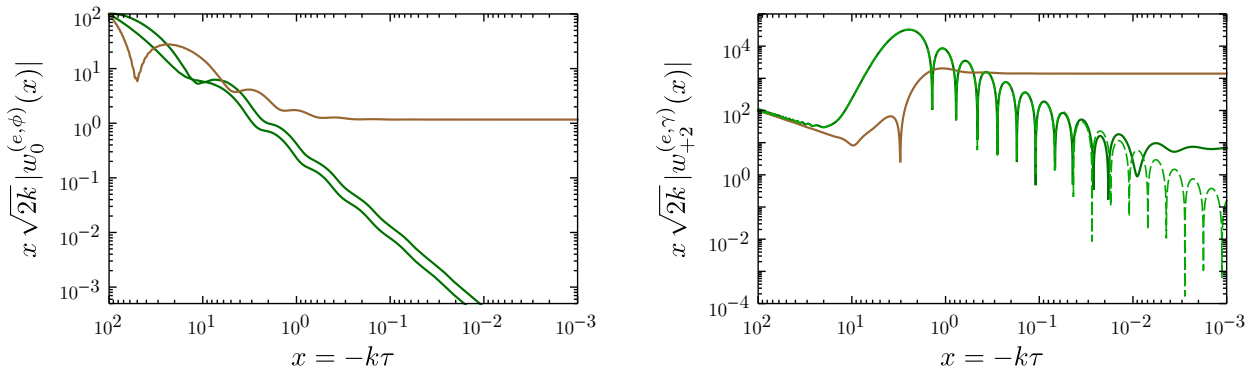

Figure 4.3: Evolution of the (physical) scalar and tensor fluctuations in a c_2-type background solution. **Left panel**: Helicity 0 modes of the gauge field (dark green) and of the inflaton (brown). **Right panel**: Helicity +2 modes of the gauge field (dark green) and the metric tensor (brown). For reference, the dashed green curve shows the gauge field mode in the absence of a coupling to the metric tensor mode. Here we have set $\xi = 5$, $e = 5 \times 10^{-3}$, $H = 10^{-5} M_P$, $\alpha/\Lambda = 30$. Moreover, working in slow-roll approximation, we have set $V_{,\phi\phi} = 0$.

corresponds precisely to the catastrophic instability observed in [4] for $m_g > 2H$, where in our notation $m_g = \sqrt{2} e f(\tau)/a \mapsto \sqrt{2} c_2 \xi H$.

Our study so far is based on the linearized system of equations given in Sec. 4.1, which forbids a coupling between the enhanced helicity +2 mode and the helicity 0 modes. To higher orders in δA, this is not longer true since two tensor mdoes can combine into a scalar mode. Schematically, e.g. a term bi-linar in A in the action can be expressed as

$$\text{linear: } f \cdot w_0^{(e)} + h.c.\,, \qquad \text{quadratic: } |w_{+2}^{(e)}|^2 \tag{4.53}$$

at the linearized level and to next order, respectively. With $\delta A \sim |w_{+2}^{(e)}| \gg |w_0^{(e)}|$, the condition $\delta A \ll f(\tau)$ is not sufficient to insure that the linear term is the dominant one. In fact, this observation is well known in the case of Abelian axion inflation, where the backreaction of the enhanced gauge fields mode occurs precisely true the $(\delta A)^2 \to \delta\phi$ process. Generalizing the procedure of Refs. [12] (see also [7]) to the non-Abelian case, we will estimate the contribution to the scalar power spectrum arising from the non-linear contributions in Sec. 5.2.[15]

Next we turn to the helicity ± 2 modes, i.e. the gravitational waves γ_{ij} coupled to the $e_{\pm 2}$ gauge field modes. We express the metric tensor perturbations in the helicity basis as

$$a\,\gamma_{ij} = \frac{1}{2} \sum_{\lambda=\pm 2} w_{\pm 2}^{(\gamma)}(x) \begin{pmatrix} 0 & 0 & 0 \\ 0 & \mp i & 1 \\ 0 & 1 & \pm i \end{pmatrix} . \tag{4.54}$$

[15] In the Abelian limit, these non-linear contribution are also responsible for a friction-type backreaction of the produced gauge fields on the background equation for the inflaton, see Eq. (2.4). On the contrary, in the non-Abelian regime (and in particular for the parameter example studied in the next section), the corresponding contribution is subdominant to the gauge field background contribution, given by the last term in Eq. (3.37), as long as $\delta A \ll f(\tau)$.

The equations of motion are then given by

$$\frac{\mathrm{d}}{\mathrm{d}x^2}\begin{pmatrix} w_{\pm 2}^{(e)}(x) \\ w_{\pm 2}^{(\gamma)}(x) \end{pmatrix} + N_{\pm 2}(x)\frac{\mathrm{d}}{\mathrm{d}x}\begin{pmatrix} w_{\pm 2}^{(e)}(x) \\ w_{\pm 2}^{(\gamma)}(x) \end{pmatrix} + M_{\pm 2}(x)\begin{pmatrix} w_{\pm 2}^{(e)}(x) \\ w_{\pm 2}^{(\gamma)}(x) \end{pmatrix} = 0\,, \tag{4.55}$$

with

$$N_{\pm 2}(x) = \frac{y'(x)Hx}{e}\begin{pmatrix} 0 & -1 \\ 4 & 0 \end{pmatrix}\,, \tag{4.56}$$

$$M_{\pm 2}(x) = \begin{pmatrix} 1 \mp \frac{2\xi}{x} + 2(\frac{\xi}{x} \mp 1)y(x) & \frac{H}{e}\left(-y'(x) - (2\xi \mp x)y(x)^2 + xy(x)^3\right) \\ -\frac{4Hxy(x)^2}{e}(y(x) \mp 1) & 1 - \frac{2}{x^2} + \frac{2H^2x^2}{e^2}\left(y(x)^4 - y'(x)^2\right) \end{pmatrix}\,. \tag{4.57}$$

where $y' \equiv \frac{\mathrm{d}}{\mathrm{d}x}y(x)$. In the large-$\xi$ limit of the c_2-solution, $y(x) = \xi/x$, this becomes

$$N_{\pm 2}(x) = \frac{H\xi}{ex}\begin{pmatrix} 0 & -1 \\ 4 & 0 \end{pmatrix}\,, \tag{4.58}$$

$$M_{\pm 2}(x) = \begin{pmatrix} 1 \mp 4\frac{\xi}{x} + 2\frac{\xi^2}{x^2} & \frac{H\xi}{ex^2}\left(\pm 1 + x\xi \mp \xi^2\right) \\ \frac{4H\xi^2}{ex^2}\left(\pm x - \xi\right) & 1 - \frac{2}{x^2} + \frac{2H^2\xi^2}{e^2x^2}(-1 + \xi^2) \end{pmatrix}\,. \tag{4.59}$$

We recognize the tachyonic instability in the +2 gauge field mode in the top left entry of M_{+2}, leading to an exponential growth for this mode for $(2-\sqrt{2})\xi \leq x \leq (2+\sqrt{2})\xi$. In the bottom right corner we find the (helicity conserving) mass for the metric tensor mode. Here the first term accounts for the free oscillation on sub-horizon scales, whereas the second term is responsible for the freeze-out on super-horizon scales. The last term is the source term arising from the background gauge field, see first term on the righthand side of Eq. (4.15), and contributes a positive mass term for $\xi > 2$. Similar to the helicity 0 case discussed above, the system reduces to $N_{\pm 2} = 0$ and $M_{\pm 2} = \mathbb{1}$ in the far past as $x \to \infty$. For sub-horizon modes ($x > 1$), the off-diagonal elements are small as long as $eM_P \ll H$, ensuring that the gauge field modes are well described by Eqs. (4.27) and (4.28). See also right panel of Fig. 4.3.

Finally, let us perform an analytical estimate of the super-horizon amplitude of the enhanced gravitational waves mode in the large-ξ limit. For $x \leq 1$, freeze-out of the gravitational wave implies $w_{+2}^{(\gamma)}(x) \propto 1/x$ and hence $\frac{d^2}{dx^2}w_{+2}^{(\gamma)}(x) = 2/x^2 w_{+2}^{(\gamma)}(x)$, thus precisely canceling the second term of the bottom right element of $M_{\pm 2}$. For $x \leq 1$, the gauge field mode $w_{+2}^{(e)}$ is well described by the solution (4.44), implying that $\overline{(w_{+2}^{(e)})'(x)} \sim \xi/x\,\overline{w_{+2}^{(e)}(x)}$ where the bar indicates an averaging over the (co)sine. With this we see that the off-diagonal first derivative term is suppressed by a factor ξ^2 compared to the off-diagonal mass term, and the equation of motion for $w_{+2}^{(\gamma)}(x)$ at $x = 1$ reads

$$-\frac{4H\xi^3}{e}w_{+2}^{(e)}(x=1) \simeq \left(1 + \frac{2H^2\xi^4}{e^2}\right)w_{+2}^{(\gamma)}(x=1)\,. \tag{4.60}$$

If furthermore $H\xi^2 \ll e$, we can immediately obtain the value of the gravitational wave mode at (and beyond) horizon crossing as

$$x\,w_{+2}^{(\gamma)}(x)\big|_{x\geq 1} = -\frac{4H\xi^3}{e}w_{+2}^{(e)}(x=1) \simeq -\frac{2H\xi^{5/2}}{e}\frac{2^{3/4}}{\sqrt{2k}}e^{(2-\sqrt{2})\pi\xi}\,, \tag{4.61}$$

where in the last step we have inserted Eq. (4.44), replacing the cosine with a factor of 1/2. For the parameter point of Fig. 4.3 this yields $\sqrt{2k}\, x\, w_{+2}^{(\gamma)}(x)\big|_{x\geq 1} \simeq 3.7 \times 10^3$, agreeing with the full numerical solution up to an order one factor. We emphasize that due to helicity conservation only one of the two metric tensor modes is enhanced in this manner, resulting in a chiral gravitational wave spectrum.
In a similar manner, the 'freeze-out'-like behaviour visible for the gauge field modes in Fig. 4.3 can be traced back to the coupling to the metric tensor perturbation through to top-right element of M_{+2}. On far super-horizon scales, the contribution from the frozen gravitational wave mode becomes comparable to the contribution from the decaying gauge field modes in the in the equation of motion for the gauge fields. In this regime, the derivative terms are supressed by a factor of ξ^{-2} compared to the M_{+2} terms. The amplitude of $w_{+2}^{(e)}$ can then be estimated by comparing the two terms in the first line of M_{+2} to get

$$w_{+2}^{(e)}(x \to 0) \simeq \frac{H\xi}{2e} w_{+2}^{(\gamma)}(x \to 0)\,, \tag{4.62}$$

For the parameter point of Fig. 4.3 this yields $w_{+2}^{(e)}(x \to 0) \simeq 10^{-2} \times w_{+2}^{(\gamma)}(x \to 0)$, in good agreement with the full numerical result. For the parameter example of this paper, the contribution of the these far super-horizon modes to both the energy and variance of the gauge fields is negligible, due to a suppression both in amplitude and momentum compared to the modes crossing the horizon at the same time. Consequently, these are well described by employing the solutions of Eq. (4.28). On the other hand, if the gauge coupling is very small, this description is no longer accurate and the gauge and gravity sector need to be treated as a fully coupled system. In this regime, the gauge field/gravity interactions induce an exchange of energy between the $e_{\pm 2}$ modes and gravitational waves [43, 44].
Both the scalar and tensor sector preserve the usual scaling behaviour of de Sitter space. In the limit of constant H and ξ, we obtain a scale invariant scalar and tensor power spectrum. The slow variation of H and ξ obtained in any realistic inflation model will lead to deviations from this exact scale invariance. We will discuss this in more detail in the next section.

5 A worked example

To illustrate the results obtained so far, we will discuss an explicit parameter example in this section. The most natural scalar potential for an axion is a periodic potential, breaking the shift symmetry of the axion down to a discrete symmetry due to non-perturbative effects,

$$V = V_0 \left[1 - \cos\left(\frac{\phi}{f_\phi}\right)\right] \simeq \frac{1}{2} m^2 \phi^2 - \frac{\lambda}{4}\phi^4\,. \tag{5.1}$$

In the following we will take $m = 7.5 \times 10^{-6}\ M_P$ and $\lambda = 1.1 \times 10^{-13}$ (corresponding to $V_0^{1/4} \simeq 8.3 \times 10^{-3}\ M_P$ and $f_\phi \simeq 9.2\ M_P$). This parameter choice ensures the correct normalization of the scalar power spectrum at CMB scales as well as a tensor-to-scalar ratio in agreement with the Planck data [2].[16] The remaining parameters are then the gauge field inflaton coupling α/Λ which directly controls the size of the parameter ξ and the gauge coupling e. In the following we choose $\alpha/\Lambda = 30$ and $e = 5 \times 10^{-3}$. As described in more detail below, the value of the gauge coupling is chosen to minimize

[16] For a discussion of the impact of different types of scalar potentials in Abelian axion inflation, see Ref. [16].

artifacts of our matching procedure between the Abelian and non-Abelian regime and the value of α/Λ is chosen so as to place the phenomenologically interesting regime within the observable last 55 e-folds of inflation. A generalization of this setup is briefly discussed at the end of Subsection 5.1.
The discussion in this section is organized as follows. In Subsection 5.1 we will discuss the growth of the gauge field fluctuations with particular emphasis on the tachyonic modes as well as their back-reaction on the homogeneous background field. Upon determining the range of validity of our linearized approach, we turn to the scalar and tensor power spectra in Subsection 5.2.

5.1 Growth of gauge field fluctutions

We first recall some key results about the homogeneous background evolution and the gauge field fluctuations from the previous sections:

- In single field inflation models, and in particular for the scalar potential considered here, the inflaton velocity $\dot{\phi}$ and hence the parameter ξ increases during inflation.
- In the far past, for $\xi \to 0$, the only stable solution for a classical isotropic gauge field background is the zero solution. General solutions are described by small perturbations around the zero solution.
- As long as the homogeneous background is sufficiently small, three of the six gauge field modes are tachyonically enhanced, corresponding to three copies of the Abelian limit described in Sec. 2.1 (see Fig. 4.2). In this Abelian limit, the variance $\langle A_{\rm ab}^2 \rangle^{1/2}$ grows exponentially with ξ and is well described by Eq. (2.11).
- When $\xi \geq 2$, a second stable, growing background solution develops (see Sec. 3). We refer to this growing solution as the "c_2-solution." It becomes possible that at some point, large fluctuations arising from the tachyonically enhanced modes will push the background away from the zero solution and towards the c_2-solution.
- The transition from an approximately-zero homogeneous background field to a growing background solution occurs once the fluctuations become large enough to trigger the c_2-solution, $e\langle A_{\rm ab}^2 \rangle^{1/2} \sim \xi/(-\tau)$, see Eq. (3.20).[17] This is depicted by the solid black line in Fig. 5.1.
- As the background grows, we enter the non-Abelian regime. In this regime, the background field evolves towards the isotropic c_2-solution where only the helicity +2-mode is enhanced.

[17] Eq. (3.20) marks the boundary to the oscillatory regime, from where c_i-type solutions spiral inwards to their asymptotic c_i values. As Fig. 3.3 illustrated, for sufficiently large ξ the c_2 solution becomes overwhelmingly likely. In the unlikely event that the classical background begins to evolve towards a c_0 solution, the gauge field background would be continued to be dominated by $\langle A_{\rm ab}^2 \rangle^{1/2}$, growing according to Eq. (2.11). The resulting stochastic initial conditions will eventually trigger a c_2-type background. Numerically, the condition $e\langle A_{\rm ab}^2 \rangle^{1/2} \sim \xi/(-\tau)$ is basically equivalent to requiring that the magnitude of the fluctuations be of the same order as the c_2 solution and very similar to the requirement of Eq. (2.18). This 'matching condition' is conservative in the sense that even smaller fluctuations which reach the c_1 saddle point solution (see Sec. 3.1.2) could (classically) evolve towards the c_2-solution. This is depicted by the dotted blue line in Fig. 5.1.

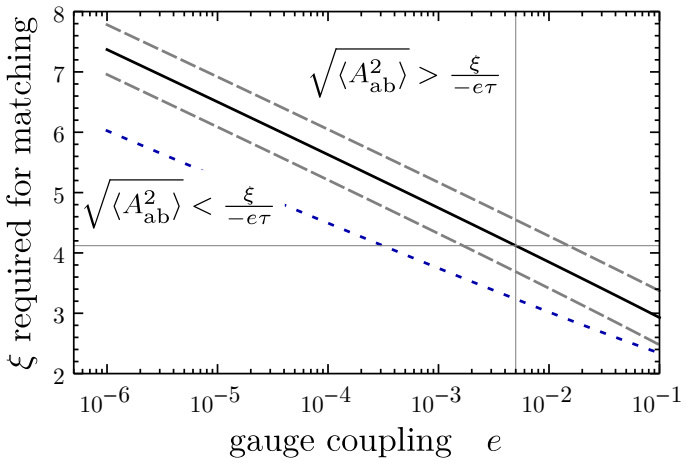

Figure 5.1: Values of ξ required to match the Abelian and non-Abelian regime as a function of the gauge coupling e. The horizontal and vertical gray lines indicates the parameter point used in this section. For reference, the dashed gray lines indicate modified matching conditions, $\langle A^2_{\rm ab}\rangle^{1/2} = \mathcal{N}\xi/(-\tau e)$ with $\mathcal{N} = \{1/3, 3\}$ parametrizing the theoretical uncertainties in the matching condition, see text. The dotted blue line indicates where $\langle A^2_{\rm ab}\rangle^{1/2}$ can reach the unstable c_1 background solution (see Sec. 3.1.2).

Based on these observations, our strategy will be the following: (i) As long as the Abelian variance $\langle A^2_{\rm ab}\rangle^{1/2}$ as given in Eq. (2.11) is much smaller than $\xi/(-\tau e)$ we work in the Abelian limit with $f(\tau) = 0$. (ii) When $\langle A^2_{\rm ab}\rangle^{1/2} \simeq \xi/(-\tau e)$ we take $f(\tau)$ to be given by the c_2-solution (3.12). We match $\phi(\tau)$ and $\phi'(\tau)$ at this point, but turning on the term on the right-hand side of Eq. (2.4) will cause a discontinuity in $\phi''(\tau)$.[18] We ensure that for the parameter point we consider this term is sub-dominant, so as to limit any unphysical effects here. (iii) We compute the evolution of all degrees of freedom in this background, tracking each mode from the sub- to the super-horizon regime. Note that for smaller values of the gauge coupling, the transition from the Abelian to the non-Abelian regime at $e\langle A^2_{\rm ab}\rangle^{1/2} = \xi/(-\tau)$ requires larger values of ξ, see Fig. 5.1.

Several comments are in order. Firstly, our matching procedure from the Abelian to the non-Abelian regime should be seen as a rough order-of-magnitude estimate only, and the results for the evolution of the background and of the fluctuations in this transition regime should be treated with care accordingly. Secondly, the linearization we are using is justified as long as $\langle \delta A^2\rangle^{1/2} \ll f(\tau)$. Once the growth of the e_{+2} mode overcomes the background evolution, a different treatment of the gauge field background becomes necessary, which is beyond the scope of this paper.

In Fig. 5.2, we depict the evolution of the homogeneous inflaton background in the Abelian (solid black curve) and in the non-Abelian regime (solid orange curve), obtained be numerically solving Eq. (3.37) with $f(\tau)$ set to 0 and to $c_2\,\xi/(-e\tau)$ in the two regimes, respectively. The matching point $\langle A^2_{\rm ab}\rangle^{1/2} = c_2\,\xi/(-e\tau)$ is indicated by the horizontal and vertical gray lines. For reference, we also show the evolution in the absence of the inflaton - gauge field coupling (dashed blue curve). The

[18] In the Abelian regime, the corresponding term is given by the right-hand side of Eq. (2.4) after inserting Eq. (2.10). For the parameter point discussed in this section, this is about a factor 10 smaller than the non-Abelian expression at the matching point.

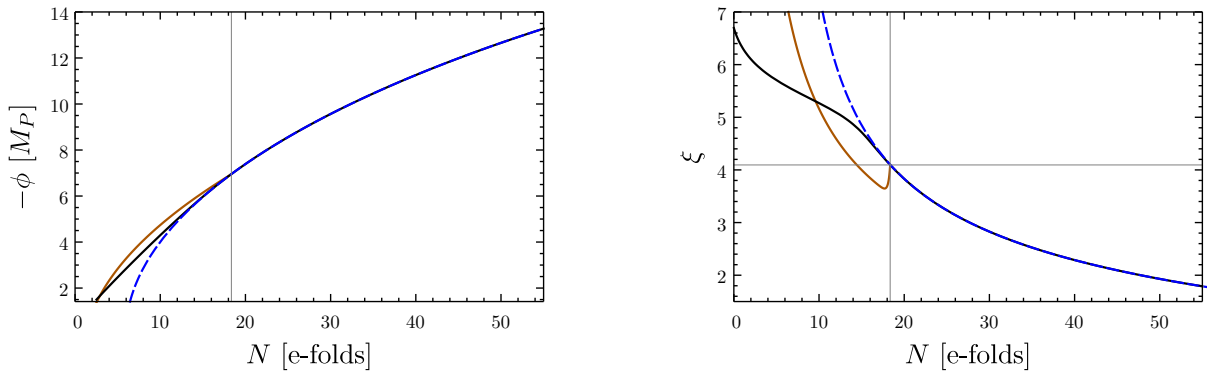

Figure 5.2: Evolution of the inflaton field ϕ for $\alpha/\Lambda = 0$ in the absence of the inflaton - gauge field coupling (dashed blue), in the Abelian limit ($\alpha\Lambda = 30$, $e = 0$, solid black) and including including non-Abelian effects in the weak coupling limit ($\alpha\Lambda = 30$, $e = 5 \times 10^{-3}$, solid orange). The gray lines indicate the matching between the Abelian and non-Abelian regime as detailed in the text.

x-axis of Fig. 5.2 is labeled in e-folds, $dN = -Hdt$, where we use the convention that inflation ends at $N = 0$ and the CMB scales exit the horizon at $N \simeq 55$.

The right panel of Fig. 5.2 shows the velocity of ϕ, encoded by the parameter ξ. After the matching, the velocity drops abruptly, since turning on the background gauge field enhances the gauge-field induced term in the inflaton equation of motion. The details are sensitive to the matching procedure we invoke, and for our computations of the scalar and tensor power spectra in Sec. 5.2 we will therefore exclude a few e-folds around this transition regime.

More importantly, after this transition regime the last term in Eq. (3.37) in only proportional to ξ^3 instead of being exponentially sensitive to ξ as in the Abelian regime (see Eq. (2.10)). Consequently, the dominant terms in the equation for ϕ in this regime are the second and third term of Eq. (3.37), and, similar to the the situation in the absence of the gauge field - inflaton coupling, $\xi \propto \sqrt{\varepsilon} \propto 1/\sqrt{N}$ [16] (see also Sec. 3.3). This in particular implies that in this regime we are not in the 'magnetic drift regime' studied in [22], which is characterized by the gauge friction dominating over the Hubble friction.

Next we consider the evolution of the gauge field fluctuations in this background. From the discussion in the previous chapter, we know that the helicity +2 mode captures the enhancement both in the Abelian and in the non-Abelian regime. For simplicity, we will restrict our discussion here to this mode, however we have checked numerically that including the full system does not lead to any significant changes. In de Sitter space, any mode with co-moving momentum k exits the horizon at $k = aH = -x/\tau$, where to good approximation $3H^2M_P^2 = V(\phi)$. Setting $a = 1$ at the end of inflation, this implies that at e-fold N, the mode $k_N = \exp(-N)H$ exits the horizon. In Fig. 5.3 we show the evolution of six modes which exit the horizon in the Abelian regime (left panel) and in the non-Abelian regime (right panel). The gradual change within each panel is due to the evolving background, i.e. the slow increase of ξ.

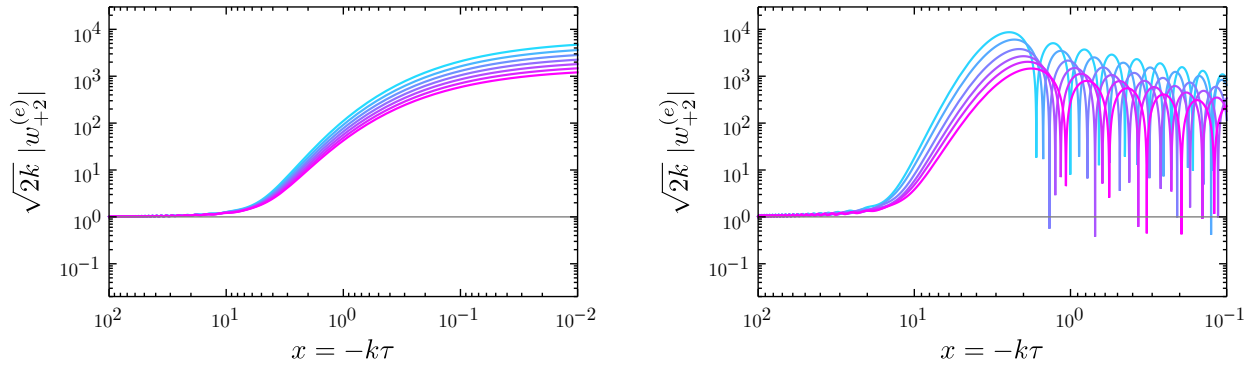

Figure 5.3: Evolution of the helicity +2 mode in a dynamical background. **Left panel**: Abelian regime, modes exiting at $N = 25, 26 \ldots 31$. **Right panel**: Non-Abelian regime, modes exiting at $N = 8, 9, \ldots 13$. In both panels, the k increases from purple to blue. Parameters as in Fig. 5.2.

Since the change of ξ is slow, we can estimate the variance of these fluctuations by

$$\langle \delta A^2 \rangle_N \simeq \int \frac{d^3k}{(2\pi)^3} |w^{(e)}_{+2,k_N}(\tau)|^2 = \frac{1}{(-\tau)^2} \int \frac{xdx}{2\pi^2} |\sqrt{k_N} w^{(e)}_{+2,k_N}(\tau)|^2 \,. \tag{5.2}$$

In the left panel of Fig. 5.4 we show the resulting variance (green dots), together with the homogeneous background solution $f(\tau)$ (solid blue). In the Abelian regime, the semi-analytical expression Eq. (2.11) (shown as dashed green line) gives a good approximation over most of this regime. The deviation at large N simply reflects that our fitting formula (2.11) is not optimized for very small values of ξ, whereas the deviations a few e-folds before the matching point reflect that the super-horizon parts of these modes are effected by the non-Abelian regime, which leads to a suppression of the variance. In the following analysis we will exclude the modes which exit the horizon within 3 e-folds before or after the matching point, so as to minimize artifacts introduced by the specific matching procedure. To illustrate the uncertainties involved, the gray curves indicate the variance we obtain in the transition region with the matching procedure above (dashed gray curve) and by imposing the matching at a later point (dotted gray curve), as indicated by the vertical dashed line.

In the non-Abelian regime, the fluctuations are initially suppressed compared to the Abelian case, due to a combination of two effects: Firstly, as is evident from Fig. 5.2, the parameter ξ, which controls the tachyonic instability in the helicity +2 gauge field mode, initially drops after switching on the background gauge field. Secondly, in the non-Abelian regime the variance grows more slowly as a function of ξ, c.f. right panel of Fig. 5.4.

Once the fluctuations reach values close to the background field we cannot trust our treatment anymore, since the motion of the background field is now no longer determined by its classical motion.[19] This regime calls for a dedicated lattice simulation to capture the non-linear effects. In the left panel of Fig. 5.4 this happens shortly before the end of inflation, at $N \simeq 10$. Note however that in Eq. (5.2)

[19]We note that the perturbativity criterion employed in [28] (see also [32, 45]), which measures the fluctuations per logarithmic frequency interval, $(\frac{d}{d\ln k}\langle \delta A^2 \rangle^{1/2})/f$ is less restrictive. This quantity does not exceed the percent level in the entire regime depicted in Fig. 5.4. This may indicate the possibility of pushing the linearized analysis somewhat further than the conservative cut-off implemented in this analysis.

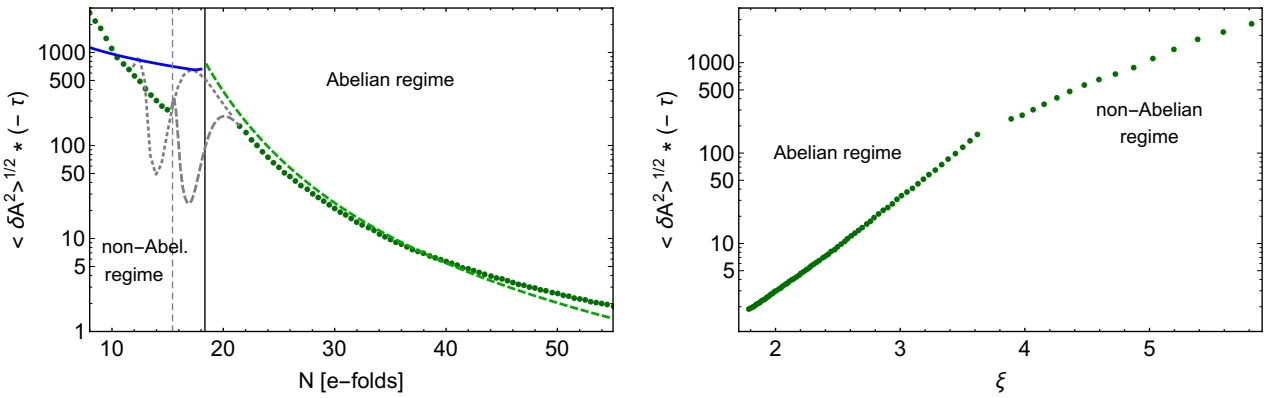

Figure 5.4: Magnitude of the gauge fields. Background solution $f(\tau)$ (blue) and estimated variance of the fluctuations (green). The solid vertical line denotes the matching point. The gray dashed lines are auxiliary quantities as described in the text. Same parameters as in Fig. 5.2.

we are overestimating the variance, since we are integrating over the super-horizon part of the mode $w^{(e)}_{+2,k_N}(\tau)$, whereas we should taking the super-horizon contributions of the modes which crossed the horizon accordingly earlier, at correspondingly smaller ξ. We thus consider it plausible that our estimate for the end of inflation at $N \simeq 0$ is relatively accurate. More reliable results can be obtained for smaller gauge - inflaton couplings α/Λ, where the matching condition occurs closer to the end of inflation. However, given the approximate nature of our matching condition, we refrain from attempting to achieve more precise results here.

The results in this section were obtained for the parameter choice given below Eq. (5.1). The parameters of the scalar potential, m and λ, are directly related to the CMB observables and do not impact the discussion of this section much. On the other hand, the coupling parameters α/Λ and e are crucial for our discussion. Increasing α/Λ increases ξ at the CMB scales and consequently leads to an earlier transition to the non-Abelian regime. Current observations constrain $\xi_{\rm CMB} \lesssim 2.5$ in the contest of Abelian axion inflation [7]. Increasing the gauge coupling e leads to a lower threshold of ξ to trigger the non-vanishing gauge field background, see Fig. 5.1. Correspondingly, the transition happens earlier and also more smoothly, since the gauge field source term in the inflaton equation of motion (3.37), proportional to ξ^3/e^2 when inserting the c_2-solution, is less important.

5.2 Scalar and tensor power spectra

We now turn to the scalar and tensor power spectra of the benchmark model of the previous section, the key observables of any inflation model (for a review, see [46]):

$$\langle \zeta_{\vec{k}} \zeta'_{\vec{k}} \rangle = (2\pi)^3 \delta(\vec{k}+\vec{k}') \mathcal{P}_\zeta(k)\,, \tag{5.3}$$

$$\langle h^\lambda_{\vec{k}} h^{\lambda'}_{\vec{k}'} \rangle = (2\pi)^3 \delta(\vec{k}+\vec{k}') \delta_{\lambda\lambda'} \mathcal{P}_{h^\lambda}(k)\,. \tag{5.4}$$

Identifying the Mukhanov variables which are canonically normalized on far sub-horizon scales as $v^\zeta = (a\,\delta\phi)$ and $v^h = (a\gamma)$ for scalars and tensors, respectively, the power spectra read

$$\mathcal{P}_\zeta(k) = \left(\frac{H}{\dot\phi}\right)^2 \left(\frac{|v_k^\zeta(x)|}{a}\right)^2 , \tag{5.5}$$

$$\mathcal{P}_{h^\lambda}(k) = \left(\frac{2}{M_P}\right)^2 \left(\frac{|v_k^h(x)|}{a}\right)^2 , \tag{5.6}$$

where ζ denotes the gauge invariant curvature perturbation and λ denotes the helicity of the gravitational wave h^λ. Due to the freeze-out of $(a\delta\phi)$ and $(a\gamma)$ on super-horizon scales (see Sec. 4.4), it suffices to evaluate these power spectra at horizon crossing ($x = 1$). Since at this point in time the coupling to the gauge fields can be very relevant, we perform this task numerically, solving the mode equations Eq. (4.48) and (4.55) in the evolving background discussed in Sec. 5.
Recalling that $\sqrt{2k}\, v_k^{\zeta,h}(x)$ is a function of x only, it is convenient to introduce

$$\Delta_s^2 = \frac{k^3}{2\pi^2}\mathcal{P}_\zeta(k)\,, \qquad (\Delta_t^\lambda)^2 = \frac{k^3}{2\pi^2}\mathcal{P}_{h^\lambda}(k)\,, \tag{5.7}$$

such that

$$\Delta_s^2 = \left(\frac{H_*}{2\pi_*}\right)^2 \left(\frac{H_*}{\dot\phi_*}\right)^2 \left(\sqrt{2k}\, x\, |w_0^{(\phi)}(x)|\right)^2 \Big|_{x\ll 1} , \tag{5.8}$$

$$(\Delta_t^\pm)^2 = \left(\frac{H_*}{2\pi}\right)^2 \left(\frac{2}{M_P}\right)^2 \left(\sqrt{2k}\, x\, |w_{\pm 2}^{(\gamma)}(x)|\right)^2 \Big|_{x\ll 1} , \tag{5.9}$$

where H_* and $\dot\phi_*$ denote the Hubble parameter and inflaton velocity at the point in time when the mode in question crosses the horizon ($x = 1$). To ensure that we are fully in the freeze-out regime, the last parenthesis in Eqs. (5.8) and (5.9) is evaluated at $x = 0.1$.

5.2.1 Scalar power spectrum

The scalar power spectrum computed in this way is subject to the caveat of Eq. (4.53). Generalizing the procedure of Ref. [12] (see also [7]) to the non-Abelian case, we can obtain an estimate for the full scalar power spectrum. For simplicity, let us consider only the helicity 0 mode associated with $\delta\phi$, whose coupling to $\langle F\tilde F\rangle$ in the action contains a coupling to two enhanced helicity +2 gauge field modes. In real space, the equation of motion for $\delta\phi$ reads,

$$\ddot{\delta\phi} + 3H\dot{\delta\phi} - \frac{\nabla^2}{a^2}\delta\phi + m_{\phi\phi}^2\delta\phi = -\frac{\alpha}{4\Lambda}\delta(\langle F\tilde F\rangle)\,, \tag{5.10}$$

where we have neglected here the couplings to the helicity 0 gauge field modes, which are discussed in depth in Sec. 4.4. The right-hand side is the variation of the Chern-Simons term with respect to the average value entering in the 0th order equation, taking also into account the $\dot\phi$-dependence of $\langle F\tilde F\rangle$ through the parameter ξ,

$$\delta(\langle F\tilde F\rangle) = [F\tilde F - \langle F\tilde F\rangle]_{\delta\phi=0} + \frac{\partial\langle F\tilde F\rangle}{\partial\dot\phi}\dot{\delta\phi}\,. \tag{5.11}$$

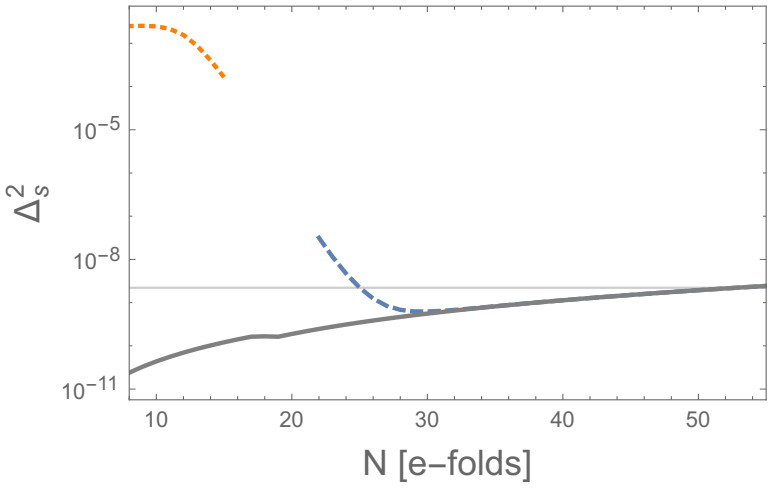

Figure 5.5: Scalar power spectrum. Our semi-analytical estimate (5.16) in the non-Abelian regime is shown as dotted orange line. For reference, we show the standard contribution of the vacuum fluctuations which also well describe the results of the linearized analysis (solid gray) and the (non-linear) contribution in the Abelian regime (dashed blue). Same parameters as in Fig. 5.2.

As demonstrated in App. C, this can be re-expressed as

$$\delta(\langle F\tilde{F}\rangle) = \frac{H^4}{\pi^2} e^{2\pi(\kappa-\mu)} \left[\left(\frac{\tilde{T}_1 + \tilde{T}_2}{5} \right)^{1/2} + \frac{2\pi\alpha(\kappa-\mu)}{2\Lambda\xi}\, \tilde{T}_0\, \delta\phi \right] . \tag{5.12}$$

with

$$\tilde{T}_1 = 0.0082 \cdot \xi^8 \,, \quad \tilde{T}_2 = 0.051 \cdot \xi^6 \,, \quad \tilde{T}_0 = -0.24 \cdot \xi^3 \,, \tag{5.13}$$

where κ and μ are defined below Eq. (4.43). Around horizon crossing, neglecting the slow-roll supressed term proportional to $m^2_{\phi\phi}$ and using $\dot{\delta\phi} \simeq H\delta\phi$, we obtain

$$\delta\phi \simeq \frac{-\frac{e^{2\pi(\kappa-\mu)}}{12\pi^2} \frac{\alpha}{\Lambda} H^2 \sqrt{\frac{\tilde{T}_1+\tilde{T}_2}{5}}}{1 + \frac{e^{2\pi(\kappa-\mu)}}{24\pi^2} \left(\frac{\alpha}{\Lambda}\right)^2 \frac{2\pi(\kappa-\mu)}{\xi} H^2 \tilde{T}_0} \,, \tag{5.14}$$

which for sufficiently large ξ, when the right-hand side dominates Eq. (5.10) simply becomes

$$\delta\phi \simeq \frac{-2\xi\Lambda}{2\pi\alpha(\kappa-\mu)} \left(\frac{\tilde{T}_1 + \tilde{T}_2}{5} \right)^{1/2} \frac{1}{\tilde{T}_0} \,, \tag{5.15}$$

and hence

$$\left(\Delta_s^2\right)^{\rm 2nd} \sim \left(\frac{H}{\dot{\phi}} \delta\phi \right)^2 \simeq \begin{cases} \left(\frac{\alpha H}{2\pi\Lambda}\right)^4 \frac{\tilde{T}_1+\tilde{T}_2}{180\,\xi^2} e^{4\pi(\kappa-\mu)} & \text{for } \xi^3 e^{2\pi(\kappa-\mu)} \ll 270 \left(\frac{\Lambda}{\alpha H}\right)^2 \\ \frac{\tilde{T}_1+\tilde{T}_2}{5\,\tilde{T}_0^2} \left[2\pi(\kappa-\mu)\right]^{-2} & \text{for } \xi^3 e^{2\pi(\kappa-\mu)} \gg 270 \left(\frac{\Lambda}{\alpha H}\right)^2 \end{cases} . \tag{5.16}$$

We note that initially, for small values of ξ, this grows as $\exp[4\pi(\kappa-\mu)] \simeq \exp[4\pi\xi(2-\sqrt{2})]$ whereas for large values of ξ we find the same $1/\xi^2$ dependence as in the Abelian case [12]. The total scalar power spectrum is the sum of the vacuum contribution (5.8) and the contribution sourced by the

enhanced gauge field mode (5.16).[20] In Fig. 5.5, we show the resulting estimate for scalar spectrum in the non-Abelian regime (dotted orange). The 'strong backreaction regime', where the simplified expression in the second line of Eq. (5.16) applies is reached only around $N \simeq 10$. For reference, we show also corresponding estimate in the Abelian regime (dashed blue) [12],

$$(\Delta_s^2)_{\rm ab.} = (\Delta_s^2)_{\rm vac} + (\Delta_s^2)_{\rm gauge} = \left(\frac{H^2}{2\pi\dot\phi}\right)^2 + \left(\frac{\alpha\langle\vec{E}\vec{B}\rangle}{2\beta\Lambda H\dot\phi}\right)^2 , \tag{5.17}$$

with

$$\beta = 1 - 2\pi\xi\frac{\alpha\langle\vec{E}\vec{B}\rangle}{3\Lambda H\dot\phi} , \quad \langle\vec{E}\vec{B}\rangle = -2.0\cdot 10^{-4}\frac{H^4}{\xi^4}e^{2\pi\xi} , \tag{5.18}$$

as well as the standard vacuum contribution (solid gray line, obtained by setting the last parenthesis in Eq. (5.8) to 1), which agrees well with the results obtaind from the linearized analysis. The horizontal gray line indicates the observed value at the CMB scales.

5.2.2 Gravitational wave spectrum

Next we turn to the tensor power spectrum. For the purpose of direct gravitational wave searches (Pulsar timing arrays (PTAs) and interferometers), it is customary to express the stochastic gravitational wave background (SGWB) as the energy in gravitational waves per logarithmic frequency interval normalized to the critical energy density ρ_c [47–49],

$$\Omega_{\rm GW}(k) = \frac{1}{\rho_c}\frac{\partial\rho_{GW}(k)}{\partial\ln k} = \frac{(\Delta_t^+)^2 + (\Delta_t^-)^2}{24}\Omega_r\frac{g_*^k}{g_*^0}\left(\frac{g_{*,s}^0}{g_{*,s}^k}\right)^{4/3} , \tag{5.19}$$

for modes entering during the radiation dominated epoch of the universe, where $g_*^{k,0}$ ($g_{*,s}^{k,0}$) denotes the effective number of degrees of freedom contributing to the energy (entropy) of the thermal bath at the point in time when the mode k entered the horizon and today, respectively. $\Omega_r = 8.5\times 10^{-5}$ denotes the fraction of radiation energy today. Neglecting the change in the number of degrees of freedom, this leads to

$$\Omega_{\rm GW}(k) = \frac{\Omega_r}{24}\left(\frac{H}{2\pi}\right)^2\left(\frac{2}{M_P}\right)^2\left[\left(\sqrt{2k}\,x\,|w_{-2}^{(\gamma)}(x)|\right)^2 + \left(\sqrt{2k}\,x\,|w_{+2}^{(\gamma)}(x)|\right)^2\right]\Big|_{x=1} \tag{5.20}$$

$$= \frac{\Omega_r}{24}\left(\frac{H}{2\pi}\right)^2\left(\frac{2}{M_P}\right)^2\left[1 + \left(\sqrt{2k}\,x\,|w_{+2}^{(\gamma)}(x)|\right)^2\right]\Big|_{x=1} , \tag{5.21}$$

where we have made use of the observation that the $w_{-2}^{(\gamma)}$ mode is not enhanced and hence is given by the usual solution of the Mukhanov-Sasaki equation, $\sqrt{2k}\,w_{-2}^{(\gamma)}(x=1) = 1$.

[20] As this work was being finalized, Refs. [33, 34] appeared, which also consider these nonlinear couplings. The main focus of Ref. [33] is the three-point correlators between the scalar and tensor perturbations, whereas Ref. [34] is a dedicated study of the leading nonlinear contribution to the scalar power spectrum. A direct comparsion of our results is difficult due to the different background evolution (see discussion in Sec. 3.3) and due to the fact that in our parameter space we typically encounter larger values of ξ than encountered in [34]. Using a very different methodology than presented here, Ref. [34] concludes that the non-linear contributions to the scalar power spectrum begin to dominate over the vacuum contributions at $m_Q \simeq 2.7$, where $m_Q \simeq c_2\,\xi$, and hence $\xi(m_Q = 2.7) \simeq 3$. From Eq. (5.16), we can estimate that in our analysis, the non-linear term comes to dominate at $\xi \simeq 2.5$. Moreover, the exponential sensitivity on ξ, $\Delta_s^2 \sim e^{2\pi m_Q}$

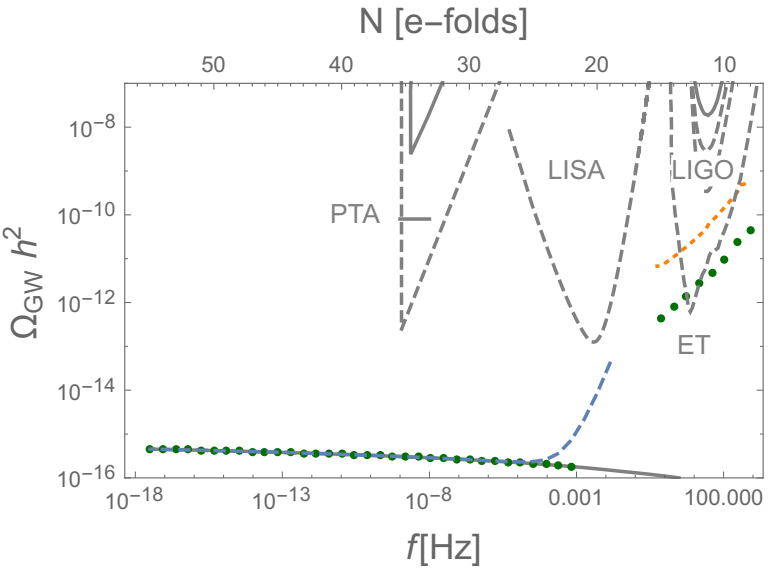

Figure 5.6: Stochastic gravitational wave background. Our semi-analytical estimate (5.23) in the non-Abelian regime is shown as dotted orange line. For reference, we show the standard contribution of the vacuum fluctuations (solid gray)and the (non-linear) contribution in the Abelian regime (dashed blue). The results of the linearized analysis are shown as green dots. Same parameters as in Fig. 5.2.

In Fig. 5.6 we show the resulting SGWB compared to current and upcoming experimental constraints from pulsar timing arrays [50, 51] and from the interferometer experiments LIGO [52], LISA [53] and the Einstein Telescope [54]. For reference, we also show the standard vacuum solution (in gray), obtained by setting $\sqrt{2k}\, w^{(\gamma,\phi)}(x=1)=1$, as well as the analytical results from the Abelian regime (dashed blue line),

$$(\Omega_{\rm GW})_{\rm ab.} = \frac{1}{24}\Omega_r \left(\frac{H}{\pi M_P}\right)^2 \left(2 + 4.3\cdot 10^{-7}\frac{2H^2}{M_P^2}\frac{e^{4\pi\xi}}{\xi^6}\right) . \tag{5.22}$$

A key feature of the non-Abelian regime is that the gravitational waves couple to the enhanced gauge field mode at the linear level, resulting in the enhanced SGWB at large frequencies [22]. In the Abelian regime, such a source term is absent at the linear level and only appears at the non-linear level. This is simply because the energy momentum tensor, the source term of the GW equation of motion, is bi-linear in the gauge fields and we do not have a background gauge field in the Abelian regime. This non-linear term is of course not captured by the linearized analysis performed here, and hence we simply include the non-linear contribution in the Abelian regime given by Eq. (5.22) a posteriori. Note that in the non-Abelian regime this non-linear contribution is sub-dominant as long as $\delta A \ll f$. For the parameter point studied here, we find the SGWB to be out of reach of the GW interferometers LIGO and LISA, and barely reachable with the Einstein Telescope. However we stress that a different parameter choice, leading e.g. to an earlier matching betwenn the Abelian and Non-Abelian regime, could change this picture. A full-flegded study of the parameter space is beyond the scope of the

in [34], is similar to what we find here. Within the uncertainties inherent to both methods, we consider this a good agreement. For related work in the Abelian case see also Refs. [6, 8].

current paper. We note that as in Ref. [55], we expect this gravitational wave background to be very non-gaussian, which may be used as a powerful model discriminator in future observations [56].
Combining Eqs. (4.61) and (5.21) we can obtain an analytical estimate of the SGWB in the non-Abelian regime,

$$\Omega_{\rm GW} \simeq \frac{1}{24}\Omega_r \left(\frac{\xi^3 H}{\pi M_P}\right)^2_{\xi=\xi_{\rm cr}} \left(\frac{2^{7/4}H}{e}\xi^{-1/2}e^{(2-\sqrt{2})\pi\xi}\right)^2_{\xi=\xi_{\rm ref}} . \tag{5.23}$$

Here, to take into account the variation of ξ, we evaluate the first parenthesis (related to the GW - gauge field coupling at horizon crossing) at $\xi_{\rm cr} = \xi(x = 1)$, whereas we evaluate the second parenthesis (describing the helicity +2 gauge field solution) at a the reference value $x = (2 + \sqrt{2})\xi_{\rm cr}$ roughly corresponding to the onset of the instability in the gauge field mode. The resulting estimate for the GW spectrum is depicted by the dotted orange line in Fig. 5.6. The discrepancy to the numerical result can be traced back to Eq. (4.61), which overestimates the GW amplitude by about a factor of three.
In summary, we re-produce the vacuum contribution for both the scalar and tensor power spectrum at large N, thus ensuring agreement with all CMB observations. As we approach smaller scales, we observe an enhancement of both spectra as we pass first through the Abelian and then through the non-Abelian regime. For the specific parameter point studied in this section, the effects are out of reach of current and upcoming experiments, however we expect this to change with increasing α/Λ and/or increasing gauge coupling, see discussion at the end of Sec. 5.1. The downside of this regime of parameter space is that the linearized treatment of the helicity +2 gauge field modes likely breaks down significantly before the end of inflation, requiring a different computational strategy to even reliably describe the background evolution in this regime.

6 Conclusions and Outlook

A shift-symmetric coupling between the inflation sector and a (non-Abelian) gauge sector opens up new avenues to probe the microphysics of inflation. Based on earlier works studying the coupling of the inflaton field to Abelian [6] and non-Abelian [4, 5, 20–22] gauge groups, we demonstrate here how the former can be understood as a limit of the latter in the far past. To this end, we extend and complement the analysis of CNI (see Refs. [4,5,22]) in the following ways: (i) Most importantly, we demonstrate how the homogeneous isotropic gauge field background, key ingredient to CNI, is generated dynamically from standard Bunch Davies initial conditions in the infinite past. The evolution of the background is then governed by two competing effects: the classical background motion and the stochastic motion due to the strong growth of gauge field perturbations. We demonstrate how the system converges to an attractor solution, where the gauge field background is dominated by the classical motion. (ii) This attractor solution is more general than the solution employed in [20], and in particular also allows us to study the parameter space in which the backreaction of the gauge fields on the equation of motion of the inflaton is small. (iii) We provide relatively simple explicit expressions for the equations of motion of the Fourier components of all physical perturbations modes, after integrating out all gauge degrees of freedom and constraint equations. Due to a slightly different choice of basis, our expressions

are somewhat simpler than those found in the literature, in particular when studying only the gauge field fluctuations. (iv) Although the bulk of our analysis is performed for the linearized system of perturbations, we highlight the importance of non-linear contributions in the scalar sector, giving an estimate for the resulting contribution to the scalar power spectrum.

In the inherently non-Abelian regime of our analysis, we reproduce the phenomenology of CNI: a single tensor (i.e. helicity 2) gauge field mode is tachyonically enhanced. A linear coupling of this mode to one helicity of the tensor metric perturbation sources a strongly enhanced, chiral gravitational wave background. We point out that the instability observed in the scalar sector in Ref. [4] only occurs in part of the parameter space (depending mainly on the value of the gauge coupling e and the coupling between the inflaton and the gauge fields, α/Λ), and is in particular absent for the parameter point studied in this paper. Large contributions to the scalar power spectrum are on the other hand sourced by non-linear contributions. We propose a method to estimate this non-linear contribution based on a generalization of the procedure described in [12] and it should be seen as an order-of-magnitude estimate only. Interestingly, we have found that the non-linear corrections are expected to quickly dominate over vacuum and linear contributions inducing a strong enhancement in the scalar power spectrum at small scales. Such an enhancement may lead to a rich phenomenology (e.g. PBH formation [12–14], μ-distortions [11], etc).

The transition between an Abelian limit at early times and a non-Abelian regime at later times provides a natural way to obtain results in agreement with all CMB constraints while obtaining a phenomenologically very interesting enhanced scalar and tensor power spectra at small scales. The key parameter driving this transition is the instability parameter ξ (see Eq. (2.7)), measuring the velocity of the inflaton. In single-field slow-roll inflation models, this parameter is small at early times but increases over the course of inflation. This parameter controls the tachyonic enhancement of the gauge field perturbations, as well as the amplitude of the homogeneous background solution. For the parameter point studied in this paper, the predicted enhancement of the scalar and tensor power spectrum is out of reach of current and upcoming experiments. A comprehensive exploration of the parameter space of these models, in particular with regarding the prospects of detecting the gravitational wave signal with LIGO, LISA or the Einstein Telescope, is left for future work.

For the numerical study in this paper, we focused on a parameter point for which the gauge friction on the inflaton motion was small at the point of transition between the Abelian and non-Abelian regime. We leave a study of the opposite regime, corresponding to the usual so-called magnetic drift regime of CNI to future work. In this case, the dynamics at the transition point change more violently, requiring a more sophisticated modeling of this transition regime. In a similar spirit, the transition region itself deserves more attention. In this paper we simply refrained from making any statements very close to the transition region, to avoid sensitivity to the precise modeling procedure of this transition. Clearly, this calls for further improvement. Finally, the restriction to a linearized system of perturbations in the bulk of our analysis limits our ability to explore parameters for which the transition to the non-Abelian regime occurs only shortly after the CMB scales exited the horizon (which may be most interesting from a phenomenological point of view). For the parameter point studied here we observe that the variance of the non-Abelian gauge field modes becomes comparable

to the classical background evolution in the last few e-folds of inflation, calling for a full non-linear treatment of the system.
Our analysis is a further step towards the embedding of axion inflation models in a fully realistic particle physics description of the early Universe. In particular, our unified framework for Abelian and Non-Abelian couplings may be applied to more complex gauge groups such as $SU(2) \times U(1)$ and eventually the full Standard Model of Particle Physics.

Acknowledgements

We thank P. Adshead, J. Beltran, D. Figueroa and M. Peloso for valuable comments and discussions at various stages of this work. M.P. acknowledges the support of the Spanish MINECOs "Centro de Excelencia Severo Ocho" Programme under grant SEV-2012-0249. This project has received funding from the European Unions Horizon 2020 research and innovation programme under the Marie Skłodowska-Curie grant agreement No 713366.

A Full equations of motion

In this Appendix we report the full computation of the equations of motion for the gauge fields and metric perturbations including the lapse and shift that were discarded in Sec. 4 of the main text. We found some minor discrepancies with respect to the results in [22] that however do not affect their results.

We start from the expressions for the action and the metric reported in sec. 4. The metric in matrix form is

$$g_{\mu\nu} = \begin{pmatrix} -N^2 + h_{ij}N^iN^j & h_{ji}N^i \\ h_{ij}N^j & h_{ij} \end{pmatrix} , \tag{A.1}$$

and it can be easily establihed that the components of the inverse matrix are

$$g^{00} = -\frac{1}{N^2} \quad g^{0i} = \frac{N^i}{N^2} \quad g^{ij} = h^{ij} - \frac{N^iN^j}{N^2} . \tag{A.2}$$

Moreover, it is useful to notice that $\sqrt{-g} = N\sqrt{h}$,[21] where $h = \det(h_{ij})$ and $h^{ij} = (h_{ij})^{-1}$. Using these definitions, the Einstein-Hilbert term takes the standard form derived in the original paper on the ADM formalism [41]

$$\mathcal{L}_{\rm EH} = \sqrt{h}\left[NR^{(3)} + \frac{1}{N}\left(E^{ij}E_{ij} - E^2\right)\right] , \tag{A.3}$$

where $R^{(3)}$ is the spatial curvature (computed using h_{ij}), while[22]

$$E_{ij} = \frac{1}{2}\left(h'_{ij} - \nabla_i N_j - \nabla_j N_i\right) , \quad E = E^i_i . \tag{A.4}$$

[21] The four-dimensional metric is always denoted by the letter g, while the three-dimensional metric is denoted by h. h_{ij}/h^{ij} is used in order to raise/lower indices in the three-dimensional space.

[22] The covariant derivative ∇ is computed using h_{ij}.

The lagrangian for the scalar field ϕ takes the form:

$$\mathcal{L}_\phi = \sqrt{h}\left[\frac{1}{2N}\left(\phi' - N^i\partial_i\phi\right)^2 - \frac{N}{2}h^{ij}\partial_i\phi\partial_j\phi - NV(\phi)\right], \tag{A.5}$$

while, after using some simple algebra, we split the Yang-Mills lagrangian as follows

$$\begin{aligned}\mathcal{L}_{\rm YM} &= \frac{\sqrt{h}}{2N}\left[h^{ij}\left(F^a_{0i}F^a_{0j} + 2F^a_{0i}F^a_{jl}N^l + F^a_{ik}F^a_{jl}N^kN^l\right)\right] - \frac{\sqrt{h}N}{4}h^{ij}h^{kl}F^a_{ik}F^a_{jl} \equiv \\ &\equiv \mathcal{L}_{\rm YM,1} + \mathcal{L}_{\rm YM,2} + \mathcal{L}_{\rm YM,3} + \mathcal{L}_{\rm YM,4}\,.\end{aligned} \tag{A.6}$$

Expanding each of the four terms in eq. (A.6) we get:

$$\begin{aligned}\mathcal{L}_{\rm YM,1} &= \frac{\sqrt{h}}{2N}h^{ij}F^a_{0i}F^a_{0j} = \\ &= \frac{\sqrt{h}}{2N}h^{ij}\left[\partial_0A^a_i\partial_0A^a_j + \partial_iA^a_0\partial_jA^a_0 - \partial_0A^a_i\partial_jA^a_0 - \partial_0A^a_j\partial_iA^a_0 + \right. \\ &+ e\varepsilon^{abc}\left(\partial_0A^a_iA^b_0A^c_j - \partial_iA^a_0A^b_0A^c_j + \partial_0A^a_jA^b_0A^c_i - \partial_jA^a_0A^b_0A^c_i\right) \\ &\left.+e^2\left(A^b_0A^b_0A^c_iA^c_j - A^b_0A^b_jA^c_0A^c_i\right)\right].\end{aligned} \tag{A.7}$$

$$\begin{aligned}\mathcal{L}_{\rm YM,2} &= \frac{\sqrt{h}}{N}h^{ij}F^a_{0i}F^a_{jl}N^l = \\ &= \frac{\sqrt{h}}{N}h^{ij}\left[\partial_0A^a_i\partial_jA^a_l - \partial_0A^a_i\partial_lA^a_j - \partial_iA^a_0\partial_jA^a_l + \partial_iA^a_0\partial_lA^a_j + \right. \\ &+ e\varepsilon^{abc}\left(\partial_0A^a_iA^b_jA^c_l - \partial_iA^a_0A^b_jA^c_l + \partial_jA^a_lA^b_0A^c_i - \partial_lA^a_jA^b_0A^c_i\right) + \\ &\left.+e^2\left(A^b_0A^b_jA^c_iA^c_l - A^b_0A^b_lA^c_iA^c_j\right)\right]N^l\,.\end{aligned} \tag{A.8}$$

$$\begin{aligned}\mathcal{L}_{\rm YM,3} &= \frac{\sqrt{h}}{2N}h^{ij}F^a_{ik}F^a_{jl}N^kN^l = \\ &= \frac{\sqrt{h}}{N}h^{ij}\left[\partial_iA^a_k\partial_jA^a_l - \partial_iA^a_k\partial_lA^a_j - \partial_kA^a_i\partial_jA^a_l + \partial_kA^a_i\partial_lA^a_j + \right. \\ &+ e\varepsilon^{abc}\left(\partial_iA^a_kA^b_jA^c_l - \partial_kA^a_iA^b_jA^c_l + \partial_jA^a_lA^b_iA^c_k - \partial_lA^a_jA^b_iA^c_k\right) + \\ &\left.+e^2\left(A^b_iA^b_jA^c_kA^c_l - A^b_iA^b_lA^c_kA^c_j\right)\right]N^kN^l\,.\end{aligned} \tag{A.9}$$

$$\begin{aligned}\mathcal{L}_{\rm YM,4} &= -\frac{\sqrt{h}}{4N}h^{ij}h^{kl}F^a_{ik}F^a_{jl} = \\ &= -\frac{\sqrt{h}N}{4}h^{ij}h^{kl}\left[\partial_iA^a_k\partial_jA^a_l - \partial_iA^a_k\partial_lA^a_j - \partial_kA^a_i\partial_jA^a_l + \partial_kA^a_i\partial_lA^a_j + \right. \\ &+ e\varepsilon^{abc}\left(\partial_iA^a_kA^b_jA^c_l - \partial_kA^a_iA^b_jA^c_l + \partial_jA^a_lA^b_iA^c_k - \partial_lA^a_jA^b_iA^c_k\right) + \\ &\left.+e^2\left(A^b_iA^b_jA^c_kA^c_l - A^b_iA^b_lA^c_kA^c_j\right)\right].\end{aligned} \tag{A.10}$$

The Chern-Simons term is

$$\begin{aligned}\mathcal{L}_{\rm CS} &= -\frac{\alpha}{8\Lambda}\phi F^a_{\mu\nu}F^a_{\rho\sigma}\varepsilon^{\mu\nu\rho\lambda} = -\frac{\alpha}{2\Lambda}\phi\left[2\varepsilon^{0ijk}\partial_0A^a_i\partial_jA^a_k - \right. \\ &\left.-2\varepsilon^{0ijk}\partial_iA^a_0\partial_jA^a_k + ef^{abc}\varepsilon^{0ijk}\left(\partial_0A^a_iA^b_jA^c_k - \partial_iA^a_0A^b_jA^c_k + 2\partial_iA^a_jA^b_0A^c_k\right)\right].\end{aligned} \tag{A.11}$$

Given the expressions for each term of the action, we can compute the expansion at quadratic order in the field fluctuations. We expand the three-dimensional metric at second order as follow

$$h_{ij} = a^2 \left(\delta_{ij} + \gamma_{ij} + \frac{\gamma_{ik}\gamma_{kj}}{2} \right) , \tag{A.12}$$

where γ_{ij} is transverse and traceless quantum fluctuation: $\gamma_{ii} = \partial_i \gamma_{ij} = 0$.[23] We also notice that, using the standard expression $\delta g = g g^{ij} \delta g_{ij}$, where $g = \det(g)$ the determinant $h = \det(h_{ij})$ can be expanded as

$$\frac{h}{a^2} = \det\left(e^{\mathrm{Tr}\left[\ln(h_{ij}/a^2)\right]} \right) = \det\left(e^{\mathrm{Tr}\left[\gamma_{ij} + \frac{\gamma_{ik}\gamma_{kj}}{2} - \frac{\gamma_{ik}\gamma_{kj}}{2}\right]} \right) = 1 . \tag{A.13}$$

We also notice that in spatially flat gauge the Christoffel symbols vanish $\Gamma^i{}_{jk} = 0$ and then $\nabla_i = \partial_i$. Finally we expand the lapse and shift around the FRW background

$$N = a\left(1 + \delta N_1 + \delta N_2\right) , \qquad N^i \equiv \delta N_1^i + \delta N_2^i , \tag{A.14}$$

where $\delta N_1, N_1^i$ are first order fluctuations while $\delta N_2, N_2^i$ are second order fluctuations. As it turns out that only the first order fluctuations are relevnat for the computation below, we just rename $\delta N_1 \equiv \delta N$ and $\delta N_1^i = \delta N^i$.

Finally we proceed with the computation of the quadratic action and we report the results term by term to make it easier tracking back the various terms. We start from the Einstein Hilbert component

$$S_{\rm EH} = \int \mathrm{d}^4x \, \frac{a^2}{2} \left[\frac{\gamma_{ij}\partial_l\partial_l\gamma_{ij}}{4} - 6\mathcal{H}^2 + \frac{\gamma'_{ij}\gamma'_{ij}}{4} + \right. \tag{A.15}$$

$$\left. + \frac{4\mathcal{H}}{a^2}(1-\delta N)\partial_i N_i + 6\mathcal{H}^2 \delta N(1-\delta N) - \left(\frac{\partial_i N_i}{a^2}\right)^2 + \frac{\partial_{(i}N_{j)}\partial_{(i}N_{j)}}{a^4} \right] , \tag{A.16}$$

where the contribution from the three-dimensional curvature $R^{(3)}$ is just the first term $a^2/8\,\gamma_{ij}\partial_l\partial_l\gamma_{ij}$. Concerning the scalar field, the second order action takes the form:

$$\delta^2 S_\phi = \int d^4x \, \left[\frac{a^2}{2}\left(\left(\delta\phi'\right)^2 - \partial_i\delta\phi\partial_i\delta\phi - a^2 V''\left(\delta\phi\right)^2 \right) - \right.$$

$$\left. - \frac{a^2}{2}\left(\frac{2}{a^2}\langle\phi'\rangle N_i \partial_i\delta\phi + 2\langle\phi'\rangle\delta N\delta\phi' + \langle\phi'\rangle^2\left(\delta N\right)^2 - 2a^2 V'\delta\phi\delta N \right) \right] . \tag{A.17}$$

Finally, we report the various contributions to the Yang-Mills $\delta^2\mathcal{S}_{\rm YM}$ and Chern-Simon $\delta^2 S_{\rm CS}$ quadratic actions

$$\delta^2\mathcal{S}_{\rm YM,1} = \int d^4x \, \left[\frac{1}{4}\left(f'\right)^2\gamma^{jk}\gamma^{kj} - f'\gamma^{aj}\partial_0\delta A^{(a}_{j)} - \right.$$

$$- \frac{1}{2}\delta A_i^a\partial_0\partial_0\delta A_i^a - \frac{1}{2}\delta A_0^a\partial_i\partial_i\delta A_0^a + \delta A_0^a\partial_0\partial_i\delta A_i^a +$$

$$+ e\varepsilon^{abi} f\partial_0\delta A_i^a\delta A_0^b + e\varepsilon^{jbc} f'\delta A_0^b\delta A_j^c - e\varepsilon^{abi} f\partial_i\delta A_0^a\delta A_0^b + e^2 f^2\delta A_0^b\delta A_0^b$$

$$\left. + \frac{3}{2}\left(f'\right)^2\delta N^2 - f'\partial_0\delta A_i^i\delta N + f'\partial_j\delta A_0^j\delta N \right] , \tag{A.18}$$

[23] Notice that spatial indices are raised and lowered by h_{ij}/h^{ij}, while gauge indices are raised and lowered with just a δ_{ij}. Everytime we write a gauge field fluctuation with two lowered indices we imply that the first one is the gauge index.

$$\delta^2\mathcal{S}_{\rm YM,2} = \int d^4x\,\frac{1}{a^2}\left[f'\partial_a\delta A^a_l N_l - f'\partial_l\delta A^a_a N_l + \right.$$
$$\left. + ef^2\varepsilon_{ail}\partial_0\delta A^a_i N_l + eff'\varepsilon_{ibl}\delta A^b_i N_l - e\varepsilon_{ail}f^2\partial_i\delta A^a_0 N_l - 2e^2f^3\delta A^l_0 N_l\right], \tag{A.19}$$

$$\delta^2\mathcal{S}_{\rm YM,3} = \int d^4x\, e^2f^4 N^k N^k\,, \tag{A.20}$$

$$\begin{aligned}\delta^2\mathcal{S}_{\rm YM,4} = \int d^4x\,\Bigg[&-\frac{3}{4}e^2f^4\delta N^2 - \frac{e^2f^4}{4}\gamma^{jk}\gamma^{kj} - \\ &- ef^2\varepsilon^{abc}\gamma^{ij}\left(\delta^b_{(i}\partial_{j)}\delta A^a_c - \delta^b_{(i}\partial_c\delta A^a_{j)}\right) + e^2f^3\gamma^{bi}\delta A^{(b}_{i)} - \\ &- ef^2\varepsilon^{abc}\partial_{[b}\delta A^a_{c]}\delta N - 2e^2f^3\delta^b_i\delta A^b_i\delta N + \\ &+ \frac{1}{2}\delta A^a_j\partial_i\partial_i\delta A^a_j + \frac{1}{2}(\partial_i\delta A^a_i)^2 - e^2f^2\left(\delta A^a_a\delta A^b_b + \frac{1}{2}\delta A^b_i\delta A^b_i - \frac{1}{2}\delta A^b_i\delta A^i_b\right) - \\ &- ef\varepsilon^{abc}\left(\delta^b_i\partial_i\delta A^a_k\delta A^c_k + \delta^c_k\partial_i\delta A^a_k\delta A^b_i\right)\Bigg]\,.\end{aligned} \tag{A.21}$$

$$\begin{aligned}\delta^2\mathcal{S}_{\rm CS} = \int d^4x\,\Bigg[&-\frac{\alpha}{2\Lambda}\langle\phi\rangle\left(2\varepsilon^{0ijk}\partial_0\delta A^a_i\partial_j\delta A^a_k - 2\varepsilon^{0ijk}\partial_i\delta A^a_0\partial_j\delta A^a_k + \right. \\ &+ 2ef\partial_0\delta A^a_a\delta A^k_k - 2ef\partial_0\delta A^c_k\delta A^k_c + ef'\delta A^b_b\delta A^c_c - ef'\delta A^b_j\delta A^j_b - \\ &\left.-2ef\partial_i\delta A^i_0\delta A^b_b + 2ef\partial_i\delta A^j_0\delta A^i_j + 2ef\partial_i\delta A^i_j\delta A^j_0 - 2ef\partial_i\delta A^j_j\delta A^i_0\right) - \\ &- \frac{\alpha}{2\Lambda}\delta\phi\left(2f'\varepsilon^{0ijk}\delta^a_i\partial_j\delta A^a_k + 4eff'\delta A^b_b + 2ef^2\partial_0\delta A^a_a - 2ef^2\partial_i\delta A^i_0\right)\Bigg]\,.\end{aligned} \tag{A.22}$$

From these expressions we can infer the full equations of motion and the constraints, that we report below.

- *Gauss' law:*

$$\begin{aligned}&-\frac{f'}{a^2}\partial_j\gamma_{gj} - f'\partial_g\delta N - \partial_i\partial_i\delta A_{g0} + \partial_0\partial_i\delta A_{gi} + e\varepsilon_{agi}f\partial_0\delta A_{ai} + e\varepsilon_{jgc}f'\delta A_{cj} + \\ &+2ef\varepsilon_{gbi}\partial_i\delta A_{b0} + 2e^2f^2\delta A_{g0} + \frac{ef^2}{a^2}\varepsilon_{gil}\partial_i N_l - \frac{2e^2f^3}{a^2}N_g - \frac{\alpha ef^2}{\Lambda}\partial_g\delta\phi = 0\,.\end{aligned} \tag{A.23}$$

- *δN-constraint:*

$$\begin{aligned}&-6a^2\mathcal{H}^2\delta N - 2\mathcal{H}\partial_i N_i - a^2\langle\phi'\rangle\delta\phi' + a^2\langle\phi'\rangle^2\delta N - a^4V'\delta\phi + \\ &+3\left(f'\right)^2\delta N - f'\partial_0\delta A^i_i + f'\partial_j\delta A^j_0 - \frac{3}{2}e^2f^4\delta N - ef^2\varepsilon^{aik}\partial_{[i}\delta A^a_{k]} - 2e^2f^3\delta A^i_i = 0\,.\end{aligned} \tag{A.24}$$

- *N_l-constraint:*

$$\begin{aligned}&2\mathcal{H}\partial_l\delta N + \frac{1}{2a^2}\left[\partial_l\partial_i N_i - \partial_i\partial_i N_l\right] - \langle\phi'\rangle\partial_i\delta\phi + \frac{2e^2f^4N_l}{a^4} + \\ &+\frac{1}{a^2}\left[f'\left(\partial_i\delta A^i_l - \partial_l\delta A^i_i\right) + ef^2\varepsilon_{lai}\partial_0\delta A^a_i - eff'\varepsilon_{lbi}\delta A^b_i - ef^2\varepsilon_{lai}\partial_i\delta A^a_0 - 2e^2f^3\delta A_{l0}\right] = 0\,.\end{aligned} \tag{A.25}$$

- *Gauge fields equation of motion*:

$$
\begin{aligned}
&- \partial_0\partial_0\delta A_i^a - 2e\varepsilon^{abi} f' \delta A_0^b + \partial_l\partial_l\delta A_i^a - \partial_i\partial_j\delta A_j^a - \\
&- e^2 f^2 (2\delta_i^a \delta A_b^b + \delta A_i^a - \delta A_a^i) + 2ef\varepsilon^{abc}\partial_b\delta A_i^c + ef\varepsilon^{abc}\partial_i\delta A_c^b + ef\varepsilon^{abi}\partial_l\delta A_l^b + \\
&+ \langle\phi'\rangle\frac{\alpha}{\Lambda}\left(\varepsilon^{ijk}\partial_j\delta A_k^a + \delta_i^a ef\delta A_b^b - ef\delta A_a^i\right) + \frac{\alpha}{\Lambda}\left[f'\varepsilon^{aji}\partial_j\delta\phi + ef^2\delta_i^a\delta\phi'\right] + \\
&+ f''\gamma_i^a + f'\gamma_i^{a\,\prime} + ef^2\varepsilon^{ajk}\partial_k\gamma_{ij} + e^2 f^3\gamma_i^a + \\
&- f'\partial_i N^a + f'\delta_i^a\partial_l N^l - e\varepsilon^{ail}(3ff'N^l + f^2 N^{l\,\prime}) + \\
&+ \delta_i^a(f''\delta N + f'\delta N') + ef^2\varepsilon^{abi}\partial_b\delta N - 2e^2 f^3\delta_i^a\delta N\,.
\end{aligned}
\tag{A.26}
$$

- *Inflaton equation of motion:*

$$
\begin{aligned}
&\Box\delta\phi - 2a'a^{-3}\delta\phi' + a^{-2}\partial_0(\langle\phi'\rangle\delta N) + 2\frac{H}{a}\langle\phi'\rangle\delta N + \frac{\langle\phi'\rangle}{a^4}\partial_i N_i - V_{,\phi\phi}\delta\phi - V_{,\phi}\delta N - \\
&\qquad - \frac{\alpha}{2\Lambda a^4}\left[2f'\varepsilon^{ijk}\partial_j\delta A_k^i + 4eff'\delta A_b^b + 2ef^2\partial_0\delta A_a^a - 2ef^2\partial_i\delta A_0^i\right] = 0\,,
\end{aligned}
\tag{A.27}
$$

where the $\Box$-operator is expressed in co-moving coordinates.

- *Gravitational waves equation of motion:*

$$
\begin{aligned}
&\frac{a}{4}\left[(a\gamma_{ij})'' + \left(-\partial_l\partial_l - \frac{a''}{a}\right)(a\gamma_{ij})\right] = \\
&+ \frac{1}{2a}(f'^{\,2} - e^2 f^4)(a\gamma_{ij}) - f'\partial_0\delta A_{j)}^{(i} + f'\partial_{(i}\delta A_0^{j)} - 2ef^2\varepsilon^{a(ic}\partial_{[j)}\delta A_{c]}^a + e^2 f^3\delta A_{j)}^{(i}\,.
\end{aligned}
\tag{A.28}
$$

B Basis vectors for the gauge fields in the helicity basis

In this appendix we collect the explicit forms of the basis vectors derived in Sec. 4.2. The six physical degrees of freedom are spanned by the helicity states $\hat{e}_\lambda$,

$$
(\hat{e}_{01})^b{}_\mu = \frac{1}{\sqrt{2}}\begin{pmatrix}0&0&0&0\\0&0&1&0\\0&0&0&1\end{pmatrix}\,,\quad (\hat{e}_{02})^b{}_\mu = \frac{1}{\sqrt{2+4y_k(x)^2}}\begin{pmatrix}0&2iy_k(x)&0&0\\0&0&0&-1\\0&0&1&0\end{pmatrix}\,,
$$

$$
(\hat{e}_{-1})^b{}_\mu = \frac{1}{\sqrt{2+4y_k(x)+4y_k(x)^2}}\begin{pmatrix}0&0&i(1+y_k(x))&1+y_k(x)\\0&iy_k(x)&0&0\\0&y_k(x)&0&0\end{pmatrix}\,,
$$

$$
(\hat{e}_{+1})^b{}_\mu = \frac{1}{\sqrt{2-4y_k(x)+4y_k(x)^2}}\begin{pmatrix}0&0&-i(1-y_k(x))&1-y_k(x)\\0&iy_k(x)&0&0\\0&-y_k(x)&0&0\end{pmatrix}\,,
$$

$$
(\hat{e}_{-2})^b{}_\mu = \frac{1}{2}\begin{pmatrix}0&0&0&0\\0&0&i&1\\0&0&1&-i\end{pmatrix}\,,\quad (\hat{e}_{+2})^b{}_\mu = \frac{1}{2}\begin{pmatrix}0&0&0&0\\0&0&-i&1\\0&0&1&i\end{pmatrix}\,,
\tag{B.1}
$$

with $y_k(x) \equiv ef(\tau)/k$. Note that in any background which is a fixed point of Eq. (3.5) (e.g. if the background follows the c_2-solution), we can drop the index k on $y_k(x)$ as this quantity becomes a function of $(-k\tau)$ only: $y_k(x) = ek^{-1}f(-k^{-1}x) = ef(-x) \equiv y(x)$.

The gauge degrees of freedom (simultaneously satisfying Eqs. (4.24) and (4.25)) read

$$(\hat{g}_{-1})^{b}{}_{\mu} = \begin{pmatrix} 0 & 0 & -y_k(x) & i\,y_k(x) \\ i\,\frac{d}{dx} & (1+y_k(x)) & 0 & 0 \\ \frac{d}{dx} & -i(1+y_k(x)) & 0 & 0 \end{pmatrix}, \tag{B.2}$$

$$(\hat{g}_{0})^{b}{}_{\mu} = \begin{pmatrix} i\,\frac{d}{dx} & 1 & 0 & 0 \\ 0 & 0 & 0 & -i\,y_k(x) \\ 0 & 0 & i\,y_k(x) & 0 \end{pmatrix}, \tag{B.3}$$

$$(\hat{g}_{+1})^{b}{}_{\mu} = \begin{pmatrix} 0 & 0 & y_k(x) & i\,y_k(x) \\ i\,\frac{d}{dx} & (1-y_k(x)) & 0 & 0 \\ -\frac{d}{dx} & i(1-y_k(x) & 0 & 0 \end{pmatrix}. \tag{B.4}$$

where the entry d/dx indicates that the corresponding coefficient $w_{\lambda}^{(g)}(x)$ is replaced by $\frac{d}{dx}w_{\lambda}^{(g)}(x)$. Finally the basis vectors encoding the constraint equations (Gauss' law) are given by

$$\left(\hat{f}_{-1}\right)^{b}{}_{\mu} = \frac{1}{\sqrt{2}}\begin{pmatrix} 0 & 0 & 0 & 0 \\ 1 & 0 & 0 & 0 \\ -i & 0 & 0 & 0 \end{pmatrix}, \tag{B.5}$$

$$\left(\hat{f}_{0}\right)^{b}{}_{\mu} = \frac{1}{\sqrt{2}}\begin{pmatrix} 1 & 0 & 0 & 0 \\ 0 & 0 & 0 & 0 \\ 0 & 0 & 0 & 0 \end{pmatrix}, \tag{B.6}$$

$$\left(\hat{f}_{+1}\right)^{b}{}_{\mu} = \frac{1}{\sqrt{2}}\begin{pmatrix} 0 & 0 & 0 & 0 \\ 1 & 0 & 0 & 0 \\ +i & 0 & 0 & 0 \end{pmatrix}. \tag{B.7}$$

C Computation of the variance of $F\tilde{F}$

In this appendix we are interested in computing the variation of $\langle F\tilde{F}\rangle$ with respect to its background value, which we employ to estimate the non-linear contribution to the scalar power spectrum in Sec. 5.2.1. In general this can be expressed as

$$\delta(\langle F\tilde{F}\rangle) = [F\tilde{F} - \langle F\tilde{F}\rangle]_{\delta\phi=0} + \frac{\partial\langle F\tilde{F}\rangle}{\partial\dot{\phi}}\dot{\delta\phi} \equiv \delta_{E\vec{B}} + \frac{\partial\langle F\tilde{F}\rangle}{\partial\dot{\phi}}\dot{\delta\phi}\,, \tag{C.1}$$

where we are using the sign convention $\dot{\phi} > 0$, $\langle F\tilde{F}\rangle > 0$ (see [12]). Notice that this corresponds at considering the variation of $\langle F\tilde{F}\rangle$ due to variations of $\delta\phi$ (second term) plus the variations of $\langle F\tilde{F}\rangle$ due to the variations of the gauge fields. In order to perform the computation of the latter it is useful to introduce the electric and magnetic fields (in conformal time)

$$F^{a}_{0i} \equiv -a^2(\tau)E^{a}_{i}\,, \qquad\qquad F^{a}_{ij} \equiv \varepsilon^{ijk}a^2(\tau)B^{a}_{k}\,. \tag{C.2}$$

With these definitions we can trivially show that:

$$F^{a}_{\mu\nu}F^{a}_{\rho\sigma}g^{\mu\rho}g^{\nu\sigma} = -\frac{2}{a^4}F^{a}_{0i}F^{a}_{0i} + \frac{1}{a^4}F^{a}_{ij}F^{a}_{ij} = -2\left[\left(\vec{E}^{a}\right)^2 - \left(\vec{B}^{a}\right)^2\right]. \tag{C.3}$$

$$F^{a}_{\mu\nu}\tilde{F}^{a}_{\rho\sigma} = \frac{4}{2\sqrt{-g}}F^{a}_{0i}F^{a}_{jk}\varepsilon^{ijk} = -2E^{a}_{i}B^{a}_{l}\varepsilon^{ijk}\varepsilon^{ljk} = -4\vec{E}^{a}\cdot\vec{B}^{a}\,. \tag{C.4}$$

We can then proceed by computing the expressions of E_i^a and B_i^a (neglecting terms depending on A_0^a) up to second order:

$$E_i^a = -\frac{1}{a^2}\left[\delta_i^a \partial_0 f + \partial_0 \delta A_i^a\right] , \tag{C.5}$$

$$B_i^a = \frac{1}{a^2}\left[\varepsilon_{ijk}\partial_j \delta A_k^a + e f^2 \delta_i^a - e f \delta A_a^i + e\frac{\varepsilon_{ijk}\varepsilon^{abc}}{2}\delta A_j^b \delta A_k^c\right] , \tag{C.6}$$

where we have neglected terms proportional to δA_a^a because it's scalar and thus it does not feature the exponential enhancement present in the e_{+2} mode. Notice that setting $e = 0$ we can easily recover all the usual Abelian terms.

With this notation it is now trivial to check that the expectation value of $F\tilde{F}$ can be expressed as:

$$\langle F_{\mu\nu}^a \tilde{F}^{a\,\mu\nu}\rangle = -4\langle \vec{E}^a \cdot \vec{B}^a\rangle \equiv -4T_0 , \tag{C.7}$$

and the variance of $F\tilde{F}$ can be expressed as

$$\delta^2_{\vec{E}\vec{B}} = \langle (F^a\tilde{F}^a)^2\rangle - \langle F^a\tilde{F}^a\rangle^2 = 16\left[\langle E_i^a E_j^b\rangle\langle B_i^a B_j^b\rangle + \langle E_i^a B_j^b\rangle\langle B_i^a E_j^b\rangle\right] , \tag{C.8}$$

that has exactly the same shape as in the Abelian limit (for comparison see appendix A of [12]). At this point it is useful to introduce

$$T_1 \equiv \left\langle E_i^a E_j^b\right\rangle\left\langle B_i^a B_j^b\right\rangle , \qquad T_2 \equiv \left\langle E_i^a B_j^b\right\rangle\left\langle B_i^a E_j^b\right\rangle , \tag{C.9}$$

so that the two contributions can be computed independently. Before substituting the explicit expressions of E and B it is important to notice that

1. In order to compute the variance we only need terms that are exactly quadratic in the fluctuations.
2. The base vectors of the ± 2 helicity modes are traceless in all bases (implying $\delta_i^a\left[e_{\pm 2}(\vec{k})\right]_i^a = 0$ for all $\vec{k}$).

We can now directly compute

$$\left\langle E_i^a E_j^b\right\rangle = \frac{1}{a^4}\left\langle \partial_0\delta A_i^a \partial_0 \delta A_j^b\right\rangle , \tag{C.10}$$

$$\begin{aligned}\left\langle B_i^a B_j^b\right\rangle =& \frac{1}{a^4}\left\langle \varepsilon_{ilk}\varepsilon_{jnm}\partial_l\delta A_k^a \partial_n \delta A_m^b + e^2 f^2 \delta A_a^i \delta A_b^j - e f \varepsilon_{ilk}\partial_l \delta A_a^k \delta A_j^b - e f \varepsilon_{jnm}\delta A_a^i \partial_n \delta A_m^b\right\rangle \\ \equiv& \left\langle B_i^a B_j^b\right\rangle_1 + \left\langle B_i^a B_j^b\right\rangle_2 + \left\langle B_i^a B_j^b\right\rangle_3 + \left\langle B_i^a B_j^b\right\rangle_4 ,\end{aligned} \tag{C.11}$$

$$\begin{aligned}\left\langle E_i^a B_j^b\right\rangle =& -\frac{1}{a^4}\left\langle \partial_0\delta A_i^a \varepsilon_{jnm}\partial_n \delta A_m^b - e f \partial_0 \delta A_i^a \delta A_b^j + e\delta_i^a \partial_0 f \frac{\varepsilon_{jnm}\varepsilon^{bdh}}{2}\delta A_n^d \delta A_m^h\right\rangle \\ \equiv& \left\langle E_i^a B_j^b\right\rangle_1 + \left\langle E_i^a B_j^b\right\rangle_2 + \left\langle E_i^a B_j^b\right\rangle_3 .\end{aligned} \tag{C.12}$$

Notice that again setting $e = 0$ our expressions reduce to the Abelian case.

At this point we can expand $\delta A^a_\nu(\tau,\vec{x})$ in terms of its Fourier modes as in Eq. (2.2). Notice that in general the basis vectors satisfy

$$\left[e^a_{\lambda,\nu}(\hat{k})\right]^* = e^a_{\lambda,\nu}(-\hat{k})\,, \qquad\qquad i\varepsilon_{ijl}k_j e^a_{\lambda,l}(\hat{k}) = \mathrm{sgn}(\lambda)|\vec{k}|e^a_{\lambda,i}(\hat{k})\,. \tag{C.13}$$

Moreover, the helicity ±2 vectors are symmetric, *i.e.*, $e^a_{\pm2,i} = e^i_{\pm2,a}$. Using the properties of the basis vectors it is possible to show that (from now on we restrict our analysis to the $+2$ mode only)

$$\left\langle E^a_i E^b_j\right\rangle = \frac{1}{a^4}\int \frac{dkd\Omega_{\vec{k}}}{(2\pi)^3}\,k^2 \frac{\partial_0\delta\tilde{A}_{+2}(\tau,k)\left[\partial_0\delta\tilde{A}_{+2}(\tau,k)\right]^* e^a_{+2,i}(\hat{k})\left[e^b_{+2,j}(\hat{k})\right]^* + h.c.}{2}\,, \tag{C.14}$$

and analogously for the terms of $\left\langle E^a_i B^b_j\right\rangle$ and $\left\langle B^a_i B^b_j\right\rangle$

$$2\left\langle E^a_i B^b_j\right\rangle_1 = -\frac{1}{a^4}\int \frac{dkd\Omega_{\vec{k}}}{(2\pi)^3}\,k^3\left\{\partial_0\delta\tilde{A}_{+2}(\tau,k)\left[\delta\tilde{A}_{+2}(\tau,k)\right]^* e^a_{+2,i}(\hat{k})\left[e^b_{+2,j}(\hat{k})\right]^* + h.c.\right\}, \tag{C.15}$$

$$2\left\langle E^a_i B^b_j\right\rangle_2 = \frac{ef}{a^4}\int \frac{dkd\Omega_{\vec{k}}}{(2\pi)^3}\,k^2\left\{\partial_0\delta\tilde{A}_{+2}(\tau,k)\left[\delta\tilde{A}_{+2}(\tau,k)\right]^* e^a_{+2,i}(\hat{k})\left[e^b_{+2,j}(\hat{k})\right]^* + h.c.\right\}, \tag{C.16}$$

$$\begin{aligned}2\left\langle E^a_i B^b_j\right\rangle_3 = &-\frac{e\partial_0 f}{a^4}\int \frac{dkd\Omega_{\vec{k}}}{(2\pi)^3}\,k^2\left\{\delta\tilde{A}_{+2}(\tau,k)\left[\delta\tilde{A}_{+2}(\tau,k)\right]^*\times\right.\\ &\left.\delta^a_i\frac{\varepsilon_{jnm}\varepsilon^{bdh}}{2}\left[e^d_{+2,n}(\hat{k})\right]\left[e^h_{+2,m}(\hat{k})\right]^* + h.c.\right\},\end{aligned} \tag{C.17}$$

$$2\left\langle B^a_i B^b_j\right\rangle_1 = \frac{1}{a^4}\int \frac{dkd\Omega_{\vec{k}}}{(2\pi)^3}\,k^4\left\{\delta\tilde{A}_{+2}(\tau,k)\left[\delta\tilde{A}_{+2}(\tau,k)\right]^* e^a_{+2,i}(\hat{k})\left[e^b_{+2,j}(\hat{k})\right]^* + h.c.\right\}, \tag{C.18}$$

$$2\left\langle B^a_i B^b_j\right\rangle_2 = \frac{e^2f^2}{a^4}\int \frac{dkd\Omega_{\vec{k}}}{(2\pi)^3}\,k^2\left\{\delta\tilde{A}_{+2}(\tau,k)\left[\delta\tilde{A}_{+2}(\tau,k)\right]^* e^a_{+2,i}(\hat{k})\left[e^b_{+2,j}(\hat{k})\right]^* + h.c.\right\}, \tag{C.19}$$

$$2\left\langle B^a_i B^b_j\right\rangle_3 = \frac{-ef}{a^4}\int \frac{dkd\Omega_{\vec{k}}}{(2\pi)^3}\,k^3\left\{\delta\tilde{A}_{+2}(\tau,k)\left[\delta\tilde{A}_{+2}(\tau,k)\right]^* e^a_{+2,i}(\hat{k})\left[e^b_{+2,j}(\hat{k})\right]^* + h.c.\right\},, \tag{C.20}$$

$$2\left\langle B^a_i B^b_j\right\rangle_4 = \frac{-ef}{a^4}\int \frac{dkd\Omega_{\vec{k}}}{(2\pi)^3}\,k^3\left\{\delta\tilde{A}_{+2}(\tau,k)\left[\delta\tilde{A}_{+2}(\tau,k)\right]^* e^a_{+2,i}(\hat{k})\left[e^b_{+2,j}(\hat{k})\right]^* + h.c.\right\}. \tag{C.21}$$

Since T_1 and T_2 are respectively given by

$$T_1 = \left\langle E^a_i E^b_j\right\rangle\left(\left\langle B^a_i B^b_j\right\rangle_1 + \left\langle B^a_i B^b_j\right\rangle_2 + \left\langle B^a_i B^b_j\right\rangle_3 + \left\langle B^a_i B^b_j\right\rangle_4\right), \tag{C.22}$$

$$T_2 = \left(\left\langle E^a_i B^b_j\right\rangle_1 + \left\langle E^a_i B^b_j\right\rangle_2 + \left\langle E^a_i B^b_j\right\rangle_3\right)\left(\left\langle B^a_i E^b_j\right\rangle_1 + \left\langle B^a_i E^b_j\right\rangle_2 + \left\langle B^a_i E^b_j\right\rangle_3\right), \tag{C.23}$$

we can immediatly see that, all the angular integrals reduce to three combinations:

$$\Omega_1 \equiv \int d\Omega_{\vec{k}}\,d\Omega_{\vec{q}}\,e^a_{+2,i}(\hat{k})\left[e^b_{+2,j}(\hat{k})\right]^* e^a_{+2,i}(\hat{q})\left[e^b_{+2,j}(\hat{q})\right]^*, \tag{C.24}$$

$$\Omega_2 \equiv \frac{3}{4}\int d\Omega_{\vec{k}}\,d\Omega_{\vec{q}}\,\varepsilon_{jnm}\varepsilon^{bdh}\left[e^d_{+2,n}(\hat{k})\right]\left[e^h_{+2,m}(\hat{k})\right]^*\varepsilon_{jlu}\varepsilon^{bpr}\left[e^p_{+2,l}(\hat{q})\right]\left[e^r_{+2,u}(\hat{q})\right]^*, \tag{C.25}$$

$$\Omega_3 \equiv \int d\Omega_{\vec{k}}\,d\Omega_{\vec{q}}\,e^a_{+2,i}(\hat{k})\left[e^b_{+2,j}(\hat{k})\right]^*\delta^a_i\frac{\varepsilon_{jnm}\varepsilon^{bdh}}{2}\left[e^d_{+2,n}(\hat{k})\right]\left[e^h_{+2,m}(\hat{k})\right]^*. \tag{C.26}$$

whose direct evaluation give

$$\Omega_1 = \frac{(4\pi)^2}{5}\,, \qquad\qquad \Omega_2 = \frac{4\pi^2}{3}\,, \qquad\qquad \Omega_3 = 0\,. \tag{C.27}$$

Notice that $\Omega_3 = 0$ can be used to simplify T_2 as:

$$T_2 = \left(\left\langle E^a_i B^b_j\right\rangle_1 + \left\langle E^a_i B^b_j\right\rangle_2\right)\left(\left\langle B^a_i E^b_j\right\rangle_1 + \left\langle B^a_i E^b_j\right\rangle_2\right) + \left\langle E^a_i B^b_j\right\rangle_3\left\langle B^a_i E^b_j\right\rangle_3, \tag{C.28}$$

At this point we are finally left with only integrals over the moduli of the momenta. In order to perform these integrals, we will employ Eq. (4.45),

$$\sqrt{2k}\, w_{+2}(x) \simeq e^{(\kappa-\mu)\pi}\sqrt{4\pi}\left(\frac{\zeta(x)}{V(x)}\right)^{1/4} \mathrm{Ai}\left(\zeta(x)\right) \equiv e^{(\kappa-\mu)\pi}\tilde{w}(x)\,. \tag{C.29}$$

We have verified that integrating this approximate expression over the range $0 \leq x \leq 2\xi$ agrees with the integral over the exact expression (4.30) extremely well, and we are moreover insensitive to the choice of the UV-cutoff. Let us start by computing for example:

$$4\left\langle E_i^a E_j^b\right\rangle \left\langle B_i^a B_j^b\right\rangle_1 = \frac{\Omega_1 e^{4\pi(\kappa-\mu)}}{(2\pi)^6 a^8}\int \frac{dk\, k^2}{k}\left\{\partial_0\tilde{w}(x_k)\partial_0\tilde{w}(x_k)\right\}\int\frac{dq\, q^4}{q}\left\{\tilde{w}(x_q)\tilde{w}(x_q)\right\}\,, \tag{C.30}$$

where we use the notation $x_k = -k\tau$ to keep track of the different momentum variables. We can then use $\partial_0\tilde{w}(x_k) = -k\tilde{w}(x_k)$ ($\prime$ here is used to denote the derivative with respect to x_k), $k = -x_k/\tau$ and $\tau = -1/(aH)$ to get

$$4\left\langle E_i^a E_j^b\right\rangle \left\langle B_i^a B_j^b\right\rangle_1 = \frac{\Omega_1 e^{4\pi(\kappa-\mu)}}{(2\pi)^6}H^8\int dx_k\, x_k^3\left\{\tilde{w}'(x_k)\tilde{w}'(x_k)\right\}\int dx_q\, x_q^3\ \left\{\tilde{w}(x_q)\tilde{w}(x_q)\right\}\,. \tag{C.31}$$

Since all the other terms can also be expressed as a product of two integrals it is useful to introduce the six integrals:

$$\mathcal{I}_1 = \int dx\, x^3\ \tilde{w}'(x)\tilde{w}'(x)\,, \qquad \mathcal{I}_2 = \int dx\, x^3\ \tilde{w}(x)\tilde{w}(x)\,, \qquad \mathcal{I}_3 = \int dx\, x\ \tilde{w}(x)\tilde{w}(x)\,, \tag{C.32}$$

$$\mathcal{I}_4 = \int dx\, x^2\ \tilde{w}(x)\tilde{w}(x)\,, \qquad \mathcal{I}_5 = \int dx\, x^3\ \tilde{w}'(x)\tilde{w}(x)\,, \qquad \mathcal{I}_6 = \int dx\, x^2\ \tilde{w}'(x)\tilde{w}(x) \tag{C.33}$$

So that we can easily express

$$\begin{aligned}
4\left\langle E_i^a E_j^b\right\rangle \left\langle B_i^a B_j^b\right\rangle_1 &= \frac{\Omega_1 e^{4\pi(\kappa-\mu)}}{(2\pi)^6}H^8\mathcal{I}_1\mathcal{I}_2\,, & 4\left\langle E_i^a E_j^b\right\rangle \left\langle B_i^a B_j^b\right\rangle_2 &= \frac{\Omega_1 e^{4\pi(\kappa-\mu)}}{(2\pi)^6}H^8\xi^2\mathcal{I}_1\mathcal{I}_3\,,\\
4\left\langle E_i^a E_j^b\right\rangle \left\langle B_i^a B_j^b\right\rangle_3 &= \frac{\Omega_1 e^{4\pi(\kappa-\mu)}}{(2\pi)^6}H^8(-\xi)\mathcal{I}_1\mathcal{I}_4\,, & 4\left\langle E_i^a E_j^b\right\rangle \left\langle B_i^a B_j^b\right\rangle_4 &= \frac{\Omega_1 e^{4\pi(\kappa-\mu)}}{(2\pi)^6}H^8(-\xi)\mathcal{I}_1\mathcal{I}_4\,,\\
4\left\langle E_i^a B_j^b\right\rangle_1 \left\langle B_i^a E_j^b\right\rangle_1 &= \frac{\Omega_1 e^{4\pi(\kappa-\mu)}}{(2\pi)^6}H^8\mathcal{I}_5^2\,, & 4\left\langle E_i^a B_j^b\right\rangle_1 \left\langle B_i^a E_j^b\right\rangle_2 &= \frac{\Omega_1 e^{4\pi(\kappa-\mu)}}{(2\pi)^6}H^8(-\xi)\mathcal{I}_5\mathcal{I}_6\,,\\
4\left\langle E_i^a B_j^b\right\rangle_2 \left\langle B_i^a E_j^b\right\rangle_1 &= \frac{\Omega_1 e^{4\pi(\kappa-\mu)}}{(2\pi)^6}H^8(-\xi)\mathcal{I}_5\mathcal{I}_6\,, & 4\left\langle E_i^a B_j^b\right\rangle_2 \left\langle B_i^a E_j^b\right\rangle_2 &= \frac{\Omega_1 e^{4\pi(\kappa-\mu)}}{(2\pi)^6}H^8\xi^2\mathcal{I}_6^2\,,\\
4\left\langle E_i^a B_j^b\right\rangle_3 \left\langle B_i^a E_j^b\right\rangle_3 &= \frac{\Omega_2 e^{4\pi(\kappa-\mu)}}{(2\pi)^6}H^8\xi^2\mathcal{I}_3^2\,,
\end{aligned} \tag{C.34}$$

where we have also used $ef = -\xi/\tau$ and $dkk^2 = -dx_k x_k^2/\tau^3$. At this point we have all in hand to compute T_0, T_1 and T_2. Let us start with T_0:

$$T_0 = \left\langle E_i^a B_j^b\right\rangle_1 + \left\langle E_i^a B_j^b\right\rangle_2 + \left\langle E_i^a B_j^b\right\rangle_3 = -\frac{H^4}{4\pi^2}e^{2\pi(\kappa-\mu)}\left(\mathcal{I}_5 + \frac{\xi}{2}\mathcal{I}_3 - \xi\mathcal{I}_6\right)\,. \tag{C.35}$$

which to good approximation is given by

$$T_0 = -0.24\times\frac{H^4}{4\pi^2}\times\xi^3 e^{2\pi(\kappa-\mu)} \equiv \frac{H^4}{4\pi^2}\, e^{2\pi(\kappa-\mu)}\,\tilde{T}_0\,. \tag{C.36}$$

analogously we can compute T_1 and T_2

$$T_1 = \frac{\Omega_1 H^8}{4(2\pi)^6} e^{4\pi(\kappa-\mu)}\, \mathcal{I}_1 \left[\mathcal{I}_2 + \xi^2 \mathcal{I}_3 - 2\xi \mathcal{I}_4\right] \tag{C.37}$$

$$T_2 = \frac{\Omega_1 H^8}{4(2\pi)^6} e^{4\pi(\kappa-\mu)}\, \left[\mathcal{I}_5^2 - 2\xi \mathcal{I}_5 \mathcal{I}_6 + \xi^2 \mathcal{I}_6^2 + \xi^2 \Omega_2/\Omega_1 \mathcal{I}_3^2\right] . \tag{C.38}$$

Performing the integrals yields

$$T_1 \simeq 0.0082 \times \frac{H^8}{80\pi^4} \times \xi^8 e^{4\pi(\kappa-\mu)} \equiv \frac{H^8}{80\pi^4}\, e^{4\pi(\kappa-\mu)}\, \tilde{T}_1 \,, \tag{C.39}$$

$$T_2 \simeq 0.051 \times \frac{H^8}{80\pi^4} \times \xi^6 e^{4\pi(\kappa-\mu)} \equiv \frac{H^8}{80\pi^4}\, e^{4\pi(\kappa-\mu)}\, \tilde{T}_2 \,, \tag{C.40}$$

where we have also substituted the values of Ω_1 and Ω_2.

D Supplemental material for Section 3

D.1 Asymptotics for general solutions at late time ($\tau \to 0^-$)

We provide here a complete description of the asymptotic behavior of solutions to Eq. (3.2) as $\tau \to 0^-$. For any fixed ξ, the limit

$$\lim_{\tau \to 0^-} -\tau\, ef(\tau) \tag{D.1}$$

achieves at most three distinct values as $ef(\tau)$ ranges over all solutions: $c_i \xi$ for $i \in \{0, 1, 2\}$, where c_i is defined in Eq. (3.9). In this way, each solution falls into one of three families: two two-parameter families (c_0-type and c_2-type) and a one-parameter family (c_1-type).

For each of these three families we provide the leading terms in a series expansion solution of Eq. (3.2) around $\tau = 0$. For brevity, we omit the degenerate case $\xi = 2$.

1. The c_0-type solutions with parameters β and η are

$$ef(\tau) = \beta + 2\xi\beta^2 \cdot (-\tau)\ln(-\tau) + \eta \cdot (-\tau) + \mathcal{O}\left(\left(\xi^2 \left|\beta^3 \ln(-\tau)\right| + \xi\eta^2\right)(-\tau)^2\right),\ \tau \to 0^-. \tag{D.2}$$

   Under Eq. (3.5) the parameters transform as $(\beta, \eta) \mapsto (\lambda\beta, \lambda^2(\eta + 2\xi\beta^2 \ln\lambda))$.

2. The c_1-type solutions with the single parameter ρ are

$$ef(\tau) = \frac{c_1\xi}{-\tau}\left(1 + \rho\,(-\tau)^{\frac{1}{2}\left(3+\sqrt{d_1}\right)} + \mathcal{O}\left(\rho^2\,(-\tau)^{3+\sqrt{d_1}}\right)\right),\ \tau \to 0^-, \tag{D.3}$$

   where

$$d_1 = 25 - 8c_1\xi^2. \tag{D.4}$$

   As ξ increases from 2 to ∞, $\sqrt{d_1}$ increases from 3 to $\sqrt{17}$. The parameter ρ transforms under Eq. (3.5) as $\rho \mapsto \lambda^{\frac{1}{2}\left(3+\sqrt{d_1}\right)}\rho$.

3. The c_2-type solutions when[24] $\xi > \sqrt{\frac{625}{136}} \approx 2.14$ with parameters υ and θ are of the form

$$ef(\tau) = \frac{c_2\xi}{-\tau}\left(1 + \nu(-\tau)^{3/2}\cos\left(\tfrac{1}{2}\sqrt{-d_2}\ln(-\tau) + \theta\right) + \mathcal{O}\left(\nu^2(-\tau)^3\right)\right),\ \tau \to 0^-, \tag{D.5}$$

[24] If $2 < \xi < \sqrt{\frac{625}{136}}$ then the square root is negative, so Eq. (D.5) must be simply be rewritten in overdamped form. The case $\xi = \sqrt{\frac{625}{136}}$ corresponds to critical damping. Qualitatively, the only difference in these cases is that the perturbations around the c_2 solution decay without oscillating.

where

$$d_2 := 25 - 8c_2\,\xi^2. \tag{D.6}$$

The parameters transform under Eq. (3.5) as $(\nu, \theta) \mapsto (\lambda^{3/2}\nu, \theta + \frac{1}{2}\sqrt{-d_2}\ln(\lambda))$.

It is clear from these formulas and the corresponding transformation laws for the parameters that in the limit $\lambda \to 0$ of Eq. (3.5), we recover the respective c_i-type solutions. Observe that in this same limit the error terms also vanish, and so these asymptotic formulas become exact.
Closely related to the c_1 solutions are the instanton-type solutions

$$ef(\tau) = \frac{c_1\xi}{-\tau}\left(1 + \rho\,(-\tau)^{\frac{1}{2}\left(3+\sqrt{d_1}\right)} + O\left(\rho^2\,(-\tau)^{3+\sqrt{d_1}}\right)\right) \tag{D.7}$$

which are vacuum-to-vacuum transitions which tunnel from the c_1 solution in the infinite past to either the c_0 solution or c_2 solution in the asymptotic future.

D.2 Proof of Theorem 1

Proof. Central to this proof is the auxiliary quantity $\omega_2(\tau)$ which we define as

$$\omega_2(\tau)^4 \equiv (ef'(\tau))^2 + (ef(\tau))^4 - \tfrac{4}{3}\xi\,(ef(\tau))^3/(-\tau). \tag{D.8}$$

Although $\omega_2(\tau)$ is not defined if the right hand side is negative, by slight abuse of notation we allow $\omega_2(\tau)^4$ to denote the right-hand side of Eq. (D.8) even when it is negative. We remark that $\omega_2(\tau)$ provides a more accurate approximation to ω than $\omega_1(\tau)$, which we recall is defined by

$$\omega_1(\tau)^4 \equiv (ef'(\tau))^2 + (ef(\tau))^4\,. \tag{D.9}$$

The contours of $-\tau\omega_2(\tau)$ are plotted as dashed lines in Fig. 3.4, and are very close to the contours of $-\omega\tau$ in the oscillatory regime.
The proof will be in two steps. Firstly we show that if there exists some τ_1 such that $\omega_1(\tau_1) > \frac{4}{3}\xi/(-\tau_1)$ then $\omega_2(\tau_1) > 0$. Secondly we show that if $\omega_2(\tau_1) > 0$ then $\omega > 0$.
For the first step, note that

$$|ef(\tau)| = \sqrt[4]{(ef(\tau))^4} \le \omega_1(\tau). \tag{D.10}$$

Thus

$$\left|\omega_2(\tau)^4 - \omega_1(\tau)^4\right| = \tfrac{4}{3}\xi\,|ef(\tau)|^3/(-\tau) \le \tfrac{4}{3}\xi\omega_1(\tau)^3/(-\tau). \tag{D.11}$$

It directly follows that

$$\left(1 - \tfrac{4}{3}\xi/(-\tau\omega_1(\tau))\right)\omega_1(\tau)^4 \le \omega_2(\tau)^4 \le \left(1 + \tfrac{4}{3}\xi/(-\tau\omega_1(\tau))\right)\omega_1(\tau)^4, \tag{D.12}$$

and thus if $\omega_1(\tau_1) > \frac{4}{3}\xi/(-\tau_1)$ then the left hand side of Eq. (D.12) is positive, so $\omega_2(\tau_1)^4 > 0$.
Now supposing that $\omega_2(\tau_1) > 0$ we must show that $\omega > 0$. By using Eq. (3.2) we verify that $\omega_2(\tau)$ satisfies the differential equation

$$\frac{d}{d\tau}(-\tau\omega_2(\tau)^4) = -\omega_1(\tau)^4. \tag{D.13}$$

Since the right hand side is negative, it follows that $-\tau\omega_2(\tau)^4$ is a decreasing quantity. Thus if $\omega_2(\tau_1)^4$ is positive for some τ_1, then $-\tau\omega_2(\tau)^4 < -\tau_1\omega_2(\tau_1)^4$ for all $\tau < \tau_1$, and so $\omega_2(\tau)^4 > C/(-\tau)$ for $\tau < \tau_1$. Now we argue that if ω were zero, it would contradict the bound $\omega_2(\tau)^4 > C/(-\tau)$. By using Eq. (3.2) once again,

$$\frac{d}{d\tau}\omega_2(\tau)^4 = -\frac{4\xi f(\tau)^3}{3\tau^2}. \tag{D.14}$$

By the fundamental theorem of calculus,

$$\omega_2(\tau)^4 = \lim_{\tau\to-\infty}\omega_2(\tau)^4 + \int_{-\infty}^{\tau}\frac{d}{d\tau'}\omega_2(\tau')^4\,d\tau' \tag{D.15}$$

$$= \omega^4 - \int_{-\infty}^{\tau}\frac{4\xi f(\tau')^3}{3\tau'^2}\,d\tau'. \tag{D.16}$$

Now if $\omega = 0$ then $f(\tau) = \mathcal{O}(-\tau^{-1})$ by Conjecture 1. Therefore

$$\omega_2(\tau)^4 = 0 + \int \tau'^{-2}\mathcal{O}\left(-\tau^{-3}\right)\,d\tau' = \mathcal{O}\left(\tau^{-4}\right), \tag{D.17}$$

but $C/(-\tau)$ is not in $\mathcal{O}\left(\tau^{-4}\right)$. To avoid the contradiction, we conclude that if $\omega_2(\tau_1)^4 > 0$ then $\omega > 0$. In summary we have proven that $\omega_1(\tau_1) > \frac{4}{3}\xi/(-\tau_1)$ implies $\omega_2(\tau_1)^4 > 0$ which implies $\omega > 0$. □

D.3 Proof of Theorem 2

Proof. The theorem follows upon showing that the $v \to \infty$ limit of any trajectory is a zero of (3.26). Every trajectory with initial conditions (q_0, p_0) either converges to a periodic orbit, is unbounded, or limits to a zero of the vector field as $v \to \infty$ (eee the Poincaré–Bendixson theorem). The divergence of (3.26) is -3, so there are no periodic orbits (see by Bendixson's criterion). Using Eq. (3.24) one computes that along trajectories, the quantity $D(p,q) \equiv p^2 + q^4 - \frac{4}{3}\xi q^3$ satisfies $\frac{\mathrm{d}D}{\mathrm{d}v} = -3D - (p^2 + q^4)$. Thus wherever $D > 0$, it is strictly decreasing along trajectories. Therefore, the trajectory remains inside the set defined by $D \le D_0$, where $D_0 \equiv \max(0, D(q_0, p_0))$. This set is readily seen to be bounded, and thus so is the trajectory. Since all other possibilities have been ruled out, the trajectory must converge to a zero of (3.26). □

E Some fundamental properties of gauge fields

E.1 Homogeneous gauge potentials have a homogeneous gauge representative

Suppose $A_\mu(\tau_0, \vec{x})$ is a gauge potential which is homogeneous. This means that for every spatial translation by $\Delta\vec{x}$, there exists a gauge transformation $g_{\Delta\vec{x}}(\tau, \vec{x})$ such that

$$A_\mu(\tau, \vec{x} + \Delta\vec{x}) = g_{\Delta\vec{x}}(\tau, \vec{x}) \cdot A_\mu(\tau, \vec{x}), \tag{E.1}$$

where $\cdot$ denotes a gauge transformation:

$$g_{\Delta\vec{x}}(\tau, \vec{x}) \cdot A_i(\tau, \vec{x}) \equiv g_{\Delta\vec{x}}(\tau, \vec{x}) A_i(\tau, \vec{x}) g_{\Delta\vec{x}}(\tau, \vec{x})^{-1} + (i/e)\left(\nabla_i g_{\Delta\vec{x}}(\tau, \vec{x})\right) g_{\Delta\vec{x}}(\tau, \vec{x})^{-1}. \tag{E.2}$$

The following theorem is unsurprising yet not completely obvious.

Theorem 3. *If $A_\mu(\tau, \vec{x})$ is homogeneous, then it is gauge-equivalent to a gauge field $A_\mu(\tau)$ which does not depend on $\vec{x}$.*

Proof. The strategy will be to use the definition of homogeneity to construct a gauge transformation $h(\tau, \vec{x})$ such that the gauge-transformed field $h(\tau, \vec{x}) \cdot A_\mu(\tau, \vec{x})$ is spatially constant. Equivalently, we want $h(\tau, \vec{x})$ to satisfy the equation

$$h(\tau, \vec{x} + \Delta\vec{x}) \cdot A_\mu(\tau, \vec{x} + \Delta\vec{x}) = h(\tau, \vec{x}) \cdot A_\mu(\tau, \vec{x}) \tag{E.3}$$

for all $\Delta\vec{x}$.

By comparing a single translation by $\Delta\vec{x}_1 + \Delta\vec{x}_2$ with two translations $\Delta\vec{x}_1$ followed by $\Delta\vec{x}_2$, we have

$$\begin{aligned} g_{\Delta\vec{x}_1+\Delta\vec{x}_2}(\tau, \vec{x}) \cdot A_\mu(\tau, \vec{x}) &= A_\mu(\tau, \vec{x} + \Delta\vec{x}_1 + \Delta\vec{x}_2) && \text{(E.4)} \\ &= g_{\Delta\vec{x}_2}(\tau, \vec{x} + \Delta\vec{x}_1) \cdot A_\mu(\tau, \vec{x} + \Delta\vec{x}_1) && \text{(E.5)} \\ &= g_{\Delta\vec{x}_2}(\tau, \vec{x} + \Delta\vec{x}_1)\, g_{\Delta\vec{x}_1}(\tau, \vec{x}) \cdot A_\mu(\tau, \vec{x}). && \text{(E.6)} \end{aligned}$$

It follows that[25]

$$g_{\Delta\vec{x}_1+\Delta\vec{x}_2}(\tau, \vec{x}) = g_{\Delta\vec{x}_2}(\tau, \vec{x} + \Delta\vec{x}_1)\, g_{\Delta\vec{x}_1}(\tau, \vec{x}). \tag{E.7}$$

By making appropriate substitutions for $\Delta\vec{x}_1$, $\Delta\vec{x}_2$ and $\vec{x}$ in this identity, immediate consequences are

$$\begin{aligned} g_0(\vec{x}) &= \mathrm{Id}, \\ g_{\Delta\vec{x}}(\vec{x})^{-1} &= g_{-\Delta\vec{x}}(\vec{x} + \Delta\vec{x}), \\ g_{\Delta\vec{x}}(\vec{x}) &= g_{\vec{x}-\vec{x}_0+\Delta\vec{x}}(\vec{x}_0)\, g_{\vec{x}-\vec{x}_0}(\vec{x}_0)^{-1}, \end{aligned} \tag{E.8}$$

for all values of $\vec{x}$, $\Delta\vec{x}$ and $\vec{x}_0$.

Now fix a basepoint $\vec{x}_0$ and define $h(\tau, \vec{x}) \equiv g_{\vec{x}-\vec{x}_0}(\tau, \vec{x}_0)^{-1}$. It follows from Eq. (E.8) that

$$g_{\Delta\vec{x}}(\tau, \vec{x}) = h(\tau, \vec{x} + \Delta\vec{x})^{-1} h(\tau, \vec{x}) \tag{E.9}$$

for all values of $\vec{x}$ and $\Delta\vec{x}$. Substituting this identity into Eq. (E.1) we obtain Eq. (E.3) as desired. □

The next theorem applies to the case where the gauge group is SU(2).

Theorem 4. *Suppose $A^a_\mu(\tau)$ is a homogeneous* SU(2) *gauge potential. Let $A_{\mathrm{sp}}(\tau) = A^a{}_i(\tau)$ denote the matrix of spatial components. Then up to gauge equivalence, there exists matrices $R(\tau) \in \mathrm{SO}(3)$ and $\Sigma(\tau)$ diagonal such that*

$$A_{\mathrm{sp}}(\tau) = \Sigma(\tau) R(\tau)^T. \tag{E.10}$$

Proof. This is a direct application of singular value decomposition. If $g(\tau)$ is any spatially constant SU(2) gauge transformation, and $G(\tau) \in \mathrm{SO}(3)$ is the corresponding adjoint representation, then

[25] Technically, we are assuming here that a gauge transformation is determined by its action on $A_\mu(\tau, \vec{x})$. It is however possible that there exist global symmetries which fix $A_\mu(\tau, \vec{x})$. In this case, the gauge transformation is determined only up to this subgroup. This issue is easily remedied by declaring that all equalities of gauge transformations are understood modulo this subgroup of symmetries. Then no further modifications to the proof are necessary.

it acts on $A_{\rm sp}(\tau)$ by $A_{\rm sp}(\tau) \mapsto G(\tau)A_{\rm sp}(\tau)$. Singular value decomposition provides matrices $U(\tau)$, $V(\tau) \in \mathrm{SO}(3)$ and $\Sigma(\tau)$ diagonal such that

$$A_{\rm sp}(\tau) = U(\tau)\Sigma(\tau)V(\tau)^T. \tag{E.11}$$

Thus after transforming $A_{\rm sp}(\tau)$ by $G(\tau) = U(\tau)^{-1}$, it satisfies Eq. (E.10) with $R(\tau) = V(\tau)$. □

E.2 Quantifying anisotropy

We want to measure the physical properties of the spatial part $A_{\rm sp}(\tau)$ of the gauge potential, which is a 3×3 matrix. We seek scalars which are invariant under both (spatially constant) SU(2) gauge transformations and SO(3) spatial rotations. Assuming that the symmetries are nondegenerate, we expect a total of $9 - 3 - 3 = 3$ scalars. From Theorem 4, such quantities are expressible in terms of the singular values. However, the singular values are determined only up to permutation, and also up to flipping pairs of signs. This non-uniqueness may be seen as follows:

$$\begin{pmatrix} 0 & 1 & 0 \\ -1 & 0 & 0 \\ 0 & 0 & 1 \end{pmatrix} \begin{pmatrix} \sigma_1 & & \\ & \sigma_2 & \\ & & \sigma_3 \end{pmatrix} \begin{pmatrix} 0 & -1 & 0 \\ 1 & 0 & 0 \\ 0 & 0 & 1 \end{pmatrix} = \begin{pmatrix} \sigma_2 & & \\ & \sigma_1 & \\ & & \sigma_3 \end{pmatrix},$$
$$\begin{pmatrix} -1 & & \\ & -1 & \\ & & 1 \end{pmatrix} \begin{pmatrix} \sigma_1 & & \\ & \sigma_2 & \\ & & \sigma_3 \end{pmatrix} \begin{pmatrix} 1 & & \\ & 1 & \\ & & 1 \end{pmatrix} = \begin{pmatrix} -\sigma_1 & & \\ & -\sigma_2 & \\ & & \sigma_3 \end{pmatrix}. \tag{E.12}$$

Thus, rather than using the singular values, invariant scalars must be invariant under these additional symmetries. Thus we must form quantities in terms of the singular values which are invariant under these additional symmetries. Denoting $A \equiv A_{\rm sp}(\tau)$, a convenient choice is the polynomials

$$I_2 \equiv |A|^2 \equiv A_i^a A_i^a = \sigma_1^2 + \sigma_2^2 + \sigma_3^2, \tag{E.13}$$
$$I_3 \equiv \det A_i^a = \sigma_1\sigma_2\sigma_3, \tag{E.14}$$
$$I_4 \equiv \tfrac{1}{6}\left(3A_i^a A_i^b - \delta^{ab} I_2\right)^2 = \tfrac{1}{6}(2\sigma_1^2 - \sigma_2^2 - \sigma_3^2)^2 + \text{cyclic permutations}. \tag{E.15}$$

These are invariant scalars, and conversely, any invariant scalar is determined as some function of these quantities.

These quantities satisfy certain inequalities. The inequality of arithmetic and geometric means implies that

$$3\sqrt{3}\,|\det A| \le |A|^3\,, \tag{E.16}$$

with equality iff A is isotropic (i.e. $\sigma_1 = \sigma_2 = \sigma_3$). Thus

$$-1 \le 3\sqrt{3}\frac{\det A}{|A|^3} \le 1, \tag{E.17}$$

with isotropy when $3\sqrt{3}\frac{\det A}{|A|^3} = \pm 1$. Similarly, one can show that

$$0 \le \frac{I_4}{|A|^4} \le 1, \tag{E.18}$$

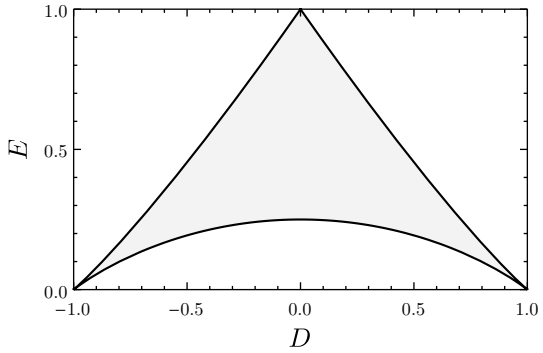

Figure E.1: Only values inside the shaded region can be realized as pairs (D, E) of an actual matrix. The left vertex corresponds to isotropy with $\sigma_i < 0$. The right vertex corresponds to isotropy with $\sigma_i > 0$. The top vertex corresponds to two singular values being zero. The boundary corresponds to when two or more singular values coincide. The lower edge corresponds to a coincidence in the larger two singular values, so it is traced out by $(1, 1, \sigma_3)$ for $\sigma_3 \in [-1, 1]$. The upper two edges correspond to a coincidence of the smaller singular values, e.g. $(\pm 1, \sigma_3, \sigma_3)$ for $\sigma_3 \in [0, 1]$.

where $I_4 = 0$ iff A is isotropic, and $I_4 / |A|^4 = 1$ iff two of the three singular values vanish.
As a sort of polar decomposition, we can consider the radial coordinate $|A|$ together with two other quantities which are invariant under scaling. As such, we define

$$(D, E) \equiv \left(3\sqrt{3} \frac{\det A}{|A|^3}, \frac{I_4}{|A|^4} \right) \in [-1, 1] \times [0, 1] \,. \tag{E.19}$$

Not all points inside this rectangle are realized. The points which are realized belong to the enclosed region in Fig. E.1 which resembles a triangle, but with curved edges.

F Asymptotics of the Whittaker W function

For convenience, throughout this appendix the factor of $1/\sqrt{2k}$ in the Bunch–Davies vacuum is ignored. For parameters k, m, and a, and a positive real variable x, the Whittaker functions

$$C_1 W_{k,m}(ax) + C_2 M_{\kappa,\mu}(ax) \tag{F.1}$$

for constants C_1 and C_2 provide the general solution to the differential equation

$$\frac{\mathrm{d}^2}{\mathrm{d}x^2} w(x) + \left(-\left(\frac{a}{2}\right)^2 + \frac{ka}{x} + \frac{\frac{1}{4} - m^2}{x^2} \right) w(x) = 0. \tag{F.2}$$

In general, given any differential equation of the form

$$\frac{\mathrm{d}^2}{\mathrm{d}x^2} w(x) + \left(A + \frac{B}{x} + \frac{C}{x^2} \right) w(x) = 0, \tag{F.3}$$

it is obviously possible to solve for (possibly complex) Whittaker function parameters k, m and a which match general parameters A, B, and C. For our purposes, it will be convenient to make the transformation $k \mapsto -i\kappa$, $m \mapsto -i\mu$ and $a \mapsto -i\alpha$. Under the assumption that that κ, μ and α

are real and positive, it will be sufficient for our purposes to take $C_2 = 0$ and consider only the "negative-imaginary Whittaker W function"

$$C_1 W_{-i\kappa,-i\mu}(-i\alpha x), \tag{F.4}$$

which solves

$$\frac{\mathrm{d}^2}{\mathrm{d}x^2} w(x) + \left(\left(\frac{\alpha}{2}\right)^2 - \frac{\kappa\alpha}{x} + \frac{\frac{1}{4}+\mu^2}{x^2} \right) w(x) = 0. \tag{F.5}$$

The case corresponding to Eq. (4.28) for $w^{(e)}_{+2}$ with the c_2-solution corresponds to the negative imaginary Whittaker W function with parameters

$$\begin{aligned} \kappa &= (1+c_2)\xi \approx 2\xi, \\ \mu &= \sqrt{2c_2 - (2\xi)^{-2}}\,\xi \approx \sqrt{2}\xi, \\ \alpha &= 2. \end{aligned} \tag{F.6}$$

F.1 Summary of asymptotics

We wish to impose the boundary condition

$$w(x) = C_1 W_{-i\kappa,-i\mu}(-i\alpha x) \sim e^{i\alpha x/2} \text{ as } x \to \infty, \tag{F.7}$$

which corresponds to the Bunch–Davies vacuum, without the factor of $\sqrt{2k}$. We discover that

$$C_1 = e^{\kappa\pi/2} e^{i\phi_0}, \tag{F.8}$$

where the phase ϕ_0 is undetermined.

Next we study the resulting behavior as $x \to 0$. As is the case in Eq. (F.6), if $\kappa > \mu$ then upon taking ϕ_0 as in Eq. (F.20), the real part is enhanced and the imaginary part is supressed. Specifically,

$$\mathrm{Re}(w(x)) \approx 2e^{(\kappa-\mu)\pi} \sqrt{\frac{\alpha x}{2\mu}} \cos\left(\mu \ln(\alpha x) + \theta_0\right), \tag{F.9}$$

$$\mathrm{Im}(w(x)) \approx \tfrac{1}{2} e^{-(\kappa-\mu)\pi} \sqrt{\frac{\alpha x}{2\mu}} \sin\left(\mu \ln(\alpha x) + \theta_0\right). \tag{F.10}$$

Note that this is a wave which decays proportional to $\sqrt{x}$. Furthermore, this wave oscillates $\mu/(2\pi)$ times per e-fold. In our case of interest $w(x) = w^{(e)}_{+2}(x)$, e-folds in x are equivalent to e-folds in τ, and the frequency is $\approx \sqrt{2}\xi/(2\pi)$ oscillations per e-fold.

For large ξ, we could approximate κ and μ to obtain

$$\begin{aligned} w^{(e)}_{+2}(x) &\approx 2^{-1/4}\sqrt{x}\left(2e^{(2-\sqrt{2})\pi\xi}\cos\theta + \tfrac{1}{2}e^{-(2-\sqrt{2})\pi\xi} i \sin\theta\right), \\ \theta &\approx \sqrt{2}\xi \ln(2x) + \theta_0, \end{aligned} \tag{F.11}$$

however due to the exponential sensitivity of κ and μ, it is preferrable to use Eq. (F.9) rather than Eq. (F.11).

Finally we approximate $\mathrm{Re}(w(x))$ around the maximum value using WKB approximation.

F.2 Asymptotics as $x \to \infty$

We now determine the magnitude $|C_1|$ by matching with the asymptotics of the Whittaker function. Let x be a positive real variable. For large x, the Whittaker function satisfies

$$W_{\kappa,\mu}(\alpha x) = e^{-\alpha x/2}(\alpha x)^{\kappa}\left(1+\epsilon_1(\alpha x)\right), \tag{F.12}$$

$$\epsilon_1(\alpha x) \equiv O\left(\frac{1+\kappa^2+\mu^2}{\alpha x}\right). \tag{F.13}$$

This asymptotic expression remains valid upon replacing $\kappa \mapsto -i\kappa$, $\mu \mapsto -i\mu$ and $\alpha \mapsto -i\alpha$, and evaluating complex exponents $b^p = e^{p\ln b}$ using the principal branch of the logarithm. Thus

$$\begin{aligned} W_{-i\kappa,-i\mu}(-i\alpha x) &= e^{i\alpha x/2}(-i\alpha x)^{-i\kappa}\left(1+\epsilon_1(\alpha x)\right) \\ &= e^{-\kappa\pi/2}\, e^{i\alpha x/2 - i\kappa\ln(\alpha x)}\left(1+\epsilon_1(\alpha x)\right) \end{aligned} \tag{F.14}$$

as $x \to \infty$. Therefore $|C_1| = e^{\kappa\pi/2}$. Note the (inconsequential) logarithmic drift in complex phase, which prevents us at this stage from selecting a distinguished phase.

F.3 Asymptotics as $x \to 0^+$

Ultimately we are interested in the resulting behavior as $x \to 0^+$, corresponding to the infinite future. In this limit we have

$$W_{-i\kappa,-i\mu}(-i\alpha x) = \sqrt{\alpha x}e^{-i\pi/4}\sum_{\pm}\frac{\Gamma\left(\mp 2i\mu\right)}{\Gamma\left(\frac{1}{2}+i\kappa\mp i\mu\right)}(-i\alpha x)^{\pm i\mu}\left(1+\epsilon_2(\alpha x)\right), \tag{F.15}$$

$$\epsilon_2(\alpha x) \equiv O\left(\frac{1+\kappa+\mu}{1+\mu}\alpha x\right). \tag{F.16}$$

To make sense of this expression, we may rewrite it in the form

$$w(x) \equiv e^{\kappa\pi/2}e^{i\phi_0}W_{-i\kappa,-i\mu}(-i\alpha x) = C_0\sqrt{\alpha x}\left(\lambda\cos\theta + i\lambda^{-1}\sin\theta + \epsilon_3(\alpha x)\right), \tag{F.17}$$

$$\theta \equiv \mu\ln(\alpha x) + \theta_0,$$

where the four constants C_0, λ, ϕ_0 and θ_0 depend only on the parameters κ and μ. After some algebra, we find the exact expressions

$$C_0 \equiv (2\mu)^{-1/2}, \tag{F.18}$$

$$\lambda \equiv e^{(\kappa-\mu)\pi}\left(\frac{\sqrt{1+e^{-2(\kappa-\mu)\pi}}+\sqrt{1+e^{-2(\kappa-\mu)\pi}e^{-4\mu\pi}}}{\sqrt{1-e^{-4\mu\pi}}}\right), \tag{F.19}$$

$$\theta_0 \equiv \tfrac{1}{2}\left(\phi_{\Gamma,1/2}(\kappa+\mu) - \phi_{\Gamma,1/2}(\kappa-\mu)\right) - \phi_{\Gamma,0}(2\mu)$$

$$\phi_0 \equiv \tfrac{\pi}{4} + \tfrac{1}{2}\left(\phi_{\Gamma,1/2}(\kappa+\mu) + \phi_{\Gamma,1/2}(\kappa-\mu)\right), \tag{F.20}$$

$$\phi_{\Gamma,a}(b) \equiv \arg\Gamma(a+ib).$$

$$\epsilon_3(\alpha x) \equiv O\left(\frac{1+\kappa+\mu}{1+\mu}(\lambda+\lambda^{-1})\alpha x\right).$$

To derive these parameters, we have made use of the following polar decomposition identities for the gamma function. For $b \in \mathbb{R}$,

$$\Gamma(ib) = \sqrt{\frac{\pi}{b\sinh(\pi b)}} e^{i\phi_{\Gamma,0}(b)}, \quad \Gamma\left(\tfrac{1}{2} + ib\right) = \sqrt{\frac{\pi}{\cosh(\pi b)}} e^{i\phi_{\Gamma,1/2}(b)}. \tag{F.21}$$

In the case of our parameters of interest F.6, namely

$$\kappa \approx 2\xi, \qquad \mu \approx \sqrt{2}\xi, \qquad \alpha = 2, \qquad \xi \geq 2, \tag{F.22}$$

we have $e^{-2\pi(\kappa-\mu)} \ll 1$ and $e^{-4\pi\mu} \ll 1$. This allows us to very accurately approximate the part of the expression for λ inside the parentheses in Eq. (F.19) by 2. Specifically,

$$\begin{aligned} &\lambda = 2e^{(\kappa-\mu)\pi}(1+\epsilon_4), \\ &0 < \epsilon_4 \leq e^{-2(\kappa-\mu)\pi} + e^{-4\mu\pi} \text{ when } \mu \geq \tfrac{1}{25}. \end{aligned} \tag{F.23}$$

In the worst case with our parameters (when $\xi = 2$), the relative error is only $\epsilon_4 \approx 3 \times 10^{-4}$.
Finally, when $e^{-2\pi(\kappa-\mu)} \ll 1$ and $e^{-4\pi\mu} \ll 1$ we obtain the formulas Eq. (F.9) and Eq. (F.10) by plugging Eq. (F.23) into Eq. (F.17).

F.4 WKB approximation

F.4.1 Review of WKB approximation

Although widely known, we briefly summarize the technique of WKB approximation as utilized here. The solutions to a differential equation of the form

$$\frac{\mathrm{d}^2}{\mathrm{d}x^2} w(x) = V(x) w(x) \tag{F.24}$$

are often not straightforward when $V(x)$ is a general function. Important exceptions are when $V(x)$ is one of the following model potentials $V_0(x)$.

- If $V_0(x) = 1$ then $w_0(x) = e^{\pm x}$ are solutions.
- If $V_0(x) = -1$ then $w_0(x) = e^{\pm ix}$ are solutions.
- If $V_0(x) = x$ then the Airy functions $w_0(x) = \mathrm{Ai}(x)$ and $w_0(x) = \mathrm{Bi}(x)$ are solutions.
- If $V_0(x) = \pm(x^2 - \alpha^2)$ for some constant α then the solutions are called parabolic cylinder functions, and they have α as a parameter.

The main idea of the WKB approximation is to perform a change of variables to make Eq. (F.24) resemble such a model equation. For context in this derivation, we recommend that the reader look ahead in Sec. F.4.2 at the end formulas.
We consider transformations of Eq. (F.24) which don't introduce a first-derivative term, and are of the form

$$w(x) \mapsto \vartheta(\zeta(x)) \cdot W(\zeta(x)), \tag{F.25}$$

where $\zeta(x)$ is an increasing change of variables ($\mathrm{d}\zeta/\mathrm{d}x > 0$), and $\vartheta(\zeta)$ is constructed to eliminate any first-derivative term introduced by ζ. Such a transformation is called a Liouville transformation. The transformed equation should be of the form

$$\frac{\mathrm{d}^2}{\mathrm{d}\zeta^2}W(\zeta) = (V_0(\zeta) + \epsilon(\zeta))\,W(\zeta), \tag{F.26}$$

where $V_0(\zeta)$ is a model potential, $\epsilon(\zeta)$ is arranged to be suitably negligible. The Liouville transformation condition that ensures no first-derivative term is equivalent to

$$\vartheta(\zeta) = \left(\frac{\mathrm{d}x}{\mathrm{d}\zeta}\right)^{1/2}. \tag{F.27}$$

A generally good choice of $\zeta(x)$ to keep $\epsilon(\zeta)$ small is

$$\frac{\mathrm{d}\zeta}{\mathrm{d}x} = +\sqrt{\frac{V(x)}{V_0(\zeta)}}. \tag{F.28}$$

Since this must be real, it must satisfy $\mathrm{sign}(V(x)) = \mathrm{sign}(V_0(\zeta))$. Thus for each zero of $V(x)$ in the domain of interest, there must be a corresponding zero in $V_0(\zeta)$. In this way, the number of roots of $V(x)$ determines the appropriate type of model potential.
Solving Eq. (F.28) gives

$$\int \sqrt{|V_0(\zeta)|}\; d\zeta = \int \sqrt{|V(x)|}\; dx, \tag{F.29}$$

which we rewrite as $Z(\zeta) = X(x)$ where Z and X are the respective antiderivatives.[26] Assuming that we can compute the antiderivatives and Z^{-1}, we have the formula

$$\zeta(x) = Z^{-1}\left(X(x)\right). \tag{F.30}$$

Working backwards to get our approximate solution, let $W_0(\zeta)$ denote a solution to Eq. (F.26) where we ignore $\epsilon(\zeta)$. Plugging this into Eq. (F.25) and using Eq. (F.27) and Eq. (F.28), we find

$$w_{\text{approx}}(x) = C\left(\frac{V_0(\zeta(x))}{V(x)}\right)^{1/4} W_0(\zeta(x)) \tag{F.31}$$

is an approximate solution to Eq. (F.24).

F.4.2 WKB approximation for various model potentials

Consider first the simple case where $V(x)$ has no zeroes so that we can take $V_0(\zeta) = \pm 1 = \mathrm{sign}V$. The model solutions are $W_0(\zeta) = e^{\pm\sqrt{\mathrm{sign}V}\zeta}$. For the reparameterization, $Z(\zeta) = \zeta$ and so

$$\zeta_{\text{exp}}(x) = X(x) = \int \sqrt{|V(x)|}\, dx. \tag{F.32}$$

Finally,

$$w_{\text{exp-approx}}(x) = C\,|V(x)|^{-1/4}\, e^{\pm\sqrt{\mathrm{sign}V}X(x)}, \tag{F.33}$$

[26] In case there are any roots $\{x_i\}$ of $V(x)$, then the constant of integration and any parameters of the model potential must be chosen so that $X(x_i) = Z(\zeta_i)$, where $\{\zeta_i\}$ are the corresponding zeroes of $V_0(\zeta)$.

which is the standard WKB approximation.

Consider next the case where $V(x)$ has a single simple zero at $x = x_1$. We take $V_0(\zeta) = \zeta$. Thus $Z(\zeta) = \operatorname{sign}(\zeta)\frac{2}{3}|\zeta|^{3/2}$, and $X(x) = \int_{x_1}^{x} \sqrt{|V(y)|}\, dy$, so

$$\zeta_{\text{Airy}}(x) = \operatorname{sign}(x - x_1)\left|\tfrac{3}{2}X(x)\right|^{2/3}, \tag{F.34}$$

$$w_{\text{Airy-approx}}(x) = C\left(\frac{\zeta(x)}{V(x)}\right)^{1/4} \operatorname{Ai}(\zeta(x)). \tag{F.35}$$

The case where $V(x)$ has two zeroes at $x_1 < x_2$ is treated in [57] and applied to the imaginary Whittaker function in [58]. As a summary, the parameter α of V_0 is determined by $\int_{-\alpha}^{\alpha} \sqrt{\alpha^2 - \zeta^2} = \int_{x_1}^{x_2} \sqrt{|V(y)|}\, dy$, which is necessary for $\zeta(x_1) = -\alpha$ and $\zeta(x_2) = +\alpha$. One complication is that although $Z(\zeta)$ has a closed form, its inverse function does not. Furthermore the parabolic cylinder functions are not as convenient. Thus for our purposes, Eq. (F.35) will suffice.

F.4.3 Airy approximation of the imaginary Whittaker W function for small x

We wish to find the constant coefficient of Eq. (F.35) which will make it agree with $\operatorname{Re}(w(x))$ from Eq. (F.9) as $x \to 0$, or equivalently as $\zeta \to -\infty$.

In the imaginary Whittaker equation Eq. (F.5) we take[27]

$$V(x) = -\left(\left(\frac{\alpha}{2}\right)^2 - \frac{\kappa\alpha}{x} + \frac{\frac{0}{4} + \mu^2}{x^2}\right), \tag{F.37}$$

To determine the proper coefficient C of Eq. (F.35), we substitute into Eq. (F.35) the asymptotic formula

$$\operatorname{Ai}(\zeta) = \pi^{-1/2}(-\zeta)^{-1/4}\sin\left(\frac{\pi}{4} + \frac{2}{3}(-\zeta)^{3/2}\right) + O(-\zeta^{-1}) \text{ as } \zeta \to -\infty \tag{F.38}$$

to obtain

$$w_{\text{approx}}(x) \approx C\pi^{-1/2}V(x)^{-1/4}\sin\left(\frac{\pi}{4} - X(x)\right). \tag{F.39}$$

As $x \to 0$ we have $V(x)^{-1/4} \approx \sqrt{x/\mu}$. Matching the magnitude with Eq. (F.9), we find $C = \sqrt{2\pi\alpha}\; e^{(\kappa-\mu)\pi}$, so

$$w_{\text{approx}}(x) = \sqrt{2\pi\alpha}\; e^{(\kappa-\mu)\pi}\left(\frac{\zeta(x)}{V(x)}\right)^{1/4} \operatorname{Ai}(\zeta(x)). \tag{F.40}$$

The exact expression for $\zeta(x)$ is complicated, but it is well-approximated for $x \approx x_1$ by

$$\zeta(x) \approx \left(2\mu^2 - \alpha\kappa x_1\right)^{1/3} \ln\frac{x}{x_1}. \tag{F.41}$$

[27] Since the WKB approximation introduces small errors, there is potential for these errors to cancel. For the Whittaker function, it is advantageous in the case of the Whittaker function to modify $V(x)$ and replace the $\frac{1}{4}$ in Eq. (F.5) with $\frac{0}{4}$ for our definition of $V(x)$. As motivation for this modification, consider $V(x) \approx -(a + \mu^2)x^{-2}$ as $x \to 0$. Then $X(x) \approx \sqrt{a + \mu^2}\ln x$. When $V(x)$ is large, the Airy approximation reduces to the exponential approximation, and thus by Eq. (F.33) the approximate solution is of the form

$$w_{\text{approx}}(x) \approx C\sqrt{x}e^{\pm i\sqrt{a+\mu^2}\ln x}. \tag{F.36}$$

By comparison of the exponent with Eq. (F.9), we see that the coefficient of $\ln x$ should be μ, and thus it is best to take $a = 0$ rather than $a = \frac{1}{4}$.

To give the exact formula for $\zeta(x)$ in the inverval $(0, x_1)$ in a concise form, we introduce

$$\chi \equiv \frac{\alpha x}{2\mu}, \quad \lambda \equiv \frac{\kappa}{\mu} > 1, \quad \chi_i \equiv \lambda + (-1)^i \sqrt{\lambda^2 - 1} \text{ for } i \in \{1, 2\}\,, \tag{F.42}$$

$$R \equiv \sqrt{\chi^2 - 2\chi\lambda + 1} = \frac{x}{\mu}\sqrt{-V(x)}. \tag{F.43}$$

It is easy to verify that

$$x_i = 2\mu\chi_i/\alpha \text{ for } i \in \{1, 2\}\,, \tag{F.44}$$

$$V(x) = V(x) = -\left(\frac{\alpha}{2\chi}\right)^2 \left(\chi^2 - 2\chi\lambda + 1\right) = -\left(\frac{\alpha}{2\chi}\right)^2 (\chi - \chi_1)\,(\chi - \chi_2)\,, \tag{F.45}$$

$$X(x) = \left(R - \ln\left(1 - \chi\lambda + R\right) - \lambda \ln\left(\lambda - \chi - R\right) + \ln\chi + \tfrac{1}{2}(1 + \lambda)\ln\left(\lambda^2 - 1\right)\right)\mu, \tag{F.46}$$

$$\zeta(x) = \text{sign}(x - x_1)\left|\tfrac{3}{2}X(x)\right|^{2/3}. \tag{F.47}$$

This expression for $X(x)$ is valid only in the interval $(0, x_1)$.

References

[1] A. H. Guth, *The Inflationary Universe: A Possible Solution to the Horizon and Flatness Problems*, *Phys. Rev.* **D23** (1981) 347–356.

[2] **Planck** Collaboration, P. A. R. Ade et al., *Planck 2015 results. XX. Constraints on inflation*, *Astron. Astrophys.* **594** (2016) A20, [arXiv:1502.02114].

[3] J. L. Cook and L. Sorbo, *Particle production during inflation and gravitational waves detectable by ground-based interferometers*, *Phys. Rev.* **D85** (2012) 023534, [arXiv:1109.0022]. [Erratum: Phys. Rev.D86,069901(2012)].

[4] E. Dimastrogiovanni and M. Peloso, *Stability analysis of chromo-natural inflation and possible evasion of Lyth's bound*, *Phys. Rev.* **D87** (2013), no. 10 103501, [arXiv:1212.5184].

[5] P. Adshead, E. Martinec, and M. Wyman, *Gauge fields and inflation: Chiral gravitational waves, fluctuations, and the Lyth bound*, *Phys. Rev.* **D88** (2013), no. 2 021302, [arXiv:1301.2598].

[6] N. Barnaby and M. Peloso, *Large Nongaussianity in Axion Inflation*, *Phys. Rev. Lett.* **106** (2011) 181301, [arXiv:1011.1500].

[7] N. Barnaby, E. Pajer, and M. Peloso, *Gauge Field Production in Axion Inflation: Consequences for Monodromy, non-Gaussianity in the CMB, and Gravitational Waves at Interferometers*, *Phys. Rev.* **D85** (2012) 023525, [arXiv:1110.3327].

[8] N. Barnaby, R. Namba, and M. Peloso, *Phenomenology of a Pseudo-Scalar Inflaton: Naturally Large Nongaussianity*, *JCAP* **1104** (2011) 009, [arXiv:1102.4333].

[9] M. Shiraishi, A. Ricciardone, and S. Saga, *Parity violation in the CMB bispectrum by a rolling pseudoscalar*, *JCAP* **1311** (2013) 051, [arXiv:1308.6769].

[10] J. L. Cook and L. Sorbo, *An inflationary model with small scalar and large tensor nongaussianities*, *JCAP* **1311** (2013) 047, [arXiv:1307.7077].

[11] P. D. Meerburg and E. Pajer, *Observational Constraints on Gauge Field Production in Axion Inflation*, *JCAP* **1302** (2013) 017, [arXiv:1203.6076].

[12] A. Linde, S. Mooij, and E. Pajer, *Gauge field production in supergravity inflation: Local non-Gaussianity and primordial black holes*, *Phys. Rev.* **D87** (2013), no. 10 103506, [arXiv:1212.1693].

[13] V. Domcke, F. Muia, M. Pieroni, and L. T. Witkowski, *PBH dark matter from axion inflation*, *JCAP* **1707** (2017) 048, [arXiv:1704.03464].

[14] J. Garcia-Bellido, M. Peloso, and C. Unal, *Gravitational waves at interferometer scales and primordial black holes in axion inflation*, *JCAP* **1612** (2016), no. 12 031, [arXiv:1610.03763].

[15] M. M. Anber and L. Sorbo, *Non-Gaussianities and chiral gravitational waves in natural steep inflation*, *Phys. Rev.* **D85** (2012) 123537, [arXiv:1203.5849].

[16] V. Domcke, M. Pieroni, and P. Binétruy, *Primordial gravitational waves for universality classes of pseudoscalar inflation*, *JCAP* **1606** (2016) 031, [arXiv:1603.01287].

[17] N. Bartolo et al., *Science with the space-based interferometer LISA. IV: Probing inflation with gravitational waves*, *JCAP* **1612** (2016), no. 12 026, [arXiv:1610.06481].

[18] M. M. Anber and L. Sorbo, *Naturally inflating on steep potentials through electromagnetic dissipation*, *Phys. Rev.* **D81** (2010) 043534, [arXiv:0908.4089].

[19] V. Domcke and K. Mukaida, *Gauge Field and Fermion Production during Axion Inflation*, arXiv:1806.08769.

[20] P. Adshead and M. Wyman, *Chromo-Natural Inflation: Natural inflation on a steep potential with classical non-Abelian gauge fields*, *Phys. Rev. Lett.* **108** (2012) 261302, [arXiv:1202.2366].

[21] E. Dimastrogiovanni, M. Fasiello, and A. J. Tolley, *Low-Energy Effective Field Theory for Chromo-Natural Inflation*, *JCAP* **1302** (2013) 046, [arXiv:1211.1396].

[22] P. Adshead, E. Martinec, and M. Wyman, *Perturbations in Chromo-Natural Inflation*, *JHEP* **09** (2013) 087, [arXiv:1305.2930].

[23] R. Namba, E. Dimastrogiovanni, and M. Peloso, *Gauge-flation confronted with Planck*, *JCAP* **1311** (2013) 045, [arXiv:1308.1366].

[24] A. Maleknejad and M. M. Sheikh-Jabbari, *Gauge-flation: Inflation From Non-Abelian Gauge Fields*, *Phys. Lett.* **B723** (2013) 224–228, [arXiv:1102.1513].

[25] A. Maleknejad and M. M. Sheikh-Jabbari, *Non-Abelian Gauge Field Inflation*, *Phys. Rev.* **D84** (2011) 043515, [arXiv:1102.1932].

[26] P. Adshead and M. Wyman, *Gauge-flation trajectories in Chromo-Natural Inflation*, *Phys. Rev.* **D86** (2012) 043530, [arXiv:1203.2264].

[27] M. M. Sheikh-Jabbari, *Gauge-flation Vs Chromo-Natural Inflation*, *Phys. Lett.* **B717** (2012) 6–9, [arXiv:1203.2265].

[28] R. R. Caldwell and C. Devulder, *Axion Gauge Field Inflation and Gravitational Leptogenesis: A Lower Bound on B Modes from the Matter-Antimatter Asymmetry of the Universe*, *Phys. Rev.* **D97** (2018), no. 2 023532, [arXiv:1706.03765].

[29] G. Dall'Agata, *Chromo-Natural inflation in Supergravity*, *Phys. Lett.* **B782** (2018) 139–142, [arXiv:1804.03104].

[30] E. Dimastrogiovanni, M. Fasiello, and T. Fujita, *Primordial Gravitational Waves from Axion-Gauge Fields Dynamics*, *JCAP* **1701** (2017), no. 01 019, [arXiv:1608.04216].

[31] E. McDonough and S. Alexander, *Observable Chiral Gravitational Waves from Inflation in String Theory*, arXiv:1806.05684.

[32] P. Adshead, E. Martinec, E. I. Sfakianakis, and M. Wyman, *Higgsed Chromo-Natural Inflation*, *JHEP* **12** (2016) 137, [arXiv:1609.04025].

[33] E. Dimastrogiovanni, M. Fasiello, R. J. Hardwick, H. Assadullahi, K. Koyama, and D. Wands, *Non-Gaussianity from Axion-Gauge Fields Interactions during Inflation*, arXiv:1806.05474.

[34] A. Papageorgiou, M. Peloso, and C. Unal, *Nonlinear perturbations from the coupling of the inflaton to a non-Abelian gauge field, with a focus on Chromo-Natural Inflation*, arXiv:1806.08313.

[35] M. S. Turner and L. M. Widrow, *Inflation Produced, Large Scale Magnetic Fields*, *Phys. Rev.* **D37** (1988) 2743.

[36] W. D. Garretson, G. B. Field, and S. M. Carroll, *Primordial magnetic fields from pseudoGoldstone bosons*, *Phys. Rev.* **D46** (1992) 5346–5351, [hep-ph/9209238].

[37] M. M. Anber and L. Sorbo, *N-flationary magnetic fields*, *JCAP* **0610** (2006) 018, [astro-ph/0606534].

[38] D. Jiménez, K. Kamada, K. Schmitz, and X.-J. Xu, *Baryon asymmetry and gravitational waves from pseudoscalar inflation*, *JCAP* **1712** (2017), no. 12 011, [arXiv:1707.07943].

[39] A. H. Guth and S.-Y. Pi, *The Quantum Mechanics of the Scalar Field in the New Inflationary Universe*, *Phys. Rev.* **D32** (1985) 1899–1920. [,1899(1985)].

[40] P. Brax, J.-F. Dufaux, and S. Mariadassou, *Preheating after Small-Field Inflation*, *Phys. Rev.* **D83** (2011) 103510, [arXiv:1012.4656].

[41] R. L. Arnowitt, S. Deser, and C. W. Misner, *The Dynamics of general relativity*, *Gen. Rel. Grav.* **40** (2008) 1997–2027, [gr-qc/0405109].

[42] M. Maggiore, *Gravitational wave experiments and early universe cosmology*, *Phys. Rept.* **331** (2000) 283–367, [gr-qc/9909001].

[43] R. R. Caldwell, C. Devulder, and N. A. Maksimova, *Gravitational wave–Gauge field oscillations*, *Phys. Rev.* **D94** (2016), no. 6 063005, [arXiv:1604.08939].

[44] R. R. Caldwell, C. Devulder, and N. A. Maksimova, *Gravitational wave–gauge field dynamics*, *Int. J. Mod. Phys.* **D26** (2017), no. 12 1742005, [arXiv:1706.00431].

[45] P. Adshead and E. I. Sfakianakis, *Higgsed Gauge-flation*, *JHEP* **08** (2017) 130, [arXiv:1705.03024].

[46] D. Baumann, *Inflation*, in *Physics of the large and the small, TASI 09, proceedings of the Theoretical Advanced Study Institute in Elementary Particle Physics, Boulder, Colorado, USA, 1-26 June 2009*, pp. 523–686, 2011. arXiv:0907.5424.

[47] M. S. Turner, M. J. White, and J. E. Lidsey, *Tensor perturbations in inflationary models as a probe of cosmology*, *Phys. Rev.* **D48** (1993) 4613–4622, [astro-ph/9306029].

[48] N. Seto and J. Yokoyama, *Probing the equation of state of the early universe with a space laser interferometer*, *J. Phys. Soc. Jap.* **72** (2003) 3082–3086, [gr-qc/0305096].

[49] T. L. Smith, M. Kamionkowski, and A. Cooray, *Direct detection of the inflationary gravitational wave background*, *Phys. Rev.* **D73** (2006) 023504, [astro-ph/0506422].

[50] R. van Haasteren et al., *Placing limits on the stochastic gravitational-wave background using European Pulsar Timing Array data*, *Mon. Not. Roy. Astron. Soc.* **414** (2011), no. 4 3117–3128, [arXiv:1103.0576]. [Erratum: Mon. Not. Roy. Astron. Soc.425,no.2,1597(2012)].

[51] M. Kramer, *Fundamental physics with the SKA: Strong-field tests of gravity using pulsars and black holes*, astro-ph/0409020.

[52] **Virgo, LIGO Scientific** Collaboration, B. P. Abbott et al., *GW150914: Implications for the stochastic gravitational wave background from binary black holes*, *Phys. Rev. Lett.* **116** (2016), no. 13 131102, [arXiv:1602.03847].

[53] **LISA** Collaboration, H. Audley et al., *Laser Interferometer Space Antenna*, arXiv:1702.00786.

[54] **ET** Collaboration, m. Abernathy et al., *Einstein gravitational wave Telescope, Conceptual Design Study*, .

[55] A. Agrawal, T. Fujita, and E. Komatsu, *Large tensor non-Gaussianity from axion-gauge field dynamics*, *Phys. Rev.* **D97** (2018), no. 10 103526, [arXiv:1707.03023].

[56] N. Bartolo, V. Domcke, D. G. Figueroa, J. Garcia-Bellido, M. Peloso, M. Pieroni, A. Ricciardone, M. Sakellariadou, L. Sorbo, and G. Tasinato, *Probing non-Gaussian Stochastic Gravitational Wave Backgrounds with LISA*, arXiv:1806.02819.

[57] F. W. J. Olver, *Second-order linear differential equations with two turning points*, *Philosophical Transactions of the Royal Society of London A: Mathematical, Physical and Engineering Sciences* **278** (1975), no. 1279 137–174.

[58] F. W. J. Olver, *Whittaker functions with both parameters large: uniform approximations in terms of parabolic cylinder functions*, *Proceedings of the Royal Society of Edinburgh: Section A Mathematics* **86** (1980), no. 3-4 213–234.